THE UNIVERSITY OF ASTON IN BIRMINGHAM

DEPARTMENT OF PHYSICS

COHERENT AND NONCOHERENT METHODS OF CORRELATION AND CONVOLUTION

By

Luay Abdul-majeed Al-Qazzaz B.Sc. M.Sc. D.I.C.

Thesis submitted for the degree of

Doctor of Philosophy.

April 1976.

ABSTRACT

Correlation and convolution are based on the idea of getting the response of one function to another. When the data is available in two dimensional transparency form it is convenient to use optical systems.

Different techniques of performing the correlation and convolution operations in coherent and noncoherent light are described. Their applications in optics are mentioned.

A random-dots code is presented. This was used for coding dilute and continuous-tone pictures. The coded pictures were decoded by correlating them with the code. Coherent and non-coherent correlation methods were employed. In the coherent method a complex filter was used and the coded pictures were decoded by coherent optical filtering. The noncoherent method is based on the idea of reversing the rays involved in the coding process. The two methods are compared, the effect of the decoding on dilute and continuous-tone objects is illustrated, noise analysis is given and the decoded images resolution is considered.

Theories of formation of Fourier images are discussed. A confusion is shown to exist between Fourier images derived from

related objects. Coherent and noncoherent correlation experiments are reported. Their results serve to confirm the possibility of confusion.

Finally a new method of noncoherent spatial filtering , using blocking filters, is presented.

To my Mother and Father

CONTENTS

INTRODUCTION

Correlation and convolution have many applications in optics particularly in optical data processing. In the first chapter of this thesis the Fourier and the Fourier transform theories are described. These are necessary for understanding the correlation and the convolution operations discussed in the same chapter.

The second chapter is a survey of the correlation and convolution techniques and applications. This chapter describes the basic idea of all the correlators and the correlation techniques used in the experimental work. It shows as well the relation between these techniques. Many other techniques and applications are described in order to give a substantial background to the use of correlation and convolution in optics. The chapter starts with an important optical principle that involves convolution viz, Image Formation. It then reviews the different techniques and applications used in coherent light. These include coherent spatial filtering, holographic and non holographic correlation techniques. The other sections of the chapter review the techniques and applications in non-coherent light.

Research was carried out on three main subjects. Chapter 3 describes the coding and the decoding of objects. Chapter 4 discusses the correlation of Fourier Images and Chapter 5 applies the idea of blocking filters, used in coherent systems, to spectra produced noncoherently by convolution.

The idea of coded sources started when Barrett thought of solving

the problem of power efficiency in X-ray imaging by constructing an anticathode in the form of a zone-plate. This would form a coded blur spot from each point in the person being X-ray photographed and a sharp picture could be subsequently recovered in coherent light. In chapter 3 a random-dots plate is presented as a new code for X-ray tube anticathodes. This was initially suggested by Dicke as a coded aperture in X-ray astronomy. The random-dots plate was, however, used in this work as a coded source.

Investigations on the effect of the number and sizes of the dots are reported. Coherent and non-coherent methods of decoding were employed. In the coherent method a Fourier transform hologram was used as a complex filter and the coded pictures were decoded by coherent spatial filtering. A novel technique of recording the hologram outside the transform lens focus is described. The non-coherent method is based on a new idea of reversing the rays involved in the process of coding.

Objects are classified into two distinctive types, continuous-tone and dilute. The effects of the decoding on dilute and continuous-tone objects are thoroughly investigated. In both decoding methods a new technique of increasing the signal to noise ratio by an appropriate control of the exposure time was used. The main conclusions of the experiments in this chapter are (1) The dilute object gets decoded better than the continuous-tone object (2) The equal dots code decodes the coded photographs better than the nonequal dots code (3) Increasing the number of dots in the code produces better results with the dilute object and worse with the continuous-tone object (4) The coherent light decodes the coded photographs better than the

non-coherent light. The basic reason lies in the fact that in any coding-decoding situation a point in the object appears as a peak in the image surrounded by a shoulder region. The effectiveness of the process depends on (a) the height of the peak/the height of the shoulder, (b) the area under the peak/area under the shoulder and (c) the percentage of the original object representing luminous or transparent points. If the percentage is small(dilute object) the effect of overlap from nearby shoulders is also small, and factor (a) is dominant. In the case of continuous tone objects the factor (b) is dominant.

It is, however, not necessary to use a random-dots or a zone-plate as a code. Any object that has an autocorrelation function close to a delta function can be used, like the spoke plate code suggested in chapter 2.

A review of the previous work carried out on Fourier images is outlined in chapter 4. A confusion is shown to exist between Fourier images derived from related repeated objects. Theories of formation of Fourier images are discussed. Fourier images derived from the same object are found to be equivalent to each other. In other words they all have the same spatial frequencies and therefore any one of them generates the others. Their Fourier transforms have been found to have the same amplitude but different phase. Coherent and noncoherent correlation experiments on Fourier images are reported. The type of results obtained from the coherent experiments is different from that in the noncoherent experiment. The results in both cases, however, confirm the idea of confusion mentioned above.

Different techniques for improving the matched filters used in the coherent experiment were tried. The best one was found to be bleaching the hologram with the reversal bleach process and centring it over the transform lens focus with the aid of a microscope. Different techniques were also tried in order to get good and uniformly exposed correlograms in the non-coherent experiment. The best technique was found to be by Dodging.

An attempt at reconstructing the Fourier images with the computer was carried out. The main order Fourier image reconstructs well. Suborders failed to reconstruct. This is attributed to the conversion of the amplitude contrast object to a phase contrast image.

Chapter 5 deals with a device for producing the Fourier transform non-coherently by convolution. An account for an experiment that uses a new method of non-coherent spatial filtering with blocking filters is present.

CHAPTER 1

INTRODUCTION TO CORRELATION AND CONVOLUTION

1.1. Fourier Series

Fourier analysis has played an important role in the development of communication theory and information processing. The concept of spatial frequencies has made it possible to apply Fourier techniques, used in the communication theory, to optics. This led to a vast development in processing the information by optical means.

In Modern optics it is possible to regard any plane object as composed of a set of spatial frequencies. That is, it may be built up by superimposing a set of gratings of different spacings, orientations and contrasts. This consideration makes the Fourier theory form the basis of optical data processing.

J.B.J.Fourier (1768 - 1830) realized that any periodic function can be represented as the sum of sinusoidal functions which have periods which are integral submultiples of the period of the original function. Full treatment of this early work is dealt with by Carslow (1).

The function f(x) is defined as a periodic function if it

is well defined, bounded, has only a finite number of maxima and minima and has only a finite number of discontinuities in the interval $-\frac{T}{2} < x < \frac{T}{2}$. These conditions are called Dirichlets conditions. The periodicity condition is $f(x) = f(x + nT)$ where n is an integer and T is the period.

According to Fourier's Theorem the series representing the periodic function f(x) is written as :

$$f(x) = \frac{C_o}{2} + \sum_{n=1}^{\infty} C_n \cos\left(\frac{2\pi nx}{T} + \phi_n\right)$$

and is called a Fourier Series. Each term in the series has an amplitude C_n and a phase angle ϕ_n. The phase angle provides the freedom necessary for relative displacements of the terms of the series along the x - axis. The determination of these quantities for each term of the series is called Fourier analysis. C_o is the average algebraic height under the curve f(x) in the interval $-\frac{T}{2} < x < \frac{T}{2}$. In optical data processing C_o corresponds to the total light flux transmitted through the data when in the form of a two dimensional transmission function contained on a photographic transparency.

Sometimes it is more convenient to write the series in the form :

$$f(x) = \frac{A_o}{2} + \sum_{n=1}^{\infty} A_n \operatorname{Cos} \frac{2\pi nx}{T} + \sum_{n=1}^{\infty} B_n \operatorname{Sin} \frac{2\pi nx}{T}$$

where $A_n = C_n \text{ Cos } \phi_n$ and $B_n = - C_n \text{ Sin}\phi_n$.

In Fourier analysis the pairs A_n and B_n have to be evaluated for each value of n.

For finding out the coefficients A_o, A_n and B_n the above series has to be integrated, multiplied by Cos $\frac{2\pi nx}{T}$ and integrated and multiplied by sin $\frac{2\pi nx}{T}$ and integrated respectively. By doing this we get:

$$A_o = \frac{1}{T} \int_{-\frac{T}{2}}^{+\frac{T}{2}} f(x) \quad dx$$

$$A_n = \frac{1}{T} \int_{-\frac{T}{2}}^{+\frac{T}{2}} f(x) \cos \frac{2\pi nx}{T} \quad dx$$

$$B_n = \frac{1}{T} \int_{-\frac{T}{2}}^{+\frac{T}{2}} f(x) \sin \frac{2\pi nx}{T} \quad dx$$

Using complex notations the Fourier series is expressed by

$$f(x) = \sum_{n=-\infty}^{\infty} D_n \; e^{\frac{2\pi inx}{T}}$$

Allowing the summation to extend over negative values of n as well as over positive values, makes it possible to express any periodic function real or imaginary by such a series.

For finding out the coefficient D_n multiply by $e^{\frac{-2\pi inx}{T}}$

and integrate over the interval $-\frac{T}{2}$ to $\frac{T}{2}$ to get

$$D_n = \frac{1}{T} \int_{-\frac{T}{2}}^{\frac{T}{2}} f(x) \quad e^{\frac{-2i\pi nx}{T}} \quad dx$$

D_n and $f(x)$ are called the Fourier transform pair for periodic functions as it will be shown in the following sections.

It is worthwhile mentioning the relation between D_n and C_n, viz:

$$D_n = \frac{1}{2} \quad C_n \quad e^{i\phi_n}$$

1.2. Even and Odd Functions

A function is defined as odd if $f(x) = -f(-x)$ and even if $f(x)=f(-x)$

The Fourier coefficient for a periodic even function $f(x)$ is

$$D_n = \frac{1}{T} \int_{-\frac{T}{2}}^{\frac{T}{2}} f(x) \quad e^{\frac{-2\pi inx}{T}} \quad dx$$

By replacing x by $-x'$ we get

$$D_n = -\frac{1}{T} \int_{-\frac{T}{2}}^{\frac{T}{2}} f(-x') \quad e^{\frac{2\pi inx'}{T}} \quad dx'$$

$$= \frac{1}{T} \int_{-\frac{T}{2}}^{\frac{T}{2}} f(x') \quad e^{\frac{2\pi inx'}{T}} \quad dx'$$

$$= D_n^*$$

Any function D_n for which $D_n = D_n^*$ must be completely real; hence the coefficients for an even function are purely real.

Similarly an odd function leads to the result $D_n = -D_n^*$ which shows that the coefficients for an odd function are purely imaginary.

1.3 Fourier Transforms.

Most functions used in optics are nonperiodic functions. A nonperiodic function is the one that varies arbitrarily within infinite limits. The generalization of Fourier theory for the inclusion of arbitrary phenomena is possible only with the aid of theory in statistics and probability (2).

There is a certain class of aperiodic functions known as transient functions. These are found to be more relevant with optical data processing. A transient function is one that varies randomly within finite interval but whose value is zero outside that interval.

Consider a wave of period T in which each unit is made of a nonperiodic function. This wave is represented by a Fourier series whose fundamental frequency is the frequency of the wave. When the period T increases without increasing the nonperiodic function's interval, the overall shape of the Fourier spectrum remains the same but the spacings between its spikes decrease.

As the period T is extended to infinity a true transient function is approached. The frequency spectrum, containing both phase and amplitude, becomes continuous and is called the Fourier transform(3). This is illustrated in Figure 1.1.

The Fourier transform is represented mathematically by an integral which replaces the summation of the Fourier series. The discrete harmonic term $\frac{2\pi n}{T}$ is replaced by variable frequency term $2\pi u$ and the coefficient D_n is replaced by the Complex frequency function F(u) multiplied by the frequency increment du. This produces the Fourier transform pair :

$$f(x) = \int_{-\infty}^{\infty} F(u) \quad e^{2\pi i u x} \quad du$$

$$F(u) = \int_{-\infty}^{\infty} f(x) \quad e^{-2\pi i u x} \quad dx$$

These are more often used in optics in the two dimensional form :

$$f(x,y) = \int_{-\infty}^{\infty}\int_{-\infty}^{\infty} F(u,v) \quad e^{2\pi i (ux + vy)} \quad du \quad dv$$

$$F(u,v) = \int_{-\infty}^{\infty}\int_{-\infty}^{\infty} f(x,y) \quad e^{-2\pi i (ux + vy)} \quad dx \quad dy$$

A common notation for the Fourier transformation operation is

$$f(x,y) \quad \overset{\rightarrow}{\leftarrow} \quad F(u,v)$$

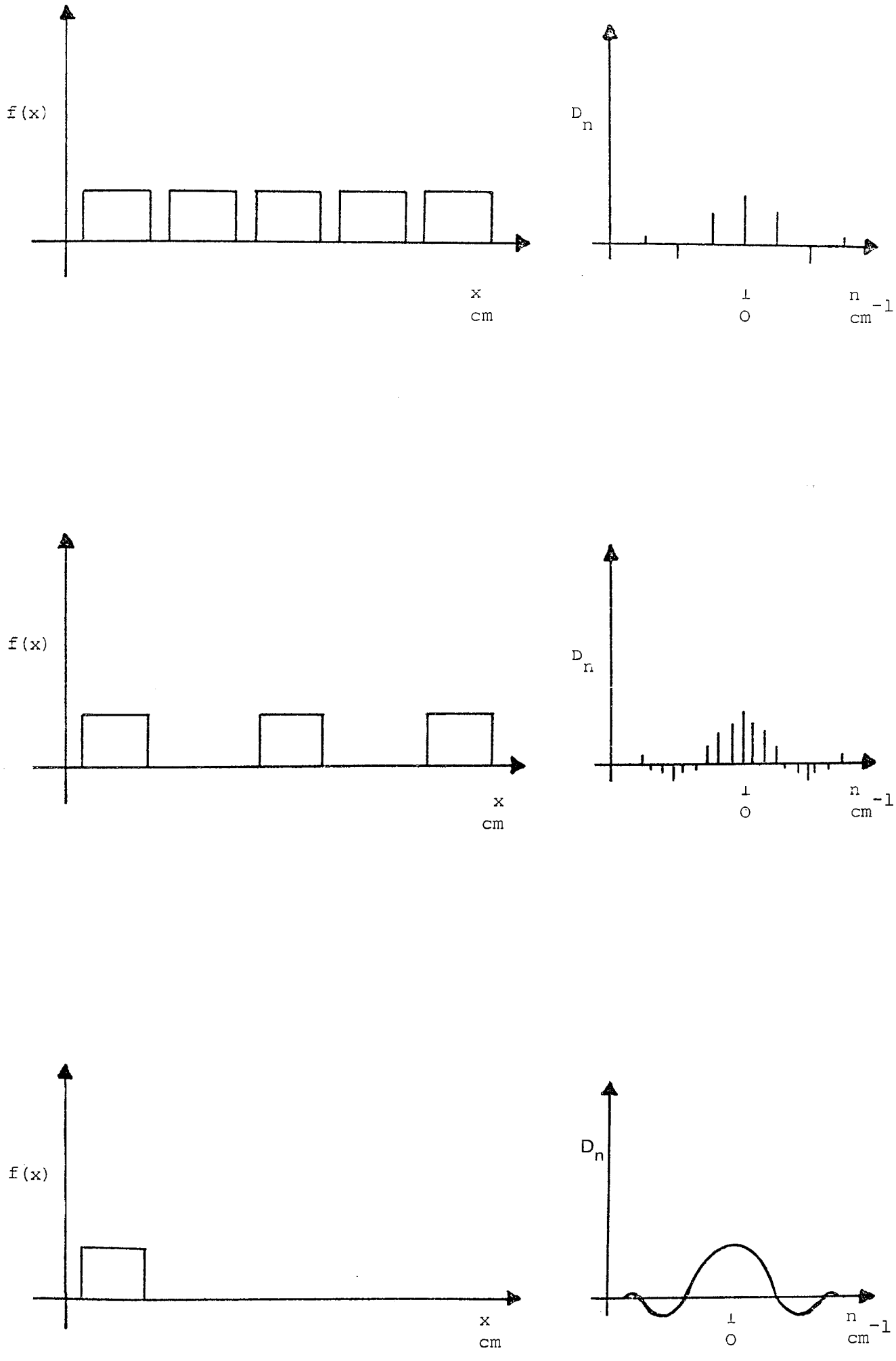

Figure 1.1 The progression from Fourier series to Fourier transform

where the forward arrow indicates the Fourier transformation and the backward arrow indicates the inverse transformation.

It should be noted in the previous equations that the only difference between direct and inverse transforms is a reversal of co-ordinates.That is, the exponent of the direct transform is written as $e^{2\pi(ux + vy)}$ and that of the inverse transform is written as $e^{-2\pi(ux + vy)}$. For this reason some books do not distinguish between the two.

If $f(x,y)$ and $F(u,v)$ are complex functions then the Fourier transformation will be :

$$f^*(x,y) \underset{\leftarrow}{\rightarrow} F^*(-u,-v)$$

1.4. Transform Theorems

Three fundamental relations, that have uses in optical data processing and wavefront reconstruction are mentioned in this section; these are :

1.4.1 Linearity Theorem

This theorem states that the transform of a sum of two functions is the sum of the transforms of these functions. This can be expressed as

$$af(x,y) + bg(x,y) \overset{\rightarrow}{\leftarrow} a F(u,v) + bG(u,v)$$

1.4.2 Similarity Theorem

A scale change in the space domain causes an inverse change in the frequency domsin, plus a change in the overall amplitude of the spectrum. This can be represented by this equation:

$$f(ax,by) \rightleftarrows \frac{1}{|ab|} F\left(\frac{u}{a}, \frac{v}{b}\right)$$

1.4.3 Shift Theorem

This theorem tells us that a translation in the position of a function in one domain results in a phase shift in the other domain. This can be written as

$$f(x-x_o, y-y_o) \rightleftarrows F(u,v)\, e^{-2\pi i(x_o u + y_c v)}$$

1.5. Transformation of a real function

In optical data processing the input data is usually real. Furthermore, complex input data can be used in coherent systems only. Real functions can be transformed into either sine or cosine transform or both while complex functions can only have the usual exponential form of Fourier transform. If f(x) is a real function then by Fourier transformation :

$$f(x) = \int_{-\infty}^{\infty} e^{2\pi iux} F(u)\, du$$

$$= \int_{-\infty}^{\infty} e^{2\pi iux} \left(\int_{-\infty}^{\infty} f(x')\, e^{-2\pi iux'} dx' \right) du$$

$$= \int_{-\infty}^{\infty}\int_{-\infty}^{\infty} f(x') \quad e^{2\pi i u(x-x')} \quad dx' \quad du$$

Since f(x') is real then by neglecting the sine term in the expansion of the exponential we get :

$$f(x) = \int_{-\infty}^{\infty}\int_{-\infty}^{\infty} f(x') \cos \left\{ 2\pi u(x-x') \right\} dx' \quad du$$

$$= 2\int_{0}^{\infty} \cos 2\pi ux \left\{ \int_{\infty}^{\infty} \cos 2\pi ux' \, f(x')dx' \right\} du$$

$$+ 2 \int_{0}^{\infty} \sin 2\pi ux \left\{ \int_{-\infty}^{\infty} \sin 2\pi ux' f(x')dx' \right\} du$$

$\int_{-\infty}^{\infty} \cos 2\pi ux' f(x') \, dx'$ is called the cosine transform and is denoted by $F_c(u)$.

$\int_{-\infty}^{\infty} \sin 2\pi ux' f(x') \, dx'$ is called the sine transform and is denoted by $F_s(u)$.

The previous equation can be written in terms of $F_s(u)$ and $F_c(u)$ as :

$$f(x) = 2\int_{0}^{\infty} \cos 2\pi ux \, F_c(u)du + 2\int_{0}^{\infty} \sin 2\pi ux \, F_s(u) \quad du$$

If f(x) is real and even then the cosine transform is the Fourier transform, and if it is real and odd then the sine transform is the Fourier transform.

1.6 Convolution

The convolution process is the one which one function is

reversed and slid along second function. The area of the product of the functions as function of the displacement is the convolution.

Mathematically the convolution is defined by :

$$g(s) = \int_{-\infty}^{\infty} f_1(x)\, f_2(s - x)\, dx$$

For simplicity it is frequently convenient to write the convolution in the form :

$$g(s) = f_1(s) \otimes f_2(s)$$

Convolution involves evaluating the integral for all the values of s in the range $-\infty<s<\infty$. In practice nonperiodic functions are sampled between finite limits and s will accordingly take finite limits. In the optical case, input functions are of the transient type and s is governed by the limits of the transcience.

1.6.1 Convolution Properties

The operation of convolution has many of the same properties of multiplication. Convolution is commutative

$$f_1 \otimes f_2 = f_2 \otimes f_1$$

associative

$$f \otimes (f_2 \otimes f_3) = (f_1 \otimes f_2) \otimes f_3$$

and distributive

$$f_1 \otimes (f_2 + f_3) = f_1 \otimes f_2 + f_1 \otimes f_3$$

These properties have many useful applications in optics since they make it more easy to manipulate relations involving convolutions.

1.6.2. Convolution Theorem

One of the main points of interest in convolution is that the transform of a product of functions results in the convolution of their transforms.

If $F_1(u)$ and $F_2(u)$ are the Fourier transforms of $f_1(x)$ and $f_2(x)$ respectively then by using the shift theorem, we get

$$f_2(s - x) = \int_{-\infty}^{\infty} F_2(u)\, e^{2\pi i u(s-x)}\, du$$

By substituting this equation into the convolution integral we get :

$$g(s) = \int_{-\infty}^{\infty} f_1(x) \left[\int_{-\infty}^{\infty} F_2(u)\, e^{2\pi i u(s-x)}\, du \right] dx$$

Reversing the order of integration:

$$g(s) = \int_{-\infty}^{\infty} F_2(u)\, e^{2\pi i u s} \left[\int_{-\infty}^{\infty} f_1(x)\, e^{-2\pi i u x}\, dx \right] du$$

now $$\int_{-\infty}^{\infty} f_1(x)\, e^{-2\pi i u x} = F_1(u)$$

The convolution integral becomes :

$$g(s) = \int_{-\infty}^{\infty} F_1(u)\, F_2(u)\, e^{2\pi i u s}\, du$$

This equation shows that "the Fourier transform of the product of two functions is the convolution of their Fourier transforms" which is the statement of the first form of the convolution theorem.

Writing the above equation using the inverse Fourier transform, gets :

$$F_1(u)\, F_2(u) = \int_{-\infty}^{\infty} g(s)\, e^{-2\pi i u s}\, ds$$

This tells us that "the Fourier transform of the convolution of two functions is the product of their Fourier transforms", which is the statement of the second form of the convolution theorem.

In general the convolution theorem is denoted by

$$f_1(x) \otimes f_2(x) \rightleftarrows F_1(u)\, F_2(u)$$

The convolution theorem is often more convenient to be used in applied optics since the absence of complex conjugates can assist analysis or interpretation of transforms. The special case of convolution when $f_1 = f_2$ is called autoconvolution.

1.7 Correlation

Correlation, in general, is the same as convolution except that there is no reversal of the sliding function. The correlation of f_1 with f_2 is defined by

$$h(s) = \int_{-\infty}^{\infty} f_1^*(x)\, f_2(s+x)\, dx$$

This, customarily, is denoted by

$$h(s) = f_1^*(s) * f_2(s)$$

$f^*(s)$ is the complex conjugate of f(s). When f(s) is real, $f^*(s) = f(s)$. The correlation integral can be written alternatively as

$$h(s) = \int_{-\infty}^{\infty} f_1^*(x-s)\, f_2(x)\, dx$$

This form is derived from the first one by substituting the variables. If $f_1(s) = f_2(s)$, the term autocorrelation is applicable. When $f_1(s) \neq f_2(s)$, the term crosscorrelation is applied.

1.7.1. Correlation properties

Correlation is similar to convolution from the point that they are both distributive and associative, but it differs from it in that it is not commutative

If $h(s) = f_1(s) * f_2(s)$

then $h(-s) = f_2(s) * f_1(s)$

Correlation becomes the same as convolution, when either function is even.

Crosscorrelation often results in a peaked distribution. This is especially true when one function is identical with part of the other. This property has applications in pattern recognition where the peak indicates the presence of the pattern to be recognized. In some pattern recognition systems the peak indicates the position as well as the presence of the wanted pattern.

Autocorrelation of random functions results in a delta function. This is used to decode previously coded pictures as will be described in Chapter 3.

1.7.2 Correlation Theorem

Consider the product $F_1(u)\ F_2(u)$. According to the convolution theorem the transform of the product of two functions is the convolution of their transforms, therefore:

$$F_1(u)\ F_2^*(u) \rightarrow f_1(x) \otimes f_2^*(-x)$$

The convolution is reversing an already reversed function. This results in no reversal of the sliding function and the convolution becomes correlation. Hence the above equation becomes

$$F_1(u)\ F_2^*(u) \rightarrow f_1(x) * f_2^*(x)$$

which is the correlation theorem formula.

(a) The Crosscorrelation Theorem

The cross correlation theorem says that the transform of the crosscorrelation of two functions is the product of their transforms. This is denoted by

$$f_1(x) * f_2^*(x) \rightleftarrows F_1(u)\, F_2^*(u)$$

(b) The autocorrelation Theorem

The autocorrelation theorem says that the transform of the autocorrelation of a function is the squared modulus of the transform of that function. This may be written as

$$f(x) * f^*(x) \rightleftarrows |F(u)|^2$$

This is derived from the crosscorrelation theorem by putting $f_1(x) = f_2(x) = f(x)$, and by using the mathematical theorem that $F(u)\, F^*(u) = |F(u)|^2$.

If x is replaced by t then the autocorrelation function will be called self coherence function and the squared modules of the Fourier transform of the function f(t) will be called power spectrum. The fact that the power spectrum is the Fourier transform of the self coherence function is known as the Wiener-Khinchin theorem.

1.7.3 Parseval's Theorem

This theorem is generally interpretable as a statement of conservation of energy. It is derived from the correlation

theorem by putting s = o. It's general form is

$$\int_{-\infty}^{\infty} f_1^*(x)\, f_2(x)dx = \int_{-\infty}^{\infty} F_1^*(u)\, F_2(u)\, du$$

In optics it is quite often quoted in the form

$$\int_{-\infty}^{\infty}\int_{-\infty}^{\infty} |f(x,y)|^2\, dx\, dy = \int_{-\infty}^{\infty}\int_{-\infty}^{\infty} |F(u,v)|^2\, du\, dv$$

1.8 Dirac Delta Function

The two-dimensional Dirac delta function $\delta(x-a, y-b)$, widely used in optical correlation technique, is a function which has infinite amplitude, zero width and unit area. The delta function can be represented as the limit, as $h \to \infty$, of a rectangular pulse of width $1/h$ and height h.

The following are the more important properties of the delta function

1. $$\delta(x,y) = \begin{cases} \infty & x = y = o \\ o & \text{otherwise} \end{cases}$$

2. $$\int_{-\varepsilon}^{\varepsilon}\int \delta(x,y)\, dx\, dy = 1 \qquad \text{any } \varepsilon > o$$

3. $$\delta(ax,by) = \frac{1}{|ab|}\, \delta(x,y)$$

4. $$\int_{-\infty}^{\infty}\int \delta(x \pm a,\ y \pm b)\ g(x,y)\, dx\, dy = g(\pm a, \pm b)$$

The last property is called the sifting property of the delta function.

The Fourier transform of $\delta(x-a, y-b)$ can be obtained by substituting $e^{-2\pi i(ux+vy)}$ for $g(x)$ in the sifting property formula.

Therefore

$$\delta(x-a,y-b) \rightleftarrows e^{-2\pi i(ua + vb)}$$

This equation shows that the amplitude spectrum of the delta function is a continuous spatial frequency function of Unit height, which extends over the whole spatial frequency domain. The phase spectrum on the other hand changes steadily with changing the value of (a,b).

The delta function is used in optics to represent a point source of light, or a spatial pulse of unit area.

References

1. Carslow H.S. "Introduction to the Theory of Fourier's Series and Integrals" McMillan 1921
2. Lee Y.W. "Statistical Theory of Communication" Wiley 1964
3. Barber, N.F. "Experimental Correlograms and Fourier Transforms" Pergamon Press 1961
4. Jennison R.C. "Fourier Transforms and Convolutions for the Experimentalist" Pergamon Press 1961

CHAPTER 2

TECHNIQUES AND APPLICATIONS OF CORRELATION AND CONVOLUTION

2.1. Image Formation

2.1.1. Coherent Light

Image formation in coherent imaging systems is based on the convolution of the amplitude point spread function (amplitude impulse response) with the object. This is represented by the equation

$$Q_i(x,y) = h(x,y) \otimes Q_o(x',y')$$

where $Q_i(x,y)$ is the image complex amplitude, $Q_o(x',y')$ is the object complex amplitude and $h(x,y)$ is the amplitude point spread function of the coherent system.

Defining the Fourier transform of these three quantities as

$$q_i(s,t) \overset{\mathcal{F}}{\rightleftarrows} Q_i(x,y)$$

$$q_o(s,t) \overset{\mathcal{F}}{\rightleftarrows} Q_o(x,y)$$

$$H(s,t) \overset{\mathcal{F}}{\rightleftarrows} h(x,y)$$

Then by applying the convolution theorem of 1.6.2 to

the convolution equation above, we get

$$q_i(s,t) = H(s,t)\, q_o(s,t)$$

This equation represents the process of image formation in the Fourier space. H(s,t) is called the coherent transfer function. It is a measure of the Imaging efficiency of the coherent system.

While H(s,t) was defined as being the transform of the coherent point spread function, the latter is itself defined as the Fourier Transform of the pupil function. This tells us that the pupil function and the coherent transfer function are equivalent. Therefore, for diffraction limited coherent systems, where the pupil function is equal to unity inside the pupil and zero outside it, the coherent transfer function has the same values of unity and zero.

2.1.2. Noncoherent light

The imaging process in the noncoherently illuminated imaging systems follows the following equation

$$G_i(x,y) = k(x,y) \otimes G_o(x',y')$$

where $G_i(x,y)$ is the image intensity distribution, $G_o(x',y')$ is the object intensity distribution and k (x,y) is the intensity point spread function of the system.

In order to write the equation of image formation in the Fourier space, let us define the Fourier transform of the above three quantitites

$$g_i(s,t) \overset{\mathcal{F}}{\rightleftarrows} G_i(x,y)$$
$$g_o(s,t) \overset{\mathcal{F}}{\rightleftarrows} G_o(x,y)$$
$$K(s,t) \overset{\mathcal{F}}{\rightleftarrows} k(x,y)$$

By applying the convolution theorem of 1.6.2 to the convolution equation above, we get

$$g_i(s,t) = K(s,t)\, g_o(s,t)$$

which is the Fourier space relation.

K(s,t) is called the optical transfer function (abbreviated OTF) of the systems. Its modulus $|K(s,t)|$ is called the modulation transfer function. As with the coherent transfer function, the O.T.F. is a measure of the efficiency of the imaging system.

Bearing in mind that k(x,y) is related to h(x,y) by the following equation

$$k(x,y) = |h(x,y)|^2 \quad ,$$

it can be seen that K(s,t) is the Fourier transform of $|h(x,y)|^2$. But the Fourier transform of $|h(x,y)|^2$, by the autocorrelation theorem of 1.7.2, is the correlation of the

coherent transfer function H(s,t) with its complex conjugate. Therefore K(s,t) is equivalent to the correlation of H(s,t) with its complex conjugate. It follows from this, after taking into account that H(s,t) is equivalent to the pupil function, that the OTF K(s,t) is represented by the area of overlap of two correlating pupil functions.

2.1.3. Examples of Imaging systems

(1) Converging lens

The point spread function of a nonaberrated converging lens is approximately a delta function. Therefore by convolving the object function with the delta function, one can get an exact representation of the object in the image plane.

If the lens is aberrated, however then the image will be modified according to the aberration function.

(2) Diffraction limited pinhole

The point spread function of a diffraction limited pinhole is approximately a delta-function. Therefore, similar to the non-aberrated lens, it produces in the image plane an exact representation of the object.

(3) Coded Aperture

If a plurality of pinholes of certain distribution

is used in forming the image then their impulse response is the convolution of the impulse response of a single pinhole with the pinholes distribution. But the impulse response of a single pinhole is a delta function, therefore the equation of image formation becomes

$$G_i(x,y) = \delta(x,y) \otimes S(x,y) \otimes G_o(x',y')$$

where $S(x,y)$ represents the pinholes distribution function

The correlation of any function with a delta function results the function, therefore

$$G_i(x,y) = S(x,y) \otimes G_o(x', y')$$

This equation can be extended to any continous-tone or dilute transparency (the definitions of these are found in 3.3) where $S(x,y)$ represents the transparency function. $G_i(x,y)$ in this case, is called the coded image and $S(x,y)$ is called the code or the coded aperture.

2.2. Coherent spatial filtering

Spatial filtering in coherent light is usually done by manipulating the Fourier Transform of the input data. The manipulation is done by inserting a spatial filter at the back focal plane of the Fourier transform lens. This multiplies the Fourier transform of the input function with the filter function. A second Fourier transform lens transforms the multiplication to a convolution which is the filtered

information. The general layout of a coherent spatial filtering apparatus is shown in Figure 2.1.

Spatial filters can be classified into the following types :

2.2.1. Blocking filters

These filters are usually opaque masks with a certain aperture (or apertures) that omit the unwanted frequencies of the spectrum. They are simple to make and to use but have the disadvantage that because of their sharp cutoff they produce at the image plane, i.e. at the second transformation plane, a diffraction pattern which is the Fourier transform of the sharp edge of the mask's aperture. This phenomenon is called ringing because of its similarity to the ringing produced in electrical circuits due to a sharp cutoff filter. A method for reducing the ringing effect is described in Chapter 5.

2.2.2. Amplitude filters

These filters operate on the amplitude, but not the phase, of the transform. They are usually produced by recording the wanted amplitude - distribution on a film or by controlled evaporation of metal on a glass substrate.

2.2.3. Phase filters

Here only the phase is operated upon but not the amplitude. The filters are often produced by using an evaporated layer of material such as magnesium fluoride or by bleaching amplitude filters that are recorded on photographic films.

2.2.4 Complex filters

This is the general type of filters, in which both the amplitude and the phase of the Fourier transform are operated

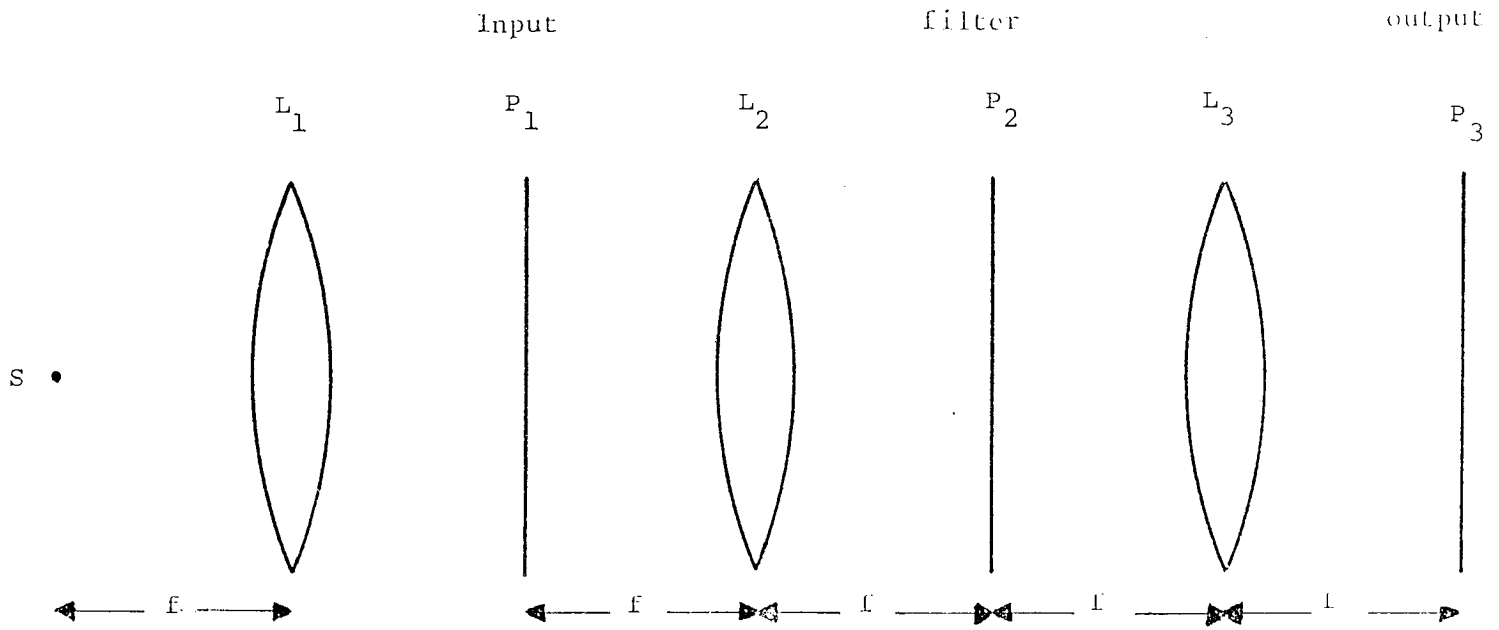

Figure 2.1 The general layout of a coherent spatial filtering apparatus

upon. Originally, the amplitude and the phase portions were made separately by the methods described above. Today the filters are produced by holography or by computer generation. Both forms of construction utilise the same basic principle to record the continuously varying phase function. By analogy with communication techniques, the function to be recorded is stored on a spatial carrier frequency, which consists of an array of fine lines drawn on a transparent substrate. The amplitude part of the filter function is recorded as a variation in contrast of the lines, whilst the phase is stored as a variation in position of the lines.

The holographically made filter is prepared on photographic film or plate of very high resolution, by making a direct recording of the interference pattern formed between the transform of the required signal and a reference wave.

The computer generated filter is prepared by computing the form of the Fourier transform with the computer. Photoreduction then yields the required filter. To avoid having to print a continuously varying grey scale, corresponding to the amplitude variations in the transform, the transform is printed as an array of small dots in much the same way as in halftones are in the printing industry.

By altering the position of the regularly spaced dots in

the transform, changes in phase can be simulated on the computer generated hologram.

2.3 Correlation and convolution with matched filters

In Figure 2.1, a matched filter is recorded using a uniform plane reference wave propagating at an angle θ with respect to the optical axis of the lenses. The total distribution in the transform plane P_2 is

$$H\left(\frac{x_2}{\lambda f}, \frac{y_2}{\lambda f}\right) + A_o \, e^{i\alpha x_2}$$

where $H\left(\frac{x_2}{\lambda f}, \frac{y_2}{\lambda f}\right)$ is the spectrum of $h(x_1, y_1)$, A_o is a real constant and $\alpha = 2\pi \sin\theta/\lambda$.

The recording of the above distribution with a photographic film results in

$$A_o^2 + |H|^2 + A_o H \, e^{-i\alpha x_2} + A_o H^* \, e^{i\alpha x_2}$$

If the information to be filtered is denoted by $g(x_1, y_1)$ then the distribution just behind the filter is

$$G\left(\frac{x_2}{\lambda f}, \frac{y_2}{\lambda f}\right)\left[A_o^2 + |H|^2 + A_o H e^{-i\alpha x_2} + A_o H^* e^{i\alpha x_2}\right]$$

Lens L_3 Fourier-transforms this distribution to give

$$A_o^2\, g(x,y) + g(x,y) \otimes \left[h(x,y) * h^*(x,y) \right] +$$

$$A_o g(x,y) \otimes h(x + f \sin\theta, y) + A_o\, g(x,y) * h^*(x - f \sin\theta, y)$$

The first term gives an image of the input $g(x_1 y_1)$ on-axis and the second adds the convolution of the input with the autocorrelation of the function for which the filter was formed. The next two terms are of greater interest. The third term shows that, centred at $x = -f \sin\theta$, the convolution of $g(x,y)$ with $h(x,y)$ is produced. The last term represents the correlation of $g(x,y)$ with $h(x,y)$ centred at $x = f \sin\theta$.

If $g(x,y)$ happens to be similar to $h(x,,y)$ then the last term of the above formula will change to an autocorrelation. The autcorrelation is originated from the multiplication of H with its complex conjugate H^*. This produces a uniform plane wave that will be focussed to a spot by the lens L_3. On the other hand, the wave giving rise to the convolution is not multiplied by its conjugate and is not converted to a plane wave. Consequently it cannot produce a spot at plane p_3 but a smeared or spread-out distribution.

The spatially filtered image is often recorded at the correlation position of the out-put of the spatial filtering system. The following are some of the applications of matched

filters

2.3.1. Image restoration

Correcting aberrated images was the prime motivation for the work in optical processing carried out by Marechal and Crose (1). Images are usually blurred due to lens aberration, defocussing or camera or object's motion. In order to correct a blurred image, its Fourier transform has to be multiplied by the inverse of the Fourier transform of the blur function. This ideally gives a straight line multiplied by the Fourier transform of the original image. The second transformation then gives the original image convolved with a delta function, which is the original image.

The filter may be synthesised by computer generation or by separate preparation of the amplitude and the phase portions.

The problem that arises quite often in synthesising the filter is that the value of the filter function is required to be infinity when the Fourier transform of the blur function contains zero values, an impossible solution. Further processing can be carried out to get a flatter transfer function, but in most cases the zero frequencies are not recovered.

Tsujiuchi illustrated the technique of image deblurring in his review paper (2). Yu discussed the problems of image restoration in his book (3) and quoted some references about the subject.

2.3.2. Decoding coded photographs

Coded apertures were suggested (4) for imaging the electromagnetic waves that cannot be imaged with ordinaty lenses. Zone-plates were first used as coded apertures. These formed coded photographs that were decoded by illuminating them with a coherent light.

If, however, the source of the electromagnetic waves is needed to be coded (but not the camera's aperture) then the coded photographs may be decoded by spatial filtering. A Fourier transform hologram of the out-of-focus point spread function of the code is made. This is used as a spatial filter in a coherent spatial filtering system. The coded photograph is correlated with the code. This produces the decoded image at the correlation position of the output of the coherent system.

Randomly distributed transparent dots on opaque surround were also used as a code (5, 6, 7). Both the random-dots code and the zone-plate have an autocorrelation function equal to a delta function. The spoke plate of Figure 2.2 may also

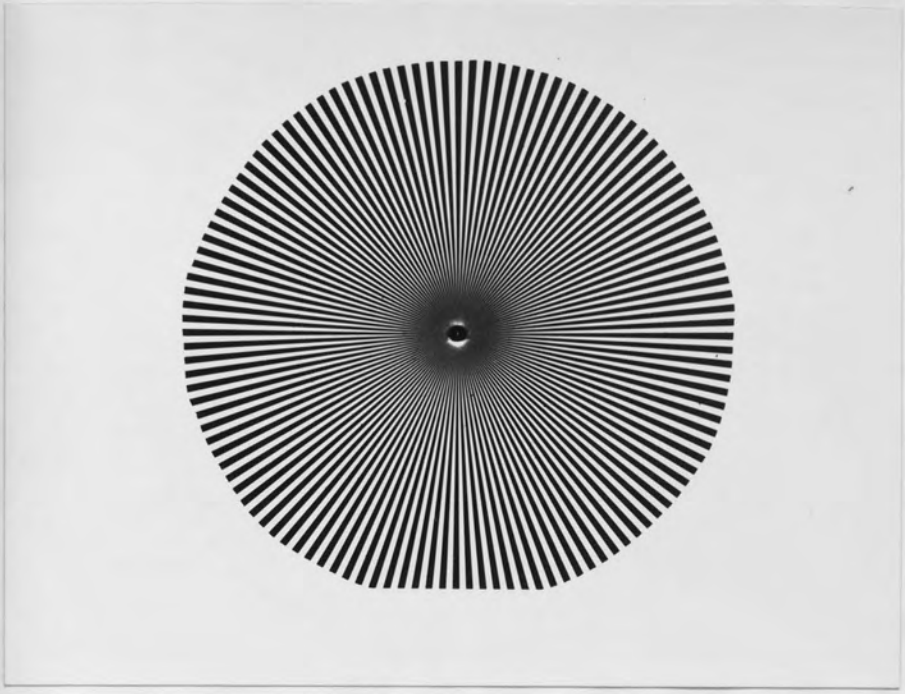

Figure 2.2 Spoke-plate code

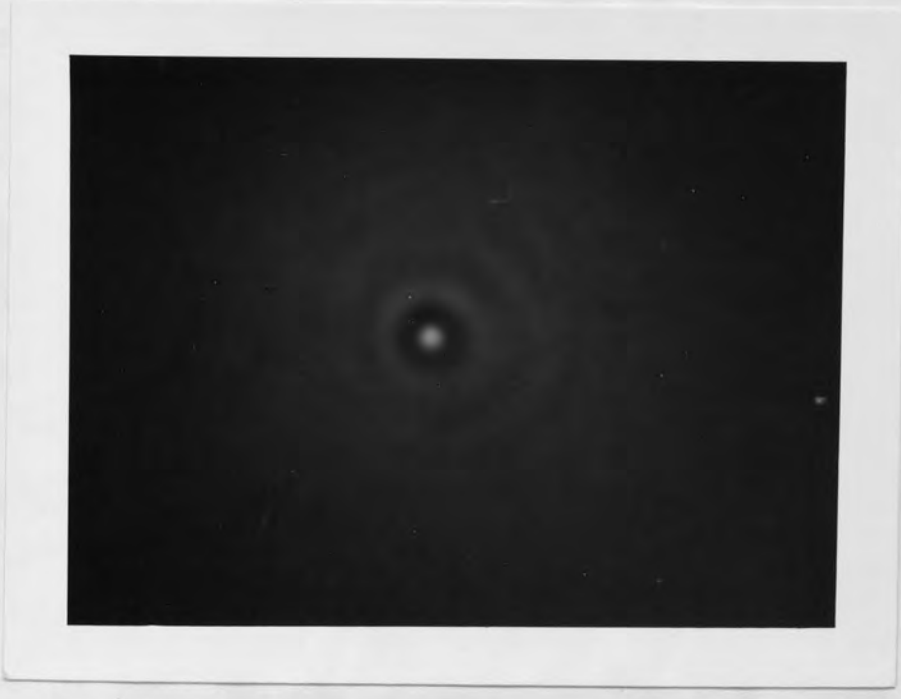

Figure 2.3 The autocorrelation pattern of the spoke plate

be used as a code since its autocorrelation function is a delta function (Figure 2.3).

The idea of coding and decoding is more fully discussed in Chapter 3 in which a coherent spatial filtering system is used to decode photographs coded with a random - dots code. 2.9 describes the methods of decoding the photographs in noncoherent light.

2.3.3. Pattern recognition

Pattern recognition in coherent light is commonly based upon the use of holographically produced matched filters. A Fourier transform hologram is usually recorded for the pattern or patterns to be recognized. The input data is then simultaneously or sequentially applied to the hologram (the matched filter). A correlation spot appears at the system's out-put whenever a pattern similar to a recorded one enters the input. In the case of filters with several recorded patterns, the position of the correlation spots indicates the pattern that exists at the input. Multiple-pattern filters are usually synthesised by recording each pattern with a different reference beam angle (8a, 9).

The earliest work on pattern recognition with a holographic spatial filtering system, was done by Vander Lugt (10). He applied his idea of holographically synthesised matched filters to

character recognition and to detection of isolated signal in random noise. Later he discussed the problem of complex spatial filtering in more detail (11, 12).

Character recognition using a similar method to that of Vander Lugt was reported by Binns, Dickinson and Watrosiewicz (13) and by Lowenthal and Belvaux (14).

A somewhat different approach to character recognition was described by Gabor (15) in which variants of letters could be identified using a single photographic plate. Keyte (16) described a character recognition system based on Gabor's method; and also discussed the problems of finger print recognition, airphotographs recognition and radar signal processing.

A main problem in pattern recognition by holography is that some cross-correlations have correlation spots with intensities comparable to those of autocorrelations. A method for discrimination enhancement is described by Cathey (17).

2.3.4. Fourier Images

Correlation and convolution with matched filters can be used for many other applications. In Chapter 4 a coherent correlation experiment is described in which Fourier images derived from different objects are correlated.

Several Fourier transform holograms were recorded. Each for a sample from one of the Fourier images. The holograms were then used as spatial filters and the samples were allowed to correlate with the rest of the images. The result of the correlation is drawn on a table. This seems to confirm the possibility of confusion in identifying images formed in coherent light (20). The Fourier images and the correlation experiment are described in more detail in Chapter 4.

2.4. Correlation using a single lensless Fresnel hologram.

In many applications of coherent optical data processing one needs to record either the Fourier transform or its interference with another (reference) wave (10). Normally, the intensity variations in these light fields are significantly larger than the dynamic range of the recording media. It was shown (18) that getting the autocorrelation using this technique was complicated by the appearance of additional (artifactual) rings that result from clipping of the power spectrum due to the limited range of the photographic film.

Bieringer(19) has shown that the effective dynamic range for optical correlation analysis can be increased by making use of holograms of diffuse objects. A Fresnel hologram is recorded for an object using a coplaner point source as reference beam. If the hologram is reconstructed using a point source at an arbitrary position in the original object

plane and a positive lens is used to record the conjugate image, then the geometric image obtained at the back focal plane of the lens is considered as the impulse response of the hologram-lens system.

Reconstruction of the hologram using, as a reference beam, a different object produces, by convolving the geometric image of this object with the geometric impulse response of the system, the desired cross-correlation (or autocorrelation, if the original object is used for the reconstruction) in the back focal plane of the lens.

2.5. Nonholographic coherent correlaters

2.5.1. Correlaters with relative motion

Many mathematical operations can be carried out using purely optical techniques (21). Multiplication can be achieved by combining together the transparencies to be multiplied and recording a contact print for their combination. Integration can be performed by simply collecting all of the light transmitted through a transparency and focussing it onto a point. A detector at that point then records the integration.

A coherent optical system performing the multiplication and the integration operations together was discussed by Curtona

et al (22). Silva and Rogers (23) described a coherent correlator working on the same principle of multiplication and integration as that of Curtona et al but the shift needed for the correlation operation is provided by scanning one transparency over the other, as shown in Figure 2.4.

Similar correlater was reported by Stroke (24). The multiplication in this correlater was performed by imaging one of the transparencies over the other. A lens then integrates the transmitted light and focuses it onto the detector.

Because of the coherent nature of the light a term of the form $e^{\frac{2\pi iux}{\lambda f}}$ appears in the correlation integral due to the Fourier transform property of the integrating lens. This term can be suppressed by minimising the area of the photodetector or by placing a suitable pinhole at the focus of the integrating lens thus making $x \to o$.

2.5.2. Spatial heterodyning

In this correlation technique, spectra of the two signals to be correlated are multiplied directly using the Fourier transforming apparatus of Figure 2.5a. The resultant record may then be retransformed to get the correlation (Figure 2.5b) (40 - 43).

This process can be used to identify spatial distributions

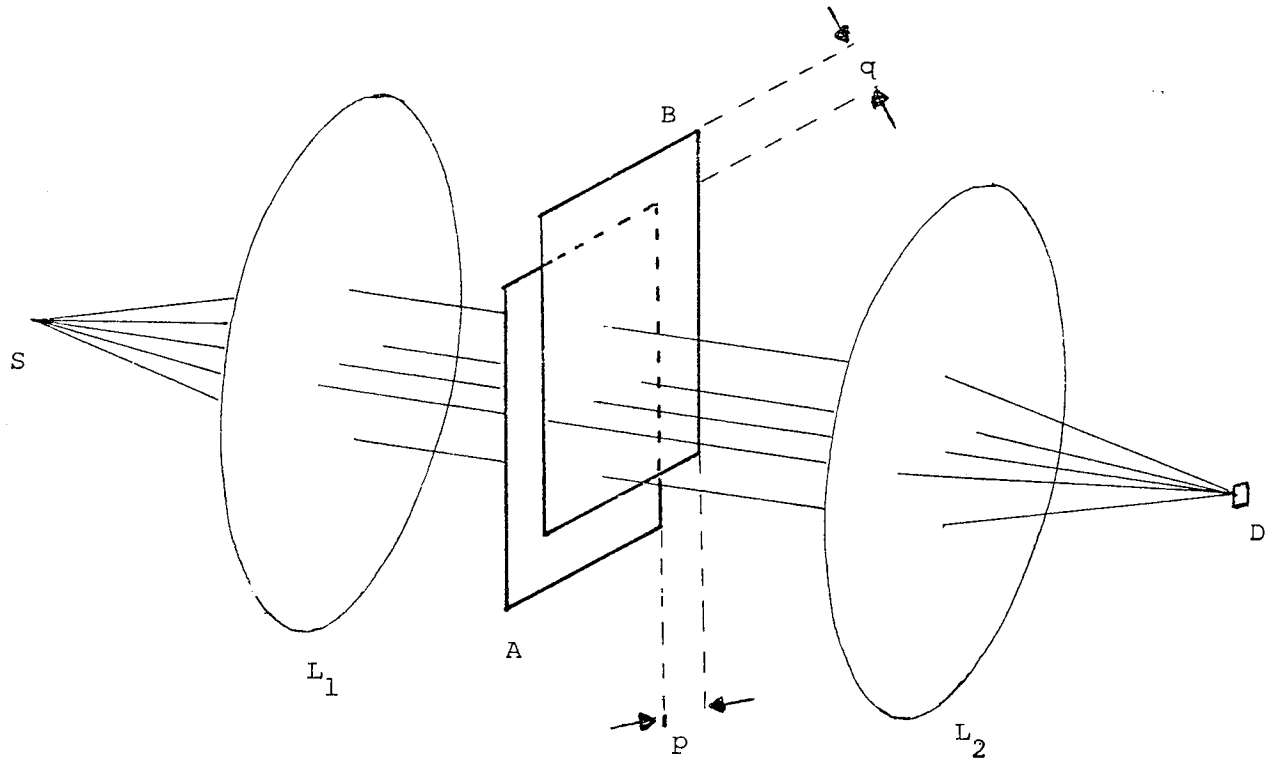

Figure 2.4 Apparatus for Correlation with relative motion. S = source; L_1 = Collimater; L_2 = Integrating lens; D = photodetector. B is scanned across A and the correlation function is obtained sequentially from the detector output

(After Silva and Rogers)

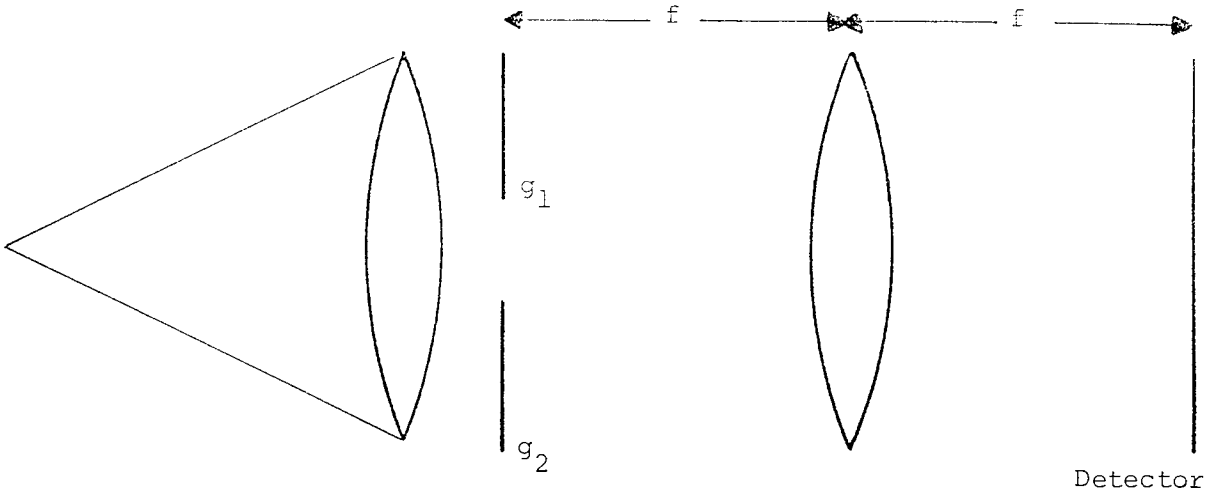

Figure 2.5(a) Heterodyning the spatial spectra

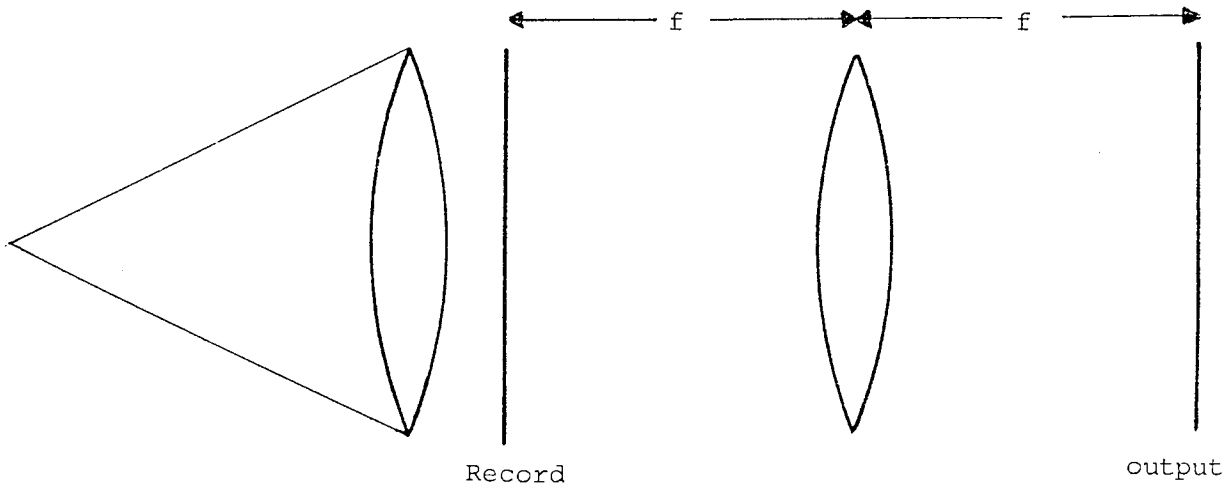

Figure 2.5 (b) Transforming the multiplied spectra

by heterodyning a reference distribution with the field of view to be searched. Its main advantage is that there is no critical positioning problem as in the spatial filtering technique.

2.6. Noncoherent correlaters

2.6.1. Advantages and limitations of noncoherent light

Using noncoherent light in correlation processes has many advantages. The most important of these advantages are redundancy (in other words the invulnerability to noise) and parallel processing (25). It has. however, the disadvantage of restriction to real positive functions. The restriction to real functions is not too serious as until now there are few transducers available in coherent optics that can modulate both amplitude and phase continously and independently. The restriction to positive functions is a very serious limitation as any function with negative values must be subject to the addition of a positive dc term throughout its range. This reduces the contrast of the input, and as processing proceeds these dc bias terms accumulate and cause very serious difficulties.

Optical modulation may be used to overcome the problem of dc bias. Examples of temporal modulation are shown References(33) and (44), and of spatial modulations in

References(6,7 and 23).

Another restriction in noncoherent systems is that a single channel cannot convey as much information as the coherent system as this leads it to depart from the laws of geometrical optics on which the noncoherent systems are designed (8b).

2.6.2. Correlation without motion

Noncoherent correlaters, in general, are based on the device suggested by Haag and others (26-28) to develop a Patterson projection. This is defined as the autocorrelation pattern of a proposed crystal structure that can be calculated easily and compared with the x-ray results.

If the system shown in Figure 2.4 is illuminated with diffuse noncoherent light it can still perform the correlation operation. The awkward and time consuming mechanical scanning, however, is not needed in this case. The two transparencies can be separated by a finite distance(Figure 3.15) and the parallax between them provides the correlation shift.

The entire correlation process is performed simultaneously and is represented as points in the focal plane of lens. A point in the correlation (x,y) plane is equivalent to a particular displacement (p,q) in the second transparency D and is related

to the separation distance d and and the focal length f by

$$\frac{\sqrt{p^2 + q^2}}{d} = \frac{\sqrt{x^2 + y^2}}{f}$$

Another advantage of this correlater is that the first pattern (the input) is not necessarily presented in the form of a transparency. Any diffusely illuminated or self illuminating object can be used. This correlater is used in Chapter 4 to correlate Fourier images derived from different objects. A full description of the experiment is reported in 4.5.

2.6.3. Autocorrelaters

If a lens is used to image the noncoherent source on the correlating transparencies then the entire optical system becomes symmetrical. A single transparency may then be used to obtain the autocorrelation. This may be done by placing a mirror at the plane of symmetry. The mirror reflects the transmitted light back through the same transparency; therefore producing autocorrelation (Figure 2.6). Optical arrangements for performing autocorrelation are described by Horwitz and Shelton (29) and Kovasznay and Arman (30).

Bromley (34) discussed a noncoherent technique for cross-correlating a one dimensional function with a library of stored signals simultaneously.

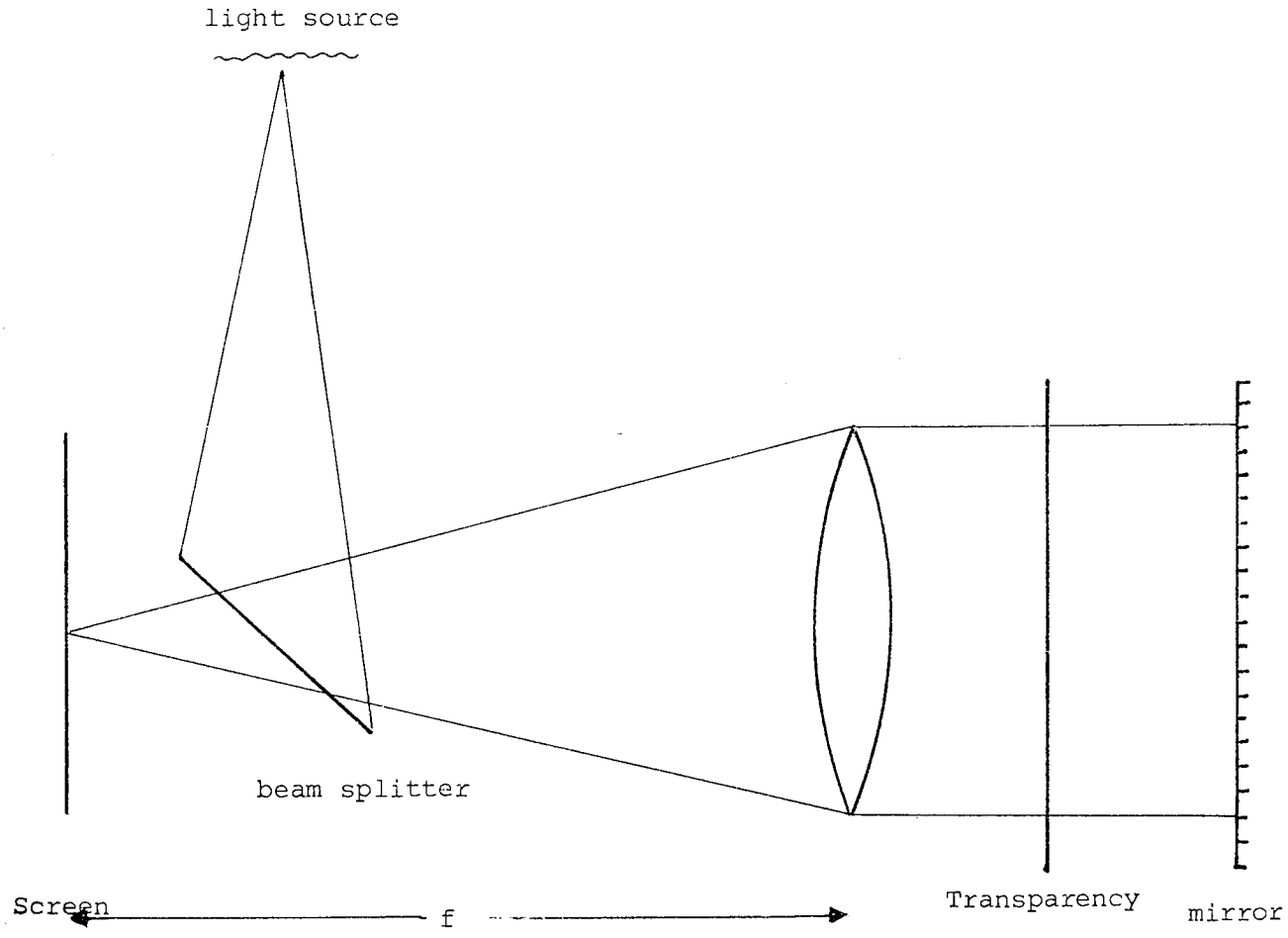

Figure 2.6 Noncoherent autocorrelater

2.6.4. Correlation with a synthesised impulse-response

It has been shown in 2.1.2 that images are formed in noncoherent light by convolving the object function with the irradiance point spread function of the optical system. If the image however is recorded at a finite distance away from the conjugate plane (Figure 2.7) then the record will represent the convolution of the object with the out of focus point spread function of the optical system. A mask may then be introduced into the system's aperture to manipulate the point spread function . This results in the convolution of the object with the mask at the out of focus plane. This principle was used by Trabka and Roetling (31) in pattern recognition. Its basic idea is similar to the idea of Haag's correlater (26) but the point of view is sufficiently different to have had a separate discussion.

2.6.5 Correlation with a spatial frequency filter

A useful variation of the correlator of Figure 3.15 is obtained by removing the lens and reducing the scale of pattern D so that the rays converge naturally on the detector plane F.

If x and t are the scales of the two correlating transparencies and p is the distance between them then the detector's location can be calculated using the theorem of similar triangles. From Figure 2.8 it can easily be shown that the detector must be placed at a distance q from the

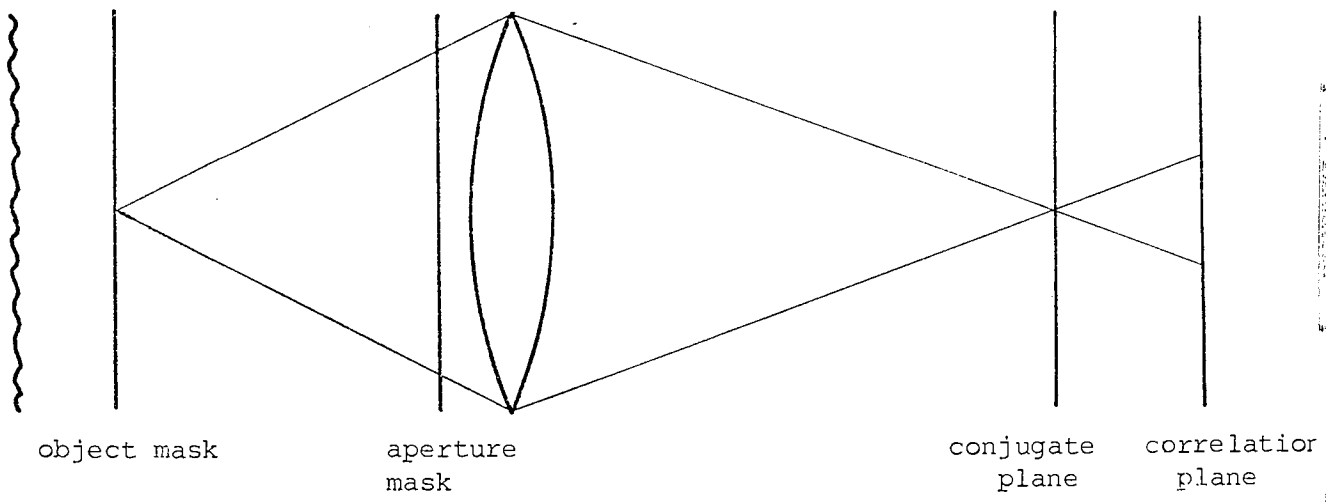

Figure 2.7 Correlation with a synthesised impulse-response

second transparency. Such correlators were used by McLachlan (32) and Leifer et al (33) in pattern recognition.

A particular case of this correlator is one which has its second transparency replaced with a linear grid having a sinisoidal variation of transmission. The new system can detect the presence of any frequency that has a certain relation with the grid's frequency. The correlation between the grid and the input transparency produces a sharp shadow on the detector plane. This shadow indicates the presence of a frequency x^{-1} in the object (the input transparency) that can be calculated using the theorem of similar triangles.

In Figure 2.8 if t is the grid's spatial period and x is the object's corresponding spatial period then it is clear from the similar triangles that

$$\frac{t}{q} = \frac{x}{p+q}$$

Therefore, the detected frequency

$$x^{-1} = \frac{q}{t(p+q)}$$

By varying the spacing and the orientation of the grid any other frequency in the input pattern can be picked up. The system is therefore acting as a spatial frequency filter or a Fourier coefficient calculator. Another way of picking up

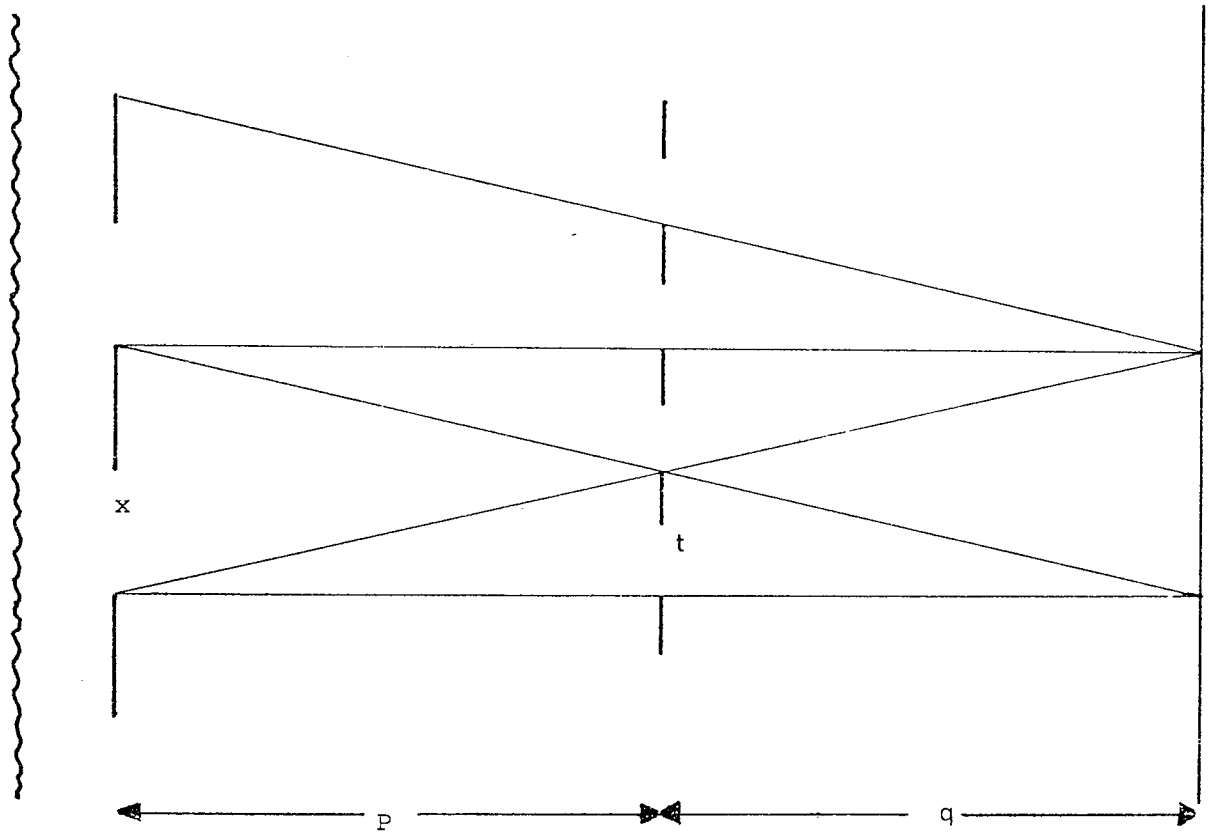

Diffuse object source

Shadowing Transparency

Ground-glass screen

Figure 2.8 The Shadowgraph

different frequencies is to move the grid between the shadowing plane (detector) and the object. This makes the system pick up frequencies between t^{-1} and o. The grid can also be rotated to detect frequencies of any orientation.

2.7 Pattern recognition with noncoherent light

There are three basic applications of correlation to the recognition of patterns.

2.7.1. General correlation

The given pattern is correlated with the set of known patterns and the one giving the best correlation (usually characterised by a bright central maximum) determined by one or more photo-detectors, provides the identity of the pattern. Disadvantages are : 180^{o} rotational ambiguity, rendering in the case of character recognition characters such as 6 and 9 indistinguishable, there is no shift variance, i.e. the position of the correlation pattern in the detector plane depends on the position of the input pattern in the object plane.

This method of recognition was discussed by McLachlan (32) who showed that identical patterns have larger common area, when they are brought into maximum coincidence, than unlike patterns. This means that an autocorrelation has a higher maximum in the centre than a cross-correlation.

2.7.2. Autocorrelation

This is only possible for the pattern in the form of a transparency. Every pattern has a certain autocorrelation function characteristic of itself. Therefore, by examining the autocorrelation plane different patterns can be identified. Autocorrelation can be made shift invariant but 180° rotational ambiguity remains. Systems using autocorrelation for pattern recognition are described by Holden(35) and Horwitz and Shelton(29).

2.7.3. Correlation with discrete frequency gratings

This is used, in character recognition, to analyse the frequency content of characters and provides a means of recognizing characters by measuring Fourier coefficients. Leifer et al[33] have shown that any character in the Arabic numerals 0,1,....,9 can be recognized by measuring a three of its Fourier coefficients. They, therefore, correlate a composite grid, consisting of the three frequencies, with the characters in the manner described in 2.6.5. The correlation of a character with one of the frequencies produces a correlation pattern. The contrast of the correlation pattern (the shadow) corresponds to the amplitude of the given Fourier coefficient and the position corresponds to the phase. Therefore, by measuring the contrast and the position of the shadow for each of the three frequencies the character can be identified.

2.8 Noncoherent Fourier transformations

It is possible to generate an entire Fourier transform temporally within practical frequency limits by convolving the input intensity distribution function optically with a single sinewave grid and continually varying the sampling frequency by controlling the spacing between the pattern and the grid. A two dimensional transform is constructed by altering the orientation of the grid after each frequency sweep. Alternatively, the grid can be continuously rotated, and the sampling frequency slowly changed. Many similar experimental correlograms and Fourier transforms are described by Barber (36).

Fourier transforms can also be obtained by convolving the input pattern with a multiplicity of sinusoidal transmission gratings of various spatial frequencies and orientations. This method is employed in the noncoherent Fourier transformer (37) and is described in more detail in Chapter 5.

2.9.Noncoherent decoding of coded pictures

2.9.1. Pictures decoding using a simple noncoherent correlater

We have seen in 2.3.2 that coded apertures can be used to image radiations that cannot be imaged by ordinary lenses. Zone-plates are usually used as coded apertures. These form coded photographs that may be decoded by reducing their scale and placing them in a coherent beam of light.

The main problem in this kind of decoding is the diffraction pattern due to the negative power of the zone-plate . If an off-axis zone-plate is used to separate spatially the dc term then a half-tone screen must be placed in front of the object to translate its low frequencies into the passband of the zone-plate. This leads to a decrease of efficiency and to addition of noise to the decoded photograph. The coherent system has the added disadvantage of vulnerability to optical disturbances like dust,flare and scatter. These drawbacks of the coherent decoding lead to the idea of using nocoherent light to decode coded photographs.

It is known that the autocorrelation function of a zone-plate is a delta function (23). Therefore, if a coded photograph (blurred zone-plate) is correlated with a sharp zone-plate, using the noncoherent correlater of Figure 3.15, then the detector at the output of the system will record the convolution of the blurred zone-plate with the sharp zone-plate.

If the sharp zone-plate is represented by Z(x,y), the original object by O(x,y) and the blurred zone-plate by B(x,y) then the correlater's output will be

$$Z(x,y) * B(x,y)$$

But $B(x,y) = Z(x,y) * O(x,y)$ (Reference 32)

Therefore the correlator's output becomes

$$Z(x,y) * Z(x,y) * O(x,y)$$

$$= \delta(x,y) * O(x,y)$$

$$= O(x,y)$$

It must be borne in mind ,however, that the autocorrelation function of a zone-plate is not exactly a delta-function. Silva and Rogers (23) have shown that the autocorrelation function of a zone-plate consists of a central peak and a shoulder. The central peak, which gives a delta-function-like effect, can be regarded as due to the positive focussing action of the zone-plate. Around it is a shoulder that corresponds to the straight-through wave and the negative focussing action of the zone-plate. In order to get better approximation to a delta-function the photographic clipping technique described by Alqazzaż and Rogers (6) must be used.

2.9.2. Noncoherent decoding by ray reversal

This method is particularly useful in decoding coded photographs produced by systems using coded-sources. In these systems random-dots are more often used, as a code, than a zone-plate (6,38,39).

The coded photograph is placed back in its original position in the coding system and a photographic plate is placed in

the position of the original object (Figure 3.43). If the code transparency is imaged on the photographic plate from the other side of the system with the same magnification as in the coding operation then the photographic plate will record the convolution of the code with the coded photograph which is the decoded image. This technique is described in more detail in 3.6.

References

1. Marechal A. and Croce P. Compt.Rendu. 237 706 (1953)
2. Tsujiuchi J. "Progress in Optics" Vol.3(Ed.E.Wolf) North Holland Publishing Co.(1963)
3. Yu F.T.S. "Introduction to Diffraction, information processing and Holography" The MIT Press P204 (1973)
4. Mertz L. and Young N.O. "Proceedings of the International Conference on Optical Instrumentations" Chapman and Hall (London) (1961) P.305.
5. Dicke R.H. Astrophysics J. 153 101 (1968)
6. Alqazzaz L. and Rogers G.L. J.Opt.Soc.Am. 65 695 (1975)
7. Weiss H."Proceedings of the International Optical Computing Conference"(Institute of Electrical and Electronics Engineers Zurich, 1974) P.41.

8a. Goodman J.W. "Introduction to Fourier Optics" McGraw-Hill(1968) P181

8b. Ibid P.164

9. Marchant A.C. and Keyte G.E. Conference on Image Detection and Processing, R.R.E. Malvern (1967)

10. Vander Lugt A. I.E.E.E. Trans.Inf.Theory 10 139 (1964)

11. Tippett J.T. et al (eds) "Optical and electro-optical information processing" The MIT press (1965) Chapter 7.

12. Vander Lugt A. Optica Acta 15 1 (1968)

13. Binns R.A.Dickinson A. and Watrasiewicz B.M. Applied Optics 7 1047 (1968)

14. Lowenthal S. and Belvaux Y. Rev. d'Optique 46 1 (1967)

15. Gabor D. Nature 208 422 (1965)

16. Keyte G.E. "The use of complex spatial frequency filters in correlation processes" Theses submitted for the Ph.D. degree, University of Aston 1970 P.159

17. Cathey W.T. "Optical Information processing and Holography" Wiley 1974 P.200

18. Yu F.T.S. and Bieringer R.J. Appl.Opt. 10 2269 (1971)

19. Bieringer R.J. Appl.Opt. 12 249 (1973)

20. Rogers G.L. J. of Micro. 89 121 (1969)

21. Mazurowski M.J.New Scientist 44 636 (1969)

22. Curtona L.J. Leith E.N. Palermo C.J. and Porcello L.J. I.R.E. Trans. Inf.Theory 6 386 (1960)

23. Silva R. and Rogers G.L. J.Opt.Soc.Am. 65 1448 (1975)

24. Stroke G.W. "An Introduction to Coherent Optics and Holography" Academic Press(1966)P.89

25. Rogers G.L. Optics and Laser Technology 7 153 (1975)

26. Haag G. Nature 153 81 (1944)

27. Robertson J.M. Nature 152 411 (1943)

28. Foster G.A.R.J.Text. Inst. 21 T18 (1930)

29. Horwitz L.P. and Shelton G.L. Proc. of the I.R.E. 49 175 (1961)

30. Kovasznay L.S.G. and Arman A. Rev.Sci.Inst. 28 793 (1957)

31. Trabka E.A and Roetling P.G. J.Opt.Soc.Am. 54 1242 (1964)

32. McLachlin D. J.Opt.Soc.Am. 52 454 (1962)

33. Leifer I. Rogers G.L. and Stephens N.W.F. Optica Acta 16 535 (1969)

34. Bromley, K. Optica Acta 21 35 (1974)

35. Holden S. J.Sci.Inst.(J. of Phys E.) 1 827 (1968)

36. Barber N.F. "Experimental Correlograms and Fourier Transforms" Pergamon Press (1961)

37. Stephens N.W.F. and Rogers G.L. Phys.Ed. 9 331 (London 1974)

38. Klotz E. and Weiss H. Optics Communications 11 368 (1974)

39. Klotz E. Linde R. and Weiss H. Optics Communications 12 183 (1974)

40. Rau J.E. J.Opt.Soc.Am. 56 541 (1966)

41. Rau J.E. J.Opt. Soc.Am. 56 1490 (1966)

42. Weaver C.S. and Goodman J.W. Appl.Opt. 5 1248 (1966)

43. Weaver C.S. Ramsey S.D. Goodmand J.W. and Rosie A.M. Appl. Opt. 9 1672 (1970)

44. Rogers G.L. "The Proceedings of the Technical programme, Electro-Optical Systems Design Conference". New York (1970) P.8.

CHAPTER 3

DECODING PREVIOUSLY CODED PICTURES

3.1 Introduction

The fundamental principles of holography were first laid down by Gabor in 1948 (1). In 1950 Rogers (2) called attention to the similarities between Gabor's holograms and Fresnel zone plates. He showed that each object point was encoded as a quasi-zone plate, with the object's transverse location given by the transverse location of the zone plate's centre, and the object's depth given by the scale of the zone plate. The object's relative intensity is given by the contrast of the zone plate. This idea leads to the shadow casting technique of Mertz and Young(3) where these zone plates are produced by a noninterferometric method. It is not practicable to focus X-rays under conditions applying in X-ray astronomy and particularly in rockets or satellites above the earth's atmosphere. On the other hand, an X-ray source can be made to cast a shadow of an etched metal mask on a photographic plate.

In the Mertz and Young technique a finite number of X-ray sources (X-ray stars) are allowed to cast the shadow of an etched metal mask representing a zone plate on a photographic plate.

Each source will throw a shadowgraph of the zone plate onto a different area of the photographic plate. The plate is then developed and if necessary its scale is photographically reduced so that each zone plate image has a convenient focal length of say 10 - 50 mm. When placed in a coherent beam each zone plate image produces a bright spot on the common focal plane. These bright spots are a map of the original X-ray stars.

In 1972 Barrett (4) and Rogers et al (5, 6) thought of applying the Mertz and Young technique to gamma ray imaging in nuclear medicine. This brings us to the coded blurring technique.

In nuclear medicine images are normally formed on a gamma ray detector by means of lead pinholes or multichannel collimators. These apertures suffer from low geometric efficiencies and low resolution. To increase these two factors the dose of the radioactive material given to the patient has to be increased. This might endanger the life of the patient.

Barrett (7) realized that if a lead zone plate is used as an aperture for imaging the gamma ray it will form a coded blur spot from each point in the person being photographed and that a sharp picture can be subsequently recovered in coherent light. This technique is found to lead to a great increase in efficiency as well as resolution. It has the added bonus that points in the patient

lying at different distances from the gamma ray detector record zone plates on a different scale and subsequently reconstruct at different distances from the record. The recording is therefore genuinely three-dimensional.

Later in the same year Barrett(8) thought of applying the idea of zone plate shadow casting to X-ray tubes.

In X-ray tubes, all the rays emanate from a small focal spot, and the image is simply a geometric shadow of the object. In order to increase the resolution of the image, a small focal spot has to be used, but this leads to loss of power or to rapid appearance of holes in the anticathode. Hence a compromise must be made between resolution and power efficiency.

Barrett constructed an X-ray anticathode with a zone plate pattern etched on it. When he allowed the electron beam to flood the anticachode the emitted X-ray formed a coded record of the object being X-ray photographed. The coded record is then recovered in coherent light.

Mertz and Young (3) had realized that the disadvantage of using a zone plate as a code is that each focal spot, produced by each zone plate image, is surrounded by a halo due to the beam diverging from the virtual focus of the zone plate. Off-axis zone plates had been used to spatially separate the dc term,

but this has the disadvantage that the object's frequencies should be in the pass_band of the zone plate.

This problem is thought to be solved (9,10) by using a halftone screen to heterodyne the object spectrum into the passband of the zone plate but this leads to a decrease of efficiency. The half tone screen tends to obstruct some of the photons and prevents them from reaching the detector .

Dicke (11) suggested use of an irregular system of pinholes as a coded aperture in X-ray astronomy and suggested several methods for decoding the coded image.

This chapter describes a code made of irregular transparent dots on opaque surrounding. Alqazzaz and Rogers (12) thought of using this type of code as a coded-source for coding pictures in noncoherent radiation. The dots can be regarded as an array of X-ray anticathodes (13); use of such an array leads to a great increase of the efficiency of the system over the efficiencies of systems that use single anticathode.

Pictures are coded by convolving them with the code. This is done by allowing each point of the code to record the whole picture on a photographic plate, the resultant photograph is the coded image.

For decoding a coded picture, the coded picture has to be convolved again with the code. Two decoding methods are described in this chapter. In the first, coherent spatial filtering system is employed while in the second a non coherent system, based on the idea of reversing the rays involved in the process of coding, is used.

3.2. Theory

To generalize the problem, we assume that a three dimensional object $f_1(x,y,z)$ is coded by the random dots code $g(x,y)$. The code lies in a plane at a distance D from the observation plane. Let x_n and y_n be the dimensions of the out-of-focus point spread function of the code produced by layer n in the object at a distance Z_n from the observation plane. The coding process is a convolution of the code with the object to be coded. Hence the coded picture is

$$f_2(x,y) = \sum_{n=1}^{m} \left\{ g(x_n,y_n) \circledast f_{1n}(x,y) \right\}$$

where $g(x_n,y_n)$ represent the out-of-focus point spread function of the code for nth layer and $f_{1n}(x,y)$ represents the nth layer of the object along the z-direction.

Two method were employed to decode the coded picture. In the first method, non-coherent light was used and the coded picture was decoded by reversing the rays involved in the coding

process. The second method employed coherent light and the coded picture was decoded by spatial filtering.

In the non_coherent way of decoding, the code transparency was put at a distance 2f from the lens and the coded picture was put on the other side of the lens, at a distance 2f-D from it.

If the code transparency is illuminated by non coherent light, the irradiance immediately behind it is

$$I = I_o \; g\,(x,y)$$

Where I_o is the irradiance at the plane of the code transparency. The lens convolves the code with the coded picture. The convolution in space is

$$\sum_{n=1}^{m} \left\{ g(x_n,y_n) \circledast h\,(x,y) \circledast f_2\,(x,y) \right\}$$

where h (x,y) is the irradiance impulse response of the optical system. If the spatial-frequency response of the signal is within the limits of the spatial-frequency response of the optical system, then h(x,y) can be approximated by a delta function. Hence the previous formula becomes

$$\sum_{n=1}^{m} \left\{ g(x_n,y_n) \circledast f_2\,(x,y) \right\}$$

By substituting for $f_2(x,y)$, we find that a photographic plate located at distance z_j from the coded picture records

$$I_j = I_o \left[\left\{ g(x_j,y_j) \; * \; g(x_j, y_j) \right\} \circledast f_{1j}(x,y) \right.$$

$$\left. + \sum_{\substack{n=1 \\ n \neq j}}^{m} \left\{ g(x_j,y_j) * g(x_n,y_n) \circledast f_{1n}(x,y) \right\} \right]$$

The autocorrelation function of random-dots is approximately a delta function; therefore

$$I_j \tilde{=} f_{1j}(x,y)$$

Hence the photographic plate records the reconstruction of the jth layer of the object. Other layers (the second part of the equation) are smeared out and contribute to the noise in the photograph.

Exact reversal of rays in the decoding process exactly reverses the magnification and the image is recovered at the same size as the object from which it formed.

The second method of decoding the coded pictures made use of Fourier transform holography (14). This was used to record a hologram of the out-of-focus point spread function of the code. The convolution of the coded picture with the code was done by using the coded picture as a signal for reconstructing the hologram.

Because coherent light was used, $h(x,y)$ becomes the

amplitude impulse response of the optical system. This was subsequently approximated by delta function. The decoded image was received at the output of the hologram by a 35 mm camera. Klotz and Weiss (15) have described a method in which different layers of object could be recovered by moving the coded picture back and forth along the optical bench.

3.3. Distinction between dilute and continuous tone objects

The extent to which the coded pictures decode depends not only on the autocorrelation pattern of the code, which must peak sharply, but also on the nature of the original picture.

Pictures are usually either continuous-tone or dilute. A picture is defined as dilute when the information carried is very much less than the theoretical maximum, as in the case of white letters on a black surround, or the case of line-drawings. The picture will often be a black and white representation with at least 90 per cent of the area either black or white, and the smaller fraction of the other colour. Continuous-tone pictures on the other hand have "grey" tone which range from black to white. Normal portraits and photographs in newspapers, are examples of the continuous-tone pictures. The dilute and the continuous-tone pictures used in the experiment are shown in Figure 3.1 and Figure 3.2 respectively.

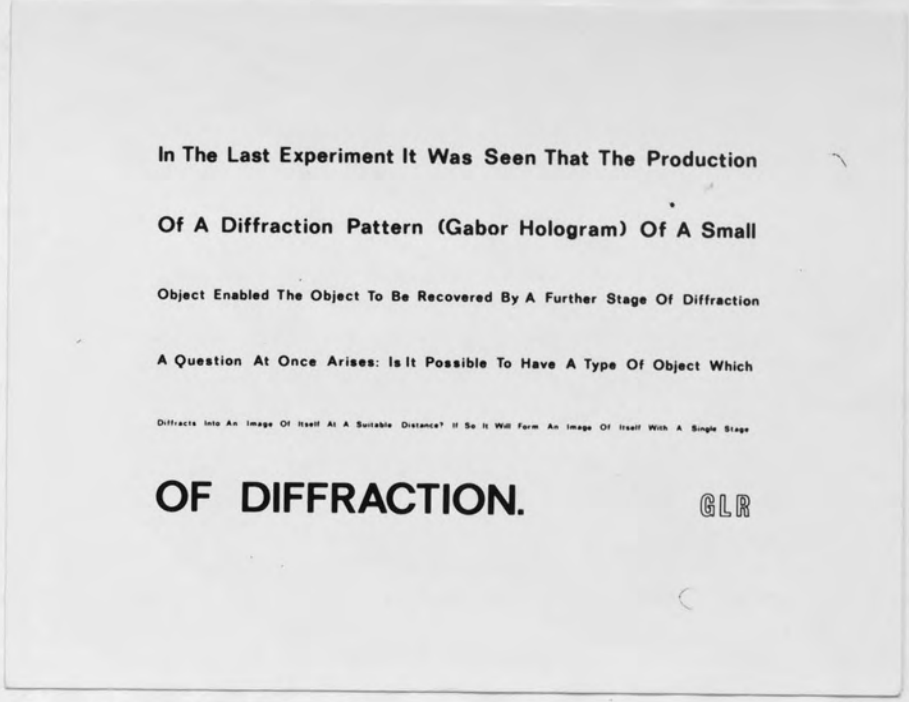

Figure 3.1 The dilute picture

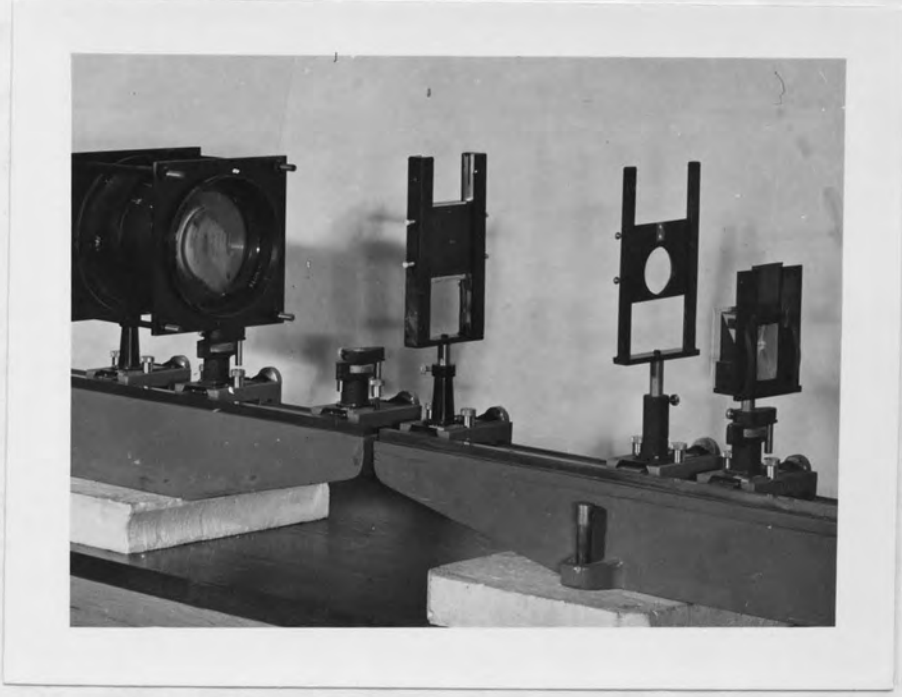

Figure 3.2 The continuous-tone picture

3.4. Noise Consideration

In the dilute decoded picture, the noise due to the shoulder of the autocorrelation pattern falls mainly or completely outside the outlines of the picture. The noise irradiance in this case is 1/N of the irradiance of the signal, where N is the number of dots in the code. Hence by decreasing the exposure time so that the density recorded on the photographic plate due to noise is approximately the same as the fog level of the plate, we can obtain a very high signal to noise ratio.

On the other hand the decoded continuous-tone picture has poor contrast, because the ratio of the integrated irradiance in the central peak to the integrated irradiance in the shoulder is low, and decreasing the exposure time cannot reduce the effect of the noise.

If we have N dots, then the central peak has weight N and the integrated surround has weight N(N-1) so that the signal-to-noise ratio will be 1/(N-1). From this, we can see that, as the number of dots decrease, the signal-to-noise ratio increases, but at the expense of efficiency, hence a compromise is necessary.

The autocorrelator pattern (Figure 3.3) of 15 random dots consists of a circular spot at the centre that has a weight equivalent to the irradiance from 15 dots, and 210 dots surrounding

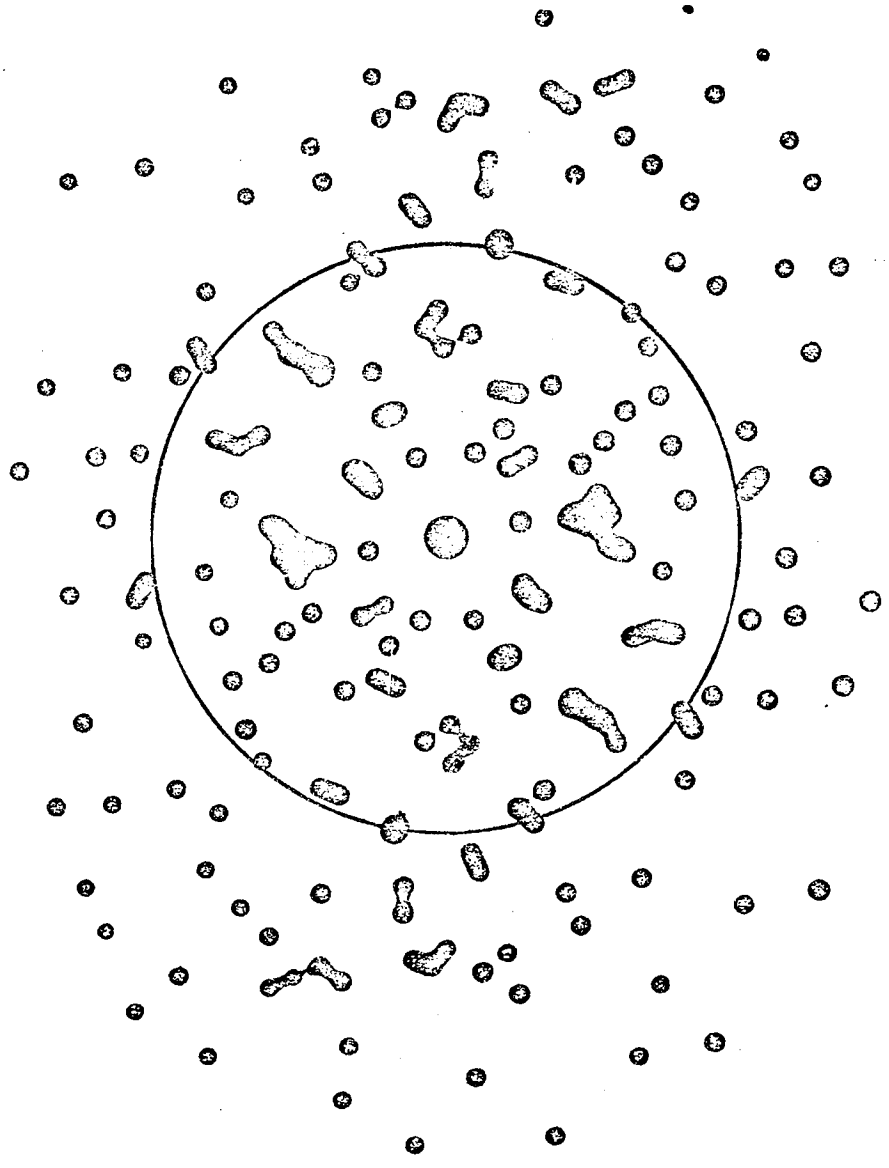

Figure 3.3 S.N.R.control circle

it. If we assume that the central half of the autocorrelation pattern is responsible for the decoding effect with a continuous tone object, then by drawing a circle (Figure 3.3) on the autocorrelation pattern such that 105 dots lie inside it, we get signal-to-noise ratio of order of magnitude 1/1.

The diameter of this 50 per cent circle is of the same order of magnitude as the spread of the original dot code. In other words we do not expect any increase of sharpness when we non coherently decode a continuous-tone object, but simply a loss of contrast.

3.5 The coherent decoding

3.5.1 The code transparency

Codes with different number of dots were used. The one which is described in this experiment consists of five randomly distributed dots. This was made as follows.

Five dots of negligible size were drawn on graph paper so that the vector differences between them had different magnitudes and orientations. To check for the randomness of the dots, their autocorrelation pattern should be drawn. This was done by allowing each dot of the five dots pattern to draw the pattern. Alternatively, each one of the dots could be passed over a certain point on the graph-paper

and the rest of the dots were drawn at each step. This point would represent a peak at the centre of the autocorrelation pattern. The peak is surrounded by 20 dots. Any aggregation of dots on some axis of the autocorrelation pattern would indicate some symmetry of the dots in the corresponding direction.

The dots pattern was then enlarged by drawing it on a graph paper using larger scale. The graph paper was put over a white cardboard and the positions of the five random dots were marked on cardboard using a pin. Circles were drawn on the cardboard with their centres at the pin-marked points. The diameter of the circles were chosen to be about 1/20 of the average distance between the dots. The circles were blackened by waterproof drawing ink using a technical pen. The cardboard was then photographed on Ilford N40 process plates. These were developed for three minutes using Kodak D8 developer, given slight rinse in clean water then put in Kodafix fixer for three minutes, washed for half an hour then left to dry. When the plates were dried they were put on a light box with the emulsion side up. Very fine holes were observed in the emulsion, these were due to dust particles attached to the emulsion before processing. The holes were spotted using Johnson liquid opaque spotter. This would prevent the extraneous holes from confusing the code.

3.5.2 Coding of pictures

The apparatus used for coding pictures is shown in Figure 3.4. It consisted of a light box with a diffuse screen on which the code plate was placed. A contact printing frame was placed 12 cm from the code plate. It contained the transparency to be coded, a spacer, and a photographic plate. The distance between the frame and the code plate controls the exposure time whilst the spacer thickness controls the amount of blurring and they are related to one another. A spacer having thickness of 3mm was found to be convenient for producing a significant blur in the photographic plate.

The photographic plate recorded the convolution of the code function with the transparency function (16) which is the coded image.

Ilford special lantern soft plates were used to produce a blurred picture for the continuous-tone object shown in Figure 3.2. For the dilute object shown in Figure 3.1 Ilford N30 ordinary plates were used. Usinga25 watts lamp for the light box, the exposure times used for recording the coded continuous-tone picture (Figure 3.5) and the coded dilute picture (Figure 3.6) were 105 seconds and 40 minutes respectively.

Because the decoding process requires the use of a positive coded transparency, the coded negative was printed by contact

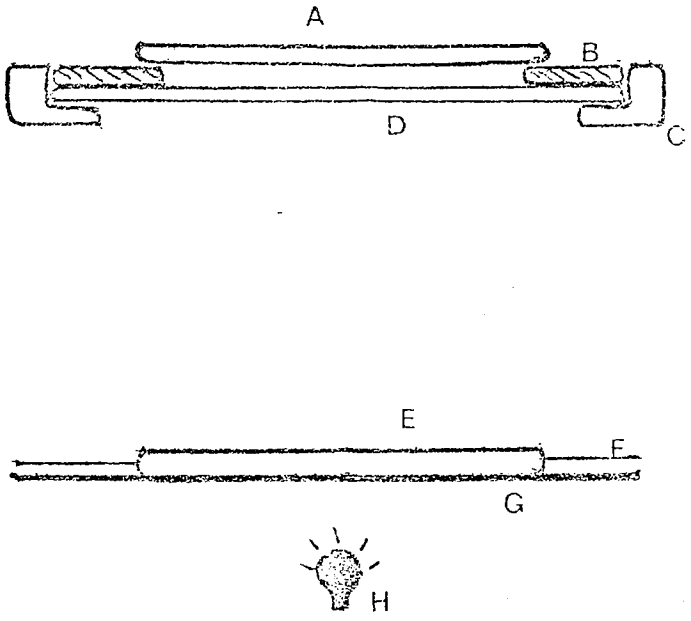

Figure 3.4 Apparatus for coding pictures. A = photographic plate; B = spacer; C = contract-printing frame; D = the picture to be coded; E = random-dots plate; F = black cover to obstruct stray light; G = ground-glass screen; H = diffuse light source

Figure 3.5 Coded continuous-tone picture (5 equal dots)

Figure 3.6 Coded dilute picture (5 equal dots)

printing,to produce a positive coded transparency. Again Ilford lantern plates were used for the continuous-tone picture and Ilford N30 plates were used for the dilute picture.

The negative transparency was put in a contact printing frame with emulsion side up and the photographic plate was put over it with emulsion side down, the back cover was put and clamped then the frame was turned, put under printing projector and the photographic plate was exposed. The projector was put in a maximum height position so that the light coming out of it expose the plate uniformly. A test strip was used to determine the right exposure time. The exposure time for both the dilute and the continuous-tone pictures was 4 seconds.

Both the N30 and the lantern plates were developed in P Q Universal developer. The developer was diluted by 1:9 and kept at 21°C. The plates were developed for three minutes, with continuous agitation of developer, rinsed with water then fixed and washed in the usual way. The back of the plates was cleaned from grit marks by cleaning tissue. The grit masks came from water and precipitate over the back of the plates.

3.5.3 Mounting the coded pictures

In coherent systems phase retardations occur when coherent light passes through a photographic plate. Such phase retardations are primarily due to emulsion thickness variations. These thickness variations are of two sorts. One

is the coarse variation, which is a departure from optical flatness of the emulsion and base. The other is the fine variation which is a result of random fluctuations in the density of developed silver grain. This fine scale variation is strongly dependent upon the exposure of the film.

Coherent spatial filtering systems are usually phase sensitive, therefore it is necessary to remove these phase retardations. For this reason, the coded transparencies were thought to be put in an index-matching liquid gate.

Glass plates, having the same size as the coded photographs viz : $3\frac{1}{4}$" x $3\frac{1}{4}$" (8.2. x 8.2 cm), were examined for optical flatness by means of Twyman-Green Interferometer. The Interferometer was first adjusted to maximum visibility by equating the optical path lengths of its two arms. The test mirror was then slightly tilted to give about 10 fringes in the field of view.

The plates were first examined for wedge existence. This was done by putting the glass plate in front of the test mirror such that it covers half of it. This enable the directions of inclination of both the fringes formed over the glass plate and the fringes formed over the uncovered part of the test mirror to be observed. If these two directions are not exactly parallel then a wedge exists in

the glass plate.

However, it is more important to examine the plates for optical hills and valleys because these are more cumbersome in coherent systems. This was done by putting the glass plate in front of the test mirror and trying to get minimum number of fringes, or no fringes if possible. No fringes indicates that the glass plate is free from optical nonuniformity. A closed fringe structure indicates the existence of either hill or valley. These could be distinguished by pressing gently the back of the test mirror, if the closed fringe structure expands then a valley exists and if it contracts then a hill exists.

Several plates with minimum number of fringes of two or less were chosen. These were cleaned by soft tissue and polishing cloth. The photographic plate to be mounted was cleaned as well, then a single drop of Sira mountant emulsion was put over the centre of the photographic plate. Another was put over the centre of one of the glass plates. The two drops then joined together by lowering the glass plate slowly over the photographic plate. This would avoid the occurrence of bubbles in the mountant. The two plates then squared up and put in a box of the same size as the plates.A 750gm weight was put over the plates and left for two days till the mountant spread uniformly over the emulsion. The other side of the photographic plate was then mounted in the same way.

The Sira mountant has a refractive index close to the

refractive indices of both the glass and the emulsion, therefore the optical path length through the liquid gate is expected to be constant.

The liquid gate was examined by Twyman-Green interferometer, several fringes were observed, indicating some inhomogeneity in the glass. This was attributed to the fact that the photographic plate had a base made from a normal window glass and therefore it was optically inhomogeneous.

The variation of optical path length along the liquid gate tends to localize the correlation effect and therefore only part of the coded picture is expected to decode. Other parts of the picture decode by scanning the hologram with the signal beam. In some cases there may exist a position on the hologram in which a large part of the coded picture is decoded.

3.5.4 The Coherent Correlator

The apparatus used in decoding the coded picture is shown in Figure 3.7. It is based on the system suggested by Vander Lugt (17) for synthesing complex spatial frequency filters and consists of

1. A heavy and rigid table with two 28 x 35 x 15 cm. pieces of expanded polystyrene over it, serving as antivibration mountings.
2. Double rail type optical bench, of length 200 cm, mounted over the polystyrene blocks and includes bench carriers which were designed to take optical components mounted on pillars 10 mm

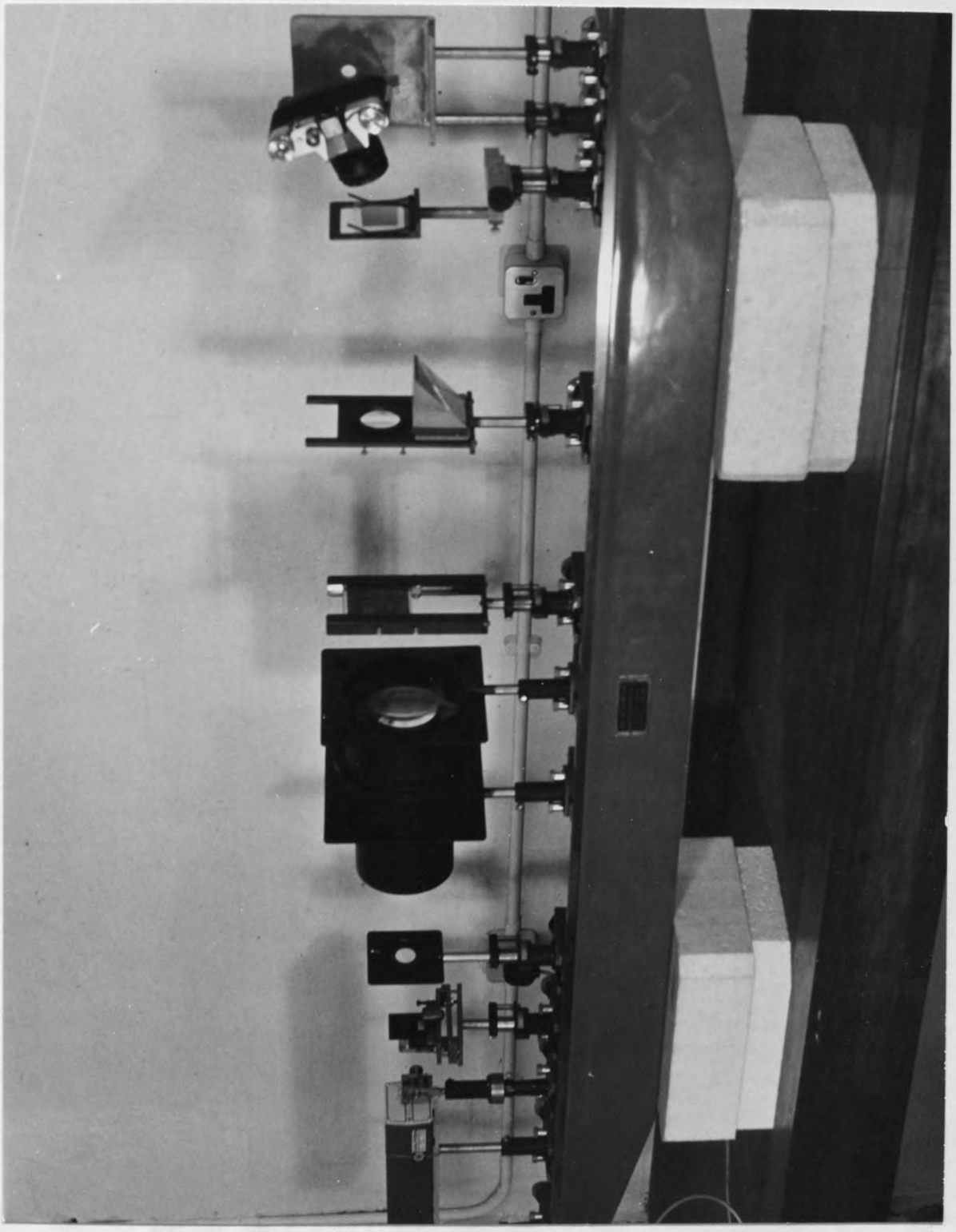

Figure 3.7 The Coherent Correleter

in diameter. The optical bench was considered too heavy for any vibration to occur.

The whole apparatus was situated in an isolated sub-basement room. This would prevent any disturbance due to vibration, temperature change or airflow from spoiling the holographic record.

3. Laser

He-Ne lasers have been found to be ideally suited for use in coherent optical systems. Their output power and wavelength are very convenient for our sort of experiment. For this reason Spectra-physics He-Ne Laser (Model 155) was used. This gave an output of 0.5 mw and wavelength 632.8 nm. The output was continuous and uniphase, i.e. the laser could be operated in the TEM_{oo} mode, giving a single output beam with an approximate Gaussian distribution of intensity across it.

An important requirement of the laser is that its output power and wavefront intensity profile must be constant during the period of experiment. This is particularly important during exposure of the hologram, when the intensity must be carefully controlled.

The output power and wavefront intensity profile depend to a large extent on the state of tuning of the laser. This refers to the alignment of the end reflectors of the resonating cavity, optimum power being obtained when the reflectors were

perfectly aligned. This also gave the best intensity profile.

A period of about twenty minutes was usually allowed, for the laser to warm up, before recording the hologram. This would enable the laser to produce more stable output. The stability of the laser output could be checked with Fabry Perot etalon. A stable laser will produce no drift and no split in the interference fringes of the etalon.

3. The beam expander and spatial filter.

A small negative lens was used to diverge slightly the laser beam from a virtual source. The beam needed to be diverged in order to fill the entrance pupil of a microscope objective. This would make full use of the objective and in particular would increase the divergence of the beam after the objective. Beck type objective of X20 power was used to bring the slightly diverging beam to a real focus. A fine pinhole, acting as spatial filter, was placed at the focus. This would block out the scattered light, due to dust, scratches or any other imperfection in the preceding optical components, and prevent it from passing beyond the focal plane of the objective. If the scattered light was passed, it would produce diffraction irregularities in the divergent beam. The pinhole was aligned with the microscope objective by the method of successive approximation described by Rogers (18).

4 Lenses

The collimator and transform lens have very similar tasks although the first was required to image an axial point source, whereas the second was required to give good performance over the range of spatial frequencies likely to be encountered.

The collimator was a large f/6.3 aircraft lens having a nominal focal length of 91.4 cm. This was placed on the optical bench such that the pinhole lies at its focal point, hence, the light emerges parallel from the other side of the lens. The focussing of the pinhole with respect to the collimator was done by viewing the pinhole, through the collimator, with a pre-set collimating telescope. A neutral density filter of value 1.0 was used for this purpose and the collimator's position was adjusted so that a sharp image of the pinhole appeared in the telescope.

The diameter of the collimated beam was 9.8 cm. Half of this beam was allowed to fall on the transparent object and the light diffracted by the object was focussed, by means of an f/3 lens, on the hologram. The lens served as a transform lens and had a focal length of about 14.6 cm. The other part of the beam was used as the reference beam in recording the hologram. This has been done by mounting a suitable right angle prism under the transform lens to refract the beam so that it falls on the hologram.

5. Object

This was a photographic plate mounted between two optical flats, as described in Section 3.5.3, and was situated at the back focal plane of the transform lens. The bench carrier holding the object was designed such that it allows the lower half of the collimated beam to pass freely to the right angle prism to provide the reference beam. It consists of two vertical rails with long slot alone one of them. The object was slid between the rails and its position was controlled with a bolt screwed to the slotted rail, as shown in Figure 3.7.

6. Hologram

The hologram was situated at the back focal plane of the transform lens. It was mounted over a carrier having three degrees of freedom. This allowed the hologram to be recorded outside the transform lens focus. It allowed it, as well, to be centred on the back focal plane of the lens. The formation of holograms beyond the focal plane will be discussed in Chapter 4.

The hologram itself was Ilford Holographic plate 9 x 6 cm in size. The plates were supplied in the standard size, viz, 9 x 12 cm. and were cut into two pieces, in a jig before being used. The cutting was done in complete darkness and the plates were kept in a light tight box until needed.

7. Telescope and Camera

The naked eye could be used to view the hologram reconstruction, but in order to view the fine details of the reconstruction, a telescope, set for viewing at infinity, was normally used. This was put in a horizontal position when the hologram response (i.e. the hologram reconstruction by the unmodulated beam) was needing to be checked. Otherwise, it was pointed along the direction of the reference beam.

The correlated image was photographed with Fed 35 mm camera. This was either set for photographing at infinity or used without a lens. It was mounted over a special carrier so that its aperture fell below the hologram (the telescope was removed) and its optical axis was along the reference beam.

Photographing the correlated images had lots of advantages. The effect of the confusing speckles could be reduced, the correlograms could be printed on larger scale and compared with each other, and the most important thing is that the unwanted noise could be minimised by making use of the nonlinearity of the photographic process, as explained in Section 3.5.6.

A schematic diagram of the apparatus is shown in Figure 3.8. Any single point on the object, since it lies in the front focal plane of the transform lens gives rise to a parallel beam of light emerging from the lens. This strikes the parallel reference

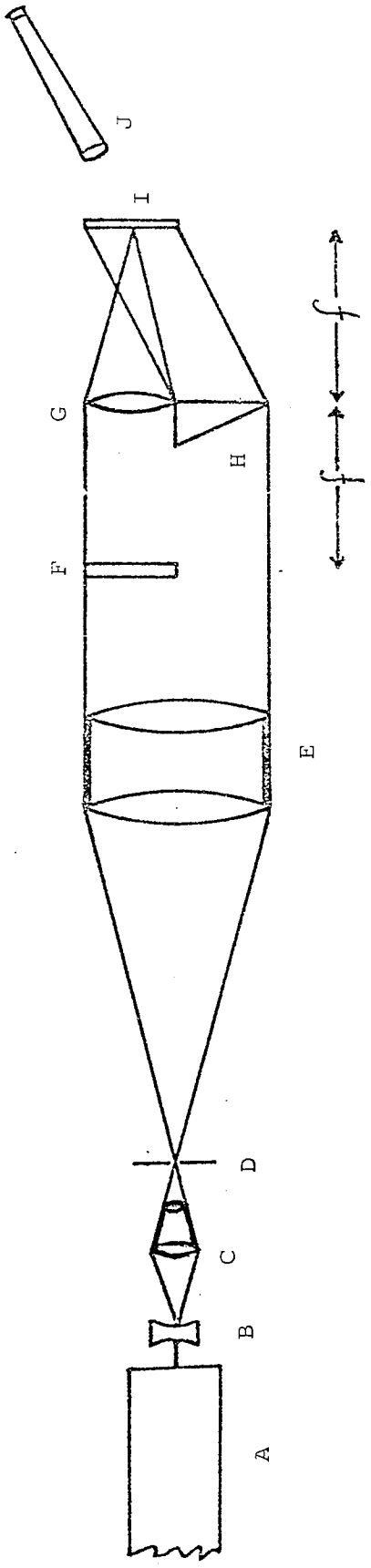

Figure 3.8 The coherent correlater. A = laser; B = divergent lens; C = microscope objective; D = pinhole; E = collimeter; F = object; G = Fourier transform lens; H = right angle prism; I = hologram; J = telescope

beam at an angle on the hologram plate producing a straight system of interference fringes. This angle varies as the single point moves over the object plane so that the spacing and orientation of the hologram fringes uniquely relate to the position of the object points.

A hologram may be recorded using this apparatus, processed and then repositioned. When the nonmodulated reference beam is allowed to interact with the recorded fringes, it reconstructs the object at infinity. This may be observed with a telescope aligned along the axis of the transform lens.

If the reference beam is now blocked up and the object beam is allowed to fall on the hologram then a fraction of the beam will pass straight through forming the zero order image of the object. There are also two diffracted beams, one upward and one downward. These may be observed in turn by tilting the telescope.

In the upward reconstruction any single point on the object reconstructs from the hologram a complete representation of the whole object. If all the points on the object act simultaneously on the hologram, the resulting image is the autocorrelation of the object with the reconstruction. The downward reconstruction on the other hand, because it is inverted, results in the convolution of the object with the reconstruction.

3.5.5. Making the filter.

A sample of the out of focus point spread function of the code was needed on the same scale as in the coded photographs to make the holographic spatial filter . For this reason the coding apparatus mentioned in section 5.2 was used. The sharp picture was replaced by a thin metal foil with a little hole in the middle. The hole was made with a watchmaker's drill of suitable diameter.A large diameter makes the dots recorded on the photographic plate overlap.A very small diameter, on the other hand, makes the exposure time, needed to record the point spread function inconveniently long. Therefore a compromise is necessary.

A hole having a diameter of 0.25 mm was used. This required an exposure time of 2½ hours for the photographic plate to record the dots with fairly good contrast. The result was checked with a microscope to confirm the photographic density and contrast.

Ilford N40 process plates were used in taking the photographs. These were developed with Kodak D8 developer diluted by 1:1.

A positive print of the dots-sample was made by contact printing (exposure time was 8 seconds), to give fine holes in a substantially black surround. The same plates and

developer were used. The dots-sample transparency was then mounted between two optically flat glass-plates and was put in the object's place of the coherent correlator. Ilford Holographic plates were used to record the fourier transform hologram.

The methods employed to improve the quality of holographic reconstruction are described in Chapter 4. The best hologram was recorded with 0.4 neutral density filter in the signal's beam. No change in the hologram's position was sought. Exposure time was six seconds and the hologram was developed with Ilford PQ Universal developer diluted by 1:9. Development time was five minutes.

3.5.6. Decoding of pictures

The coded pictures were placed in the coherent correlator with their orietnation and emulsion side corresponding to the orientation and emulsion side of the code-sample which the hologram was made from.

In decoding the coded pictures, the unmodulated reconstructing beam of the coherent correlator was not needed, therefore, it was blocked up by a black sheet of paper.

The hologram must be inserted in the focal plane of the fourier tranform lens, otherwise the correlation is only correct

at one point of the field. This was done by moving the hologram back and forth along the optical bench so that the signal beam emerging from the transform lens focuses on the emulsion of the hologram.

The signal beam should focus exactly on the holographic spot. Therefore the exact position of the holographic spot has to be found. This was done by shining white light on the hologram and trying to pick up the position of the spot by means of a high powered eyepiece. Once the position of the spot was found, the signal beam focusing on the holographic plate was brought to focus on the holographic spot.

Two reconstructions were observed,the first represents the correlation of the coded picture with the code and was viewed by looking at the hologram along the direction of the reconstructing beam (the unmodulated beam). The second represents the convolution and was viewed by looking at the hologram along a direction making the same angle with the horizontal as the direction of the reconstructing beam but with a negative sign.

The reconstruction corresponding to the correlation is the one which was expected to give a decoded image, therefore a 35 mm camera was put behind the hologram with its axis along the direction of the reconstructing beam. Since the decoded image is formed at infinity, therefore, the camera lens was

set for photographing at infinity.

First, an exposure time of one minute was tried. This would expose the film at the middle of its H & D curve. But this produced a lot of noise in the decoded photograph (Figure 3.9) due to the shoulder region of the autocorrelation pattern. Then it was decided to expose the film near the toe of its H & D curve, in order to eliminate the shoulder region. This was done by decreasing the exposure time so that the density recorded from the shoulder region was about the same as the fog level of the film, as in Figure 3.10. The exposure time needed for doing this was two seconds.

Ilford FP4 35 mm film was used. This was developed in Unitol developer diluted by 1:9. Development time was $8\frac{1}{4}$ minutes and fixing time was five minutes.

3.5.7. Convolution and correlation patterns

Figure 3.11 shows the autocorrelation pattern of the five dots. The pattern consists of a central spot which is responsible for the decoding, surrounded by twenty dots which contribute to the noise in the decoded picture. The figure illustrates as well the bisymmetry property of the autocorrelation pattern. The method employed to record the autocorrelation pattern was to use the code-sample, used to make the hologram, as a signal to reconstruct the hologram. The reconstruction

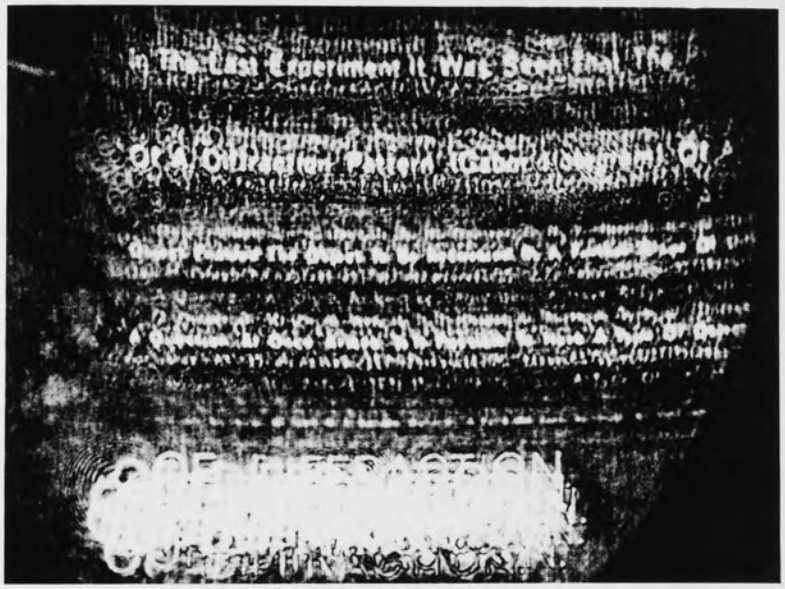

Figure 3.9 Noisy decoded photograph due to exposing the film at the middle of its H & D Curve

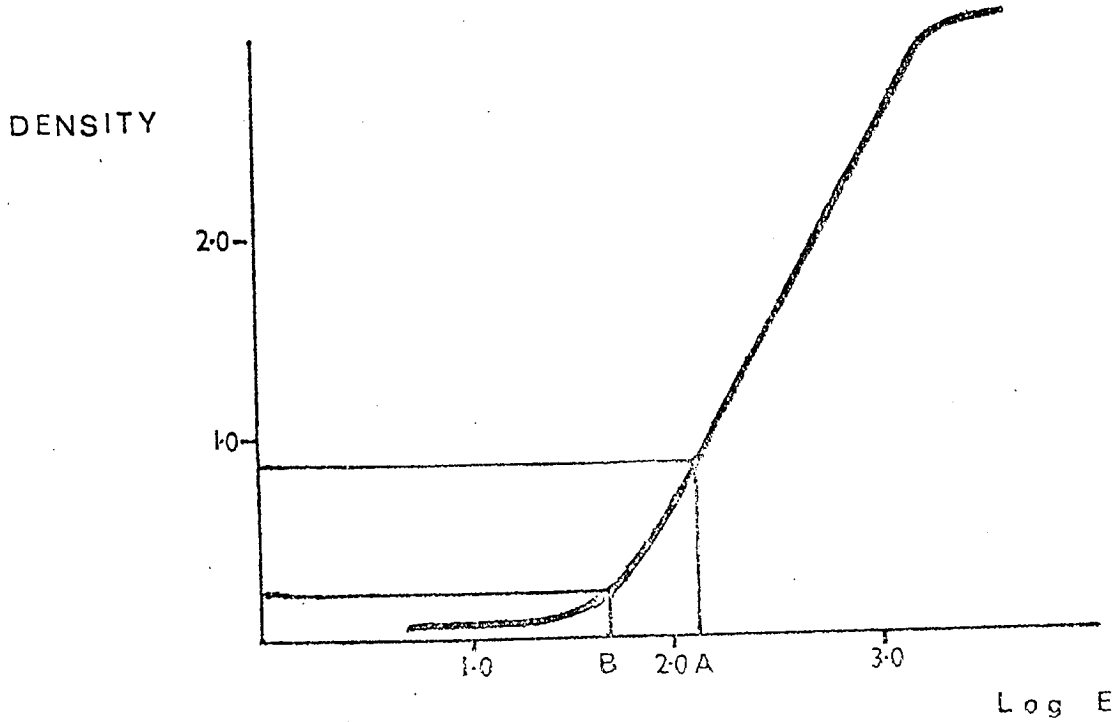

Figure 3.10 The H and D Curve of photographic emulsion of $\gamma = 1.7$ showing two exposures, the first (A) at the straight portion of the curve, corresponding to the autocorrelation peak (signal), the second (B) near the toe, corresponding to the autocorrelation shoulder (noise)

corresponding to correlation, was then photographed by the 35 mm camera.

For getting the convolution (Figure 3.12) the transparency was inverted and a photograph was taken along the same direction used before.

It was noted that the intensity of the central spot of the autocorrelation pattern decreases to a minimum (Figure 3.13) then increases again (Figure 3.14) as the hologram was shifted away from the focus of the signal beam. This was thought to be due to change in the phase of the autocorrelation pattern as the signal beam scans the hologram.

The autocorrelation and convolution patterns could be alternatively produced by using the noncoherent correlator (Figure 3.15) mentioned in Chapter 2. Two copies of the code transparency were put in the noncoherent correlator so that their orientations were the same.

The diffuse light at the input of the apparatus would produce the autocorrelation pattern on the ground glass screen at the output. The ground glass screen could be replaced by a photographic plate for recording the autocorrelation pattern. The pattern was faint, therefore a sensitive plate like Ilford HP3 was used. If one of the two transparencies was inverted, then

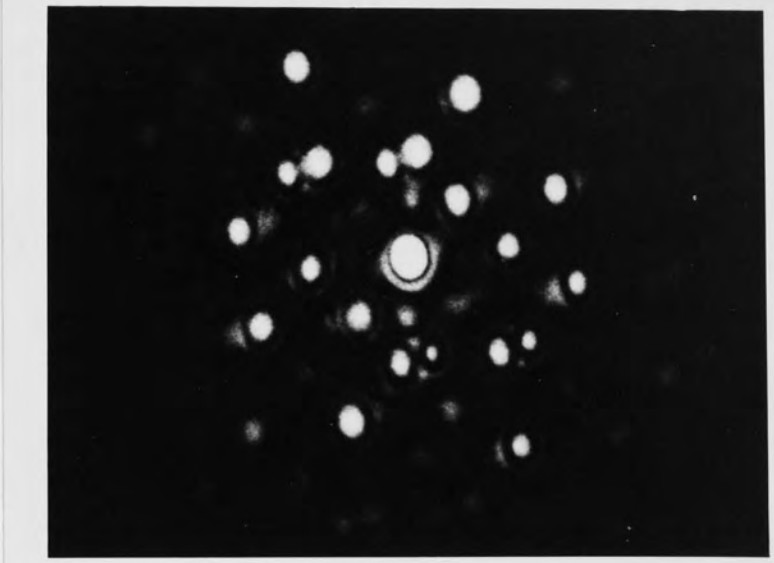

Figure 3.11 Autocorrelation pattern of the five dots; produced by the coherent correlater

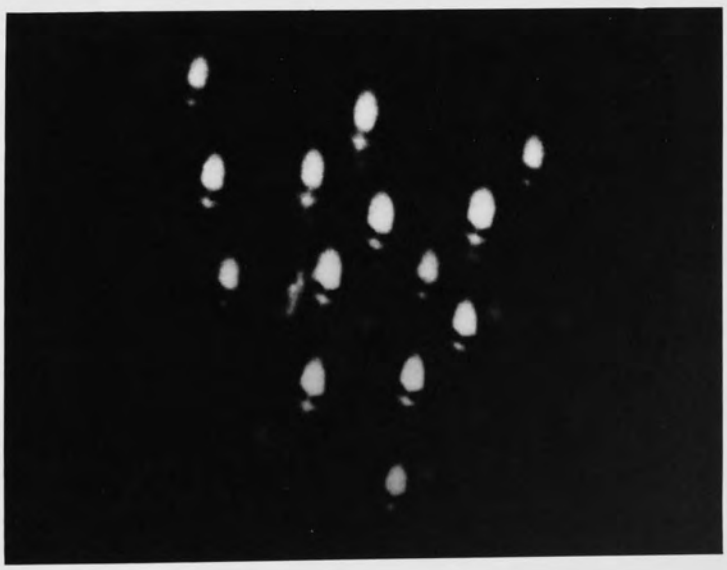

Figure 3.12 Convolution pattern of the five dots; produced by the coherent correlater

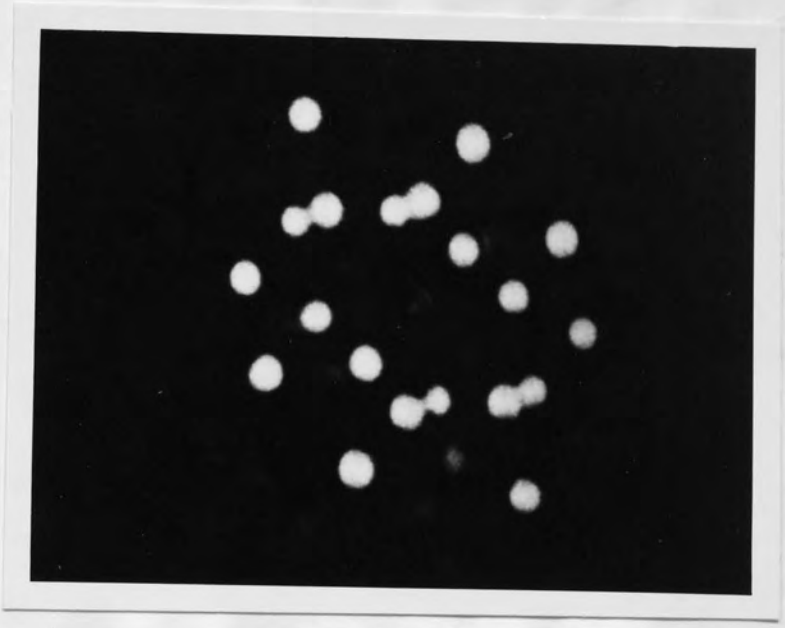

Figure 3.13 Position of minimum signal to noise ratio

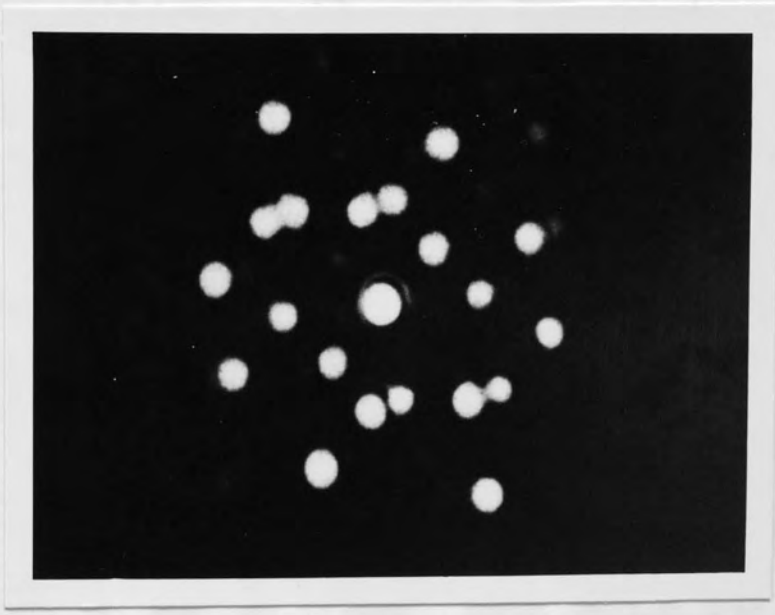

Figure 3.14 Position of maximum signal to noise ratio

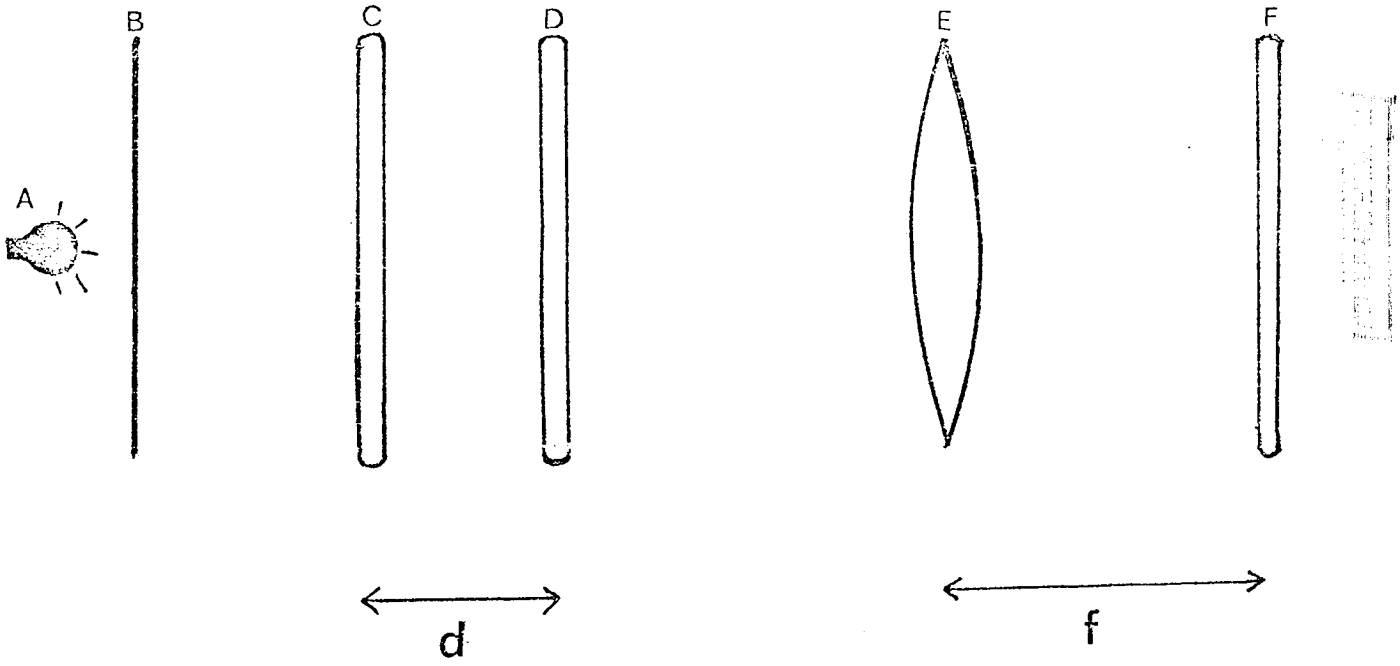

Figure 3.15 Noncoherent correlater. A = diffuse light source; B = ground-glass screen; C and D = two transparencies to be correlated; E = lens; F = Photographic plate or ground-glass screen

the photographic plate would record the convolution.

Two sorts of the 5 dots code were used in the experiments. One having dots of equal weights (i.e. their diameters are the same, Figure 3.16) and another having dots of unequal weights (i.e. their diameters are not the same, Figure 3.17) . The autocorrelation and convolution patterns of the equal and the non equal dots are shown in Figures 3.18, 3.19, 3.20 and 3.21.

Figure 3.22 shows what the noncoherent correlator records when one of the equal dots transparencies is rotated by 90 degrees while Figure 3.23 shows what it records when one of the equal dots transparencies is turned frontside back. Each one of these two figures represents a crosscorrelation pattern. The general formula for crosscorrelation is

$$\int_{-\infty}^{\infty}\int_{-\infty}^{\infty} f_1(x,y)\, f_2(x + s,\, y + r)\, dx\, dy$$

In Figure 3.22 the two functions f_1 and f_2 are similar except that one of them was rotated counterclockwise, by 90 degrees, with respect to the other. Therefore the cross correlation function can be written as

$$\int_{-\infty}^{\infty}\int_{-\infty}^{\infty} f(x,y)\, f\,(s-y,\, x + r)\, dx\, dy$$

Figure 3.23 ,on the other hand, was produced by changing the signs of the x - axis of one of the functions leaving the y - axis signs unchanged. The crosscorrelation function, in

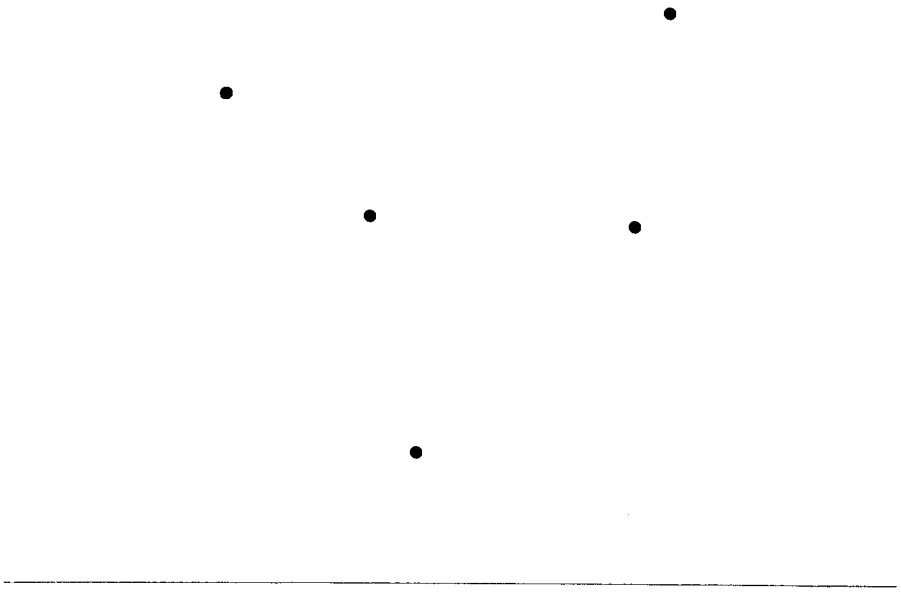

Figure 3.16 Five random-dots having equal weight

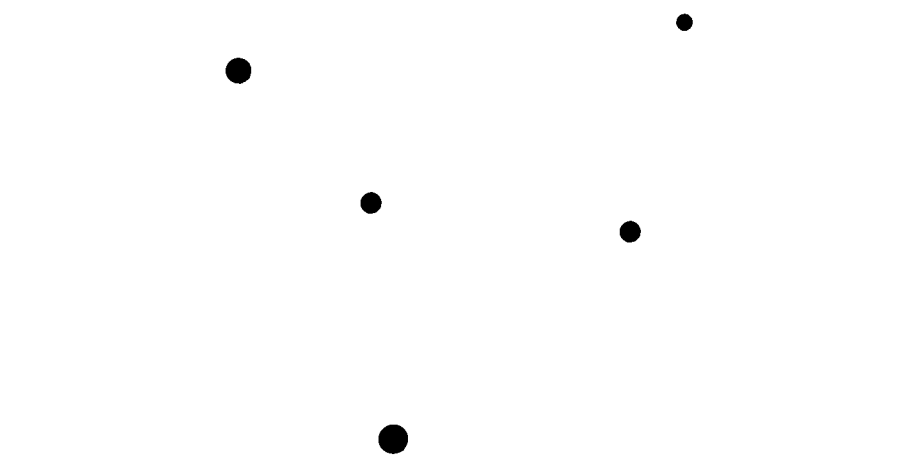

Figure 3.17 Five random-dots having nonequal weight

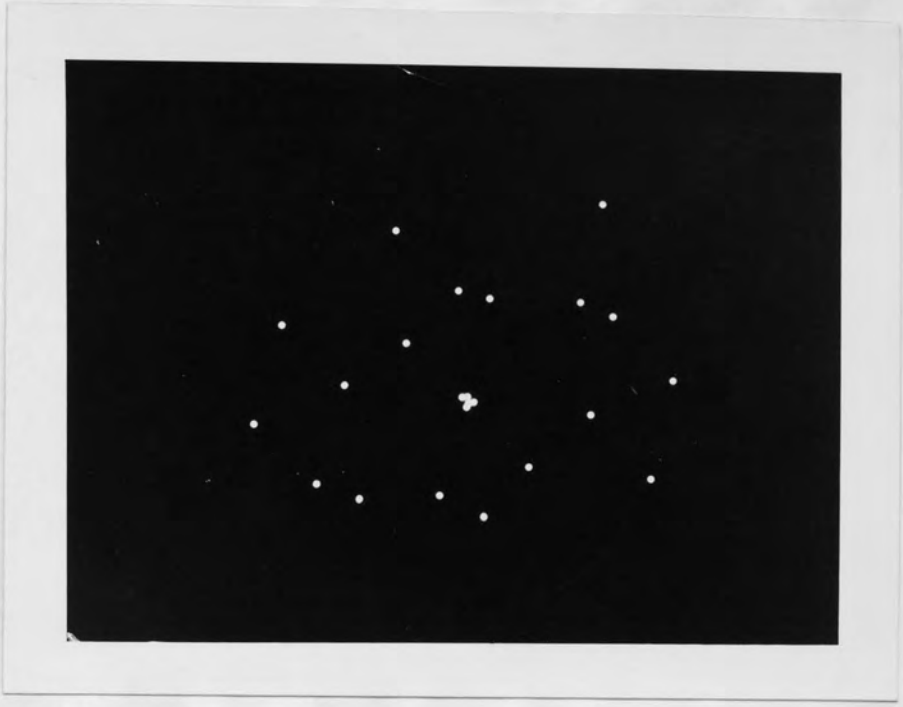

Figure 3.18 Autocorrelation pattern for the 5 random-dots of equal weight

Figure 3.19 Convolution pattern for the 5 random-dots of equal weight

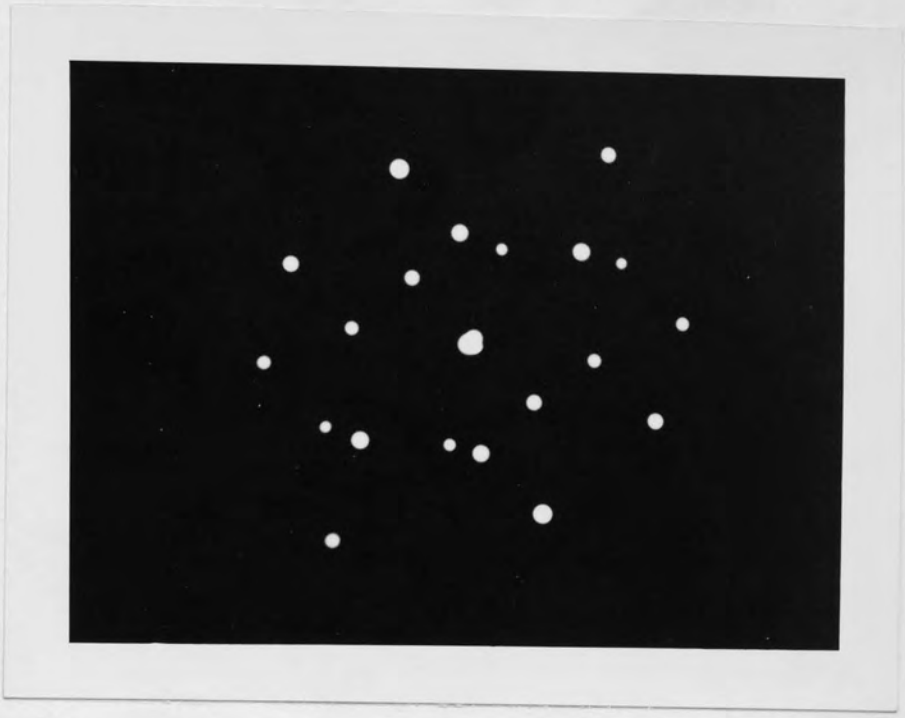

Figure 3.20 Autocorrelation pattern for the 5 random-dots of nonequal weight

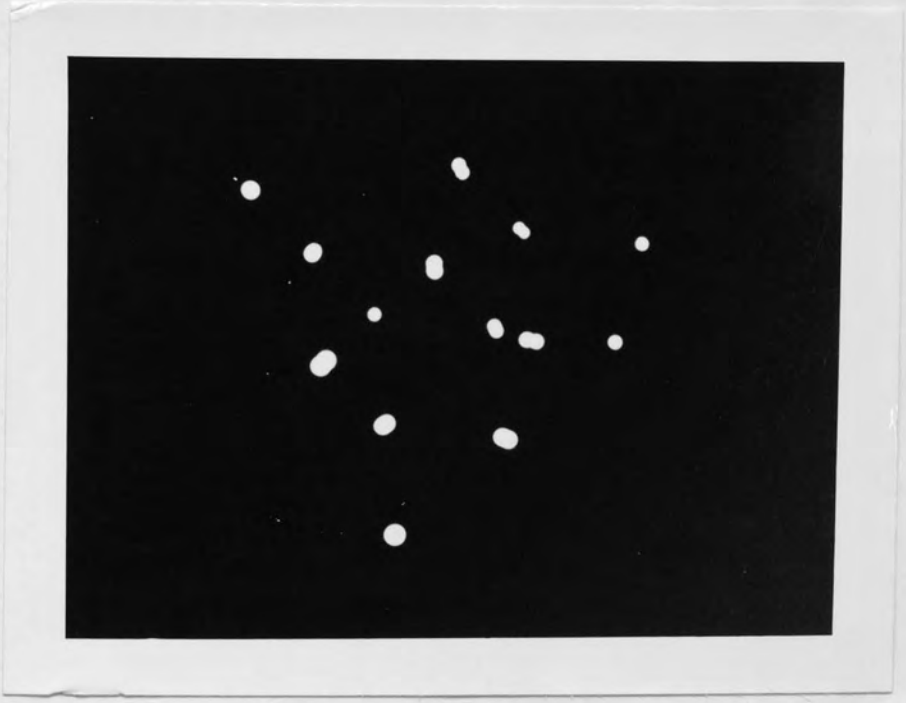

Figure 3.21 Convolution pattern for the 5 random-dots of non-equal weight

Figure 3.22 Crosscorrelation pattern of two similar 5 random-dots transparencies, one rotated by 90° with respect to the other

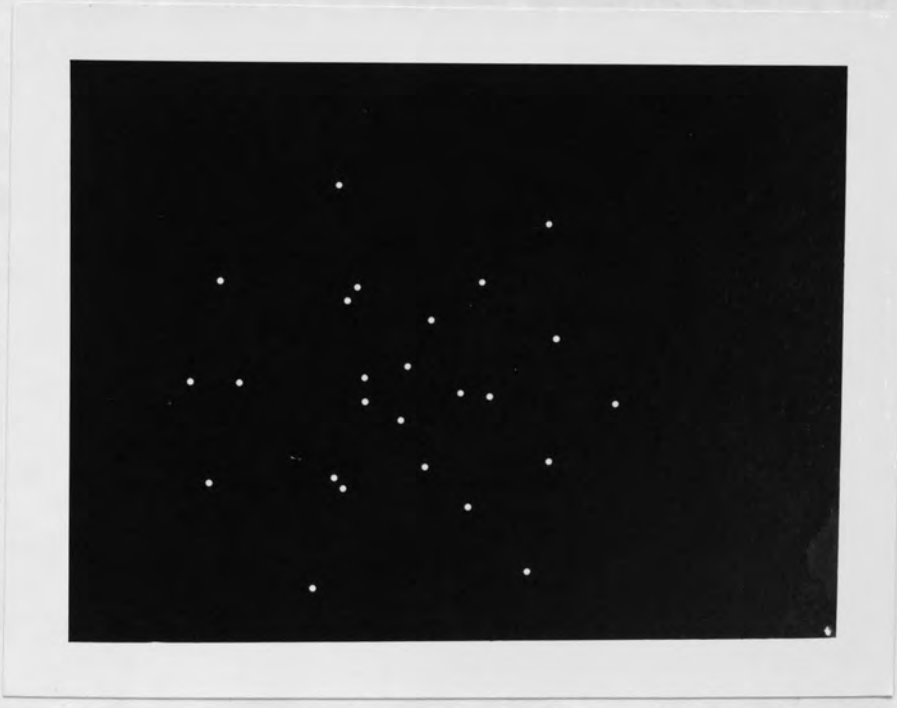

Figure 3.23 Crosscorrelation pattern of two similar 5 random-dots transparencies, one turned front side back with respect to the other

this case, is therefore

$$\int_{-\infty}^{\infty}\int_{-\infty}^{\infty} f(x,y)\ \ f(s-x,\ y+r)\ dx\ dy$$

The expected number of dots in the convolution pattern (Figures 3.19 and 3.21) is 25 while the observed one is 23. This is thought to be due to dots overlapping and lens cut off.

It can be shown in Figures 3.19 and 3.21 that the convolution pattern is asymmetrical. This property is used to distinguish the convolution pattern from the symmetrical pattern shown in Figure 3.23.

The convolution and autocorrelation patterns can be alternatively drawn by a graphical method.For drawing the convolution pattern resulting from the convolution of two systems of 5 random dots; each one of the dots,of one of the systems, is allowed to draw the 5 dots of the other system, The resulting convolution is shown in Figure 3.24.

If, on the other hand, the autocorrelation pattern is wanted, one of the 5 dots system must be rotated by 180 degrees and again each one of the dots of one of the systems is allowed to draw the five dots of the other system. The resulting autocorrelation pattern is shown in Figure 3.25.

It can be noted in the last two paragraphs that drawing

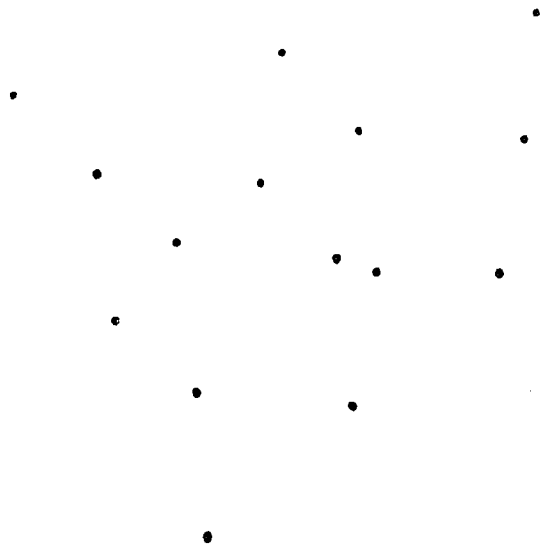

Figure 3.24 Convolution pattern of the 5 random-dots; drawn by the graphical method

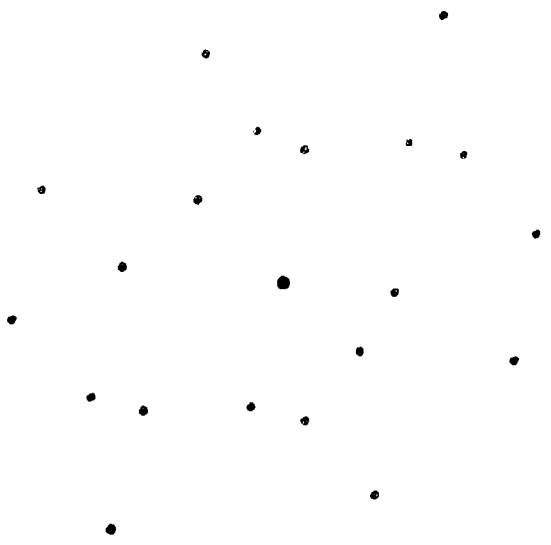

Figure 3.25 Autocorrelation pattern of the 5 random-dots; drawn by the graphical method

the autocorrelation pattern requires the inversion of one of the systems of five dots while drawing the convolution pattern does not. This is the reverse of what the experimental procedure demands.

The correlation pattern shown in Figure 3.23 can be drawn graphically by inverting one of the dots systems turning it front side back then correlating it with the same method described above (Figure 3.26). Figure 3.22 can be drawn graphically by turning one of the dots systems by 90 degrees then correlating it with the other system as shown in Figure 3.27.

3.5.8 Results

Figures 3.28 and 3.29 show the decoded dilute and continuous-tone pictures in the coherent experiment that had been coded by equal dots. Figures 3.30 and 3.31 show the decoded dilute and continuous-tone pictures that had been coded by nonequal dots. It can be noticed that the equal dots code produce better decoded pictures than the nonequal dots code. This is becuase, in the extreme case, the largest dot in the non-equal dots code behaves like a delta function. This produces five delta functions in the autocorrelation pattern. Since the decoding process needs single delta function, therefore, no decoding is expected to result.

Surprisingly some decoding was observed (Figures 3.32,

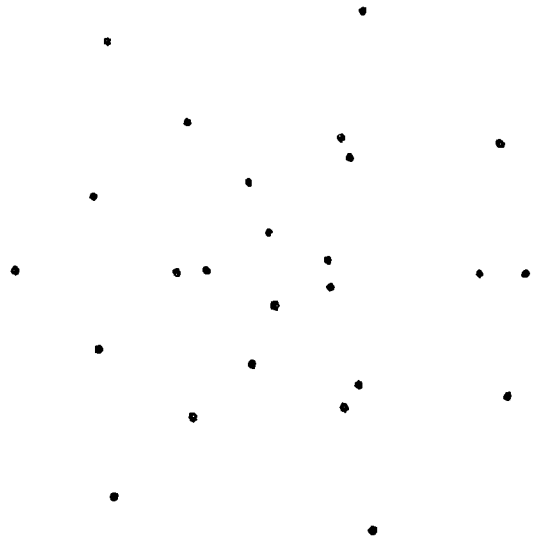

Figure 3.26 The crosscorrelation pattern of Figure 3.23 drawn by the graphical method

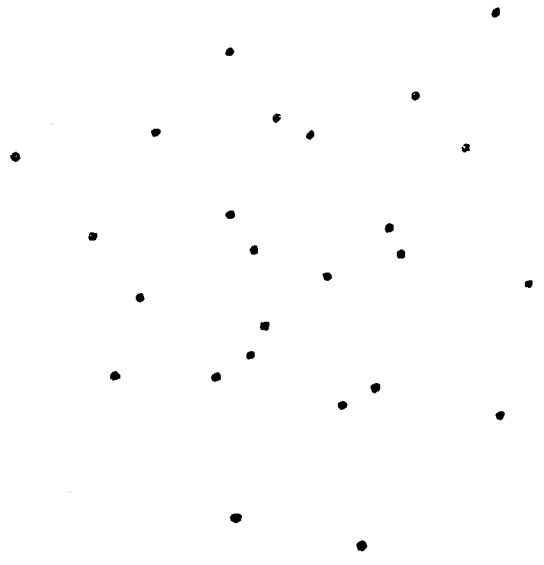

Figure 3.27 The crosscorrelation pattern of Figure 3.22 drawn by the graphical method

Figure 3.28 Decoded dilute picture (coherent experiment using 5 random-dots of equal weight)

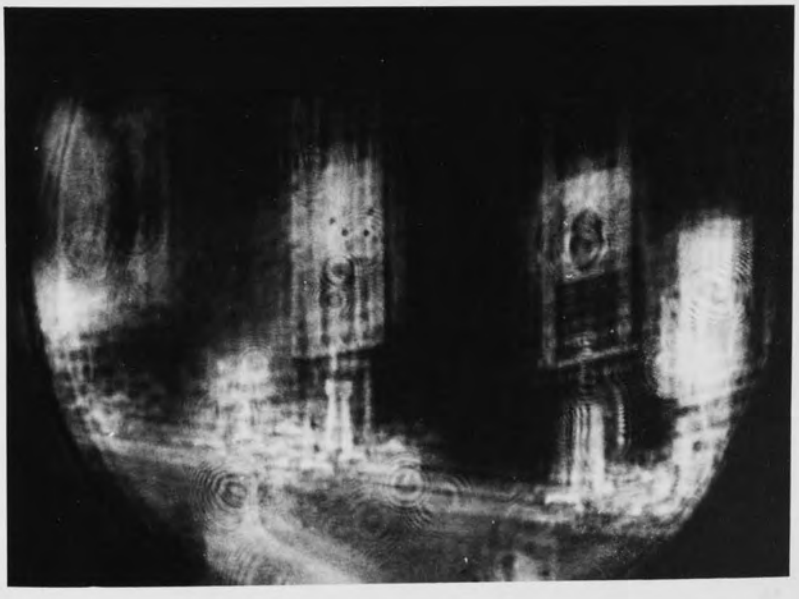

Figure 3.29 Decoded continuous-tone pictue (coherent experiment using 5 random-dots of equal weight)

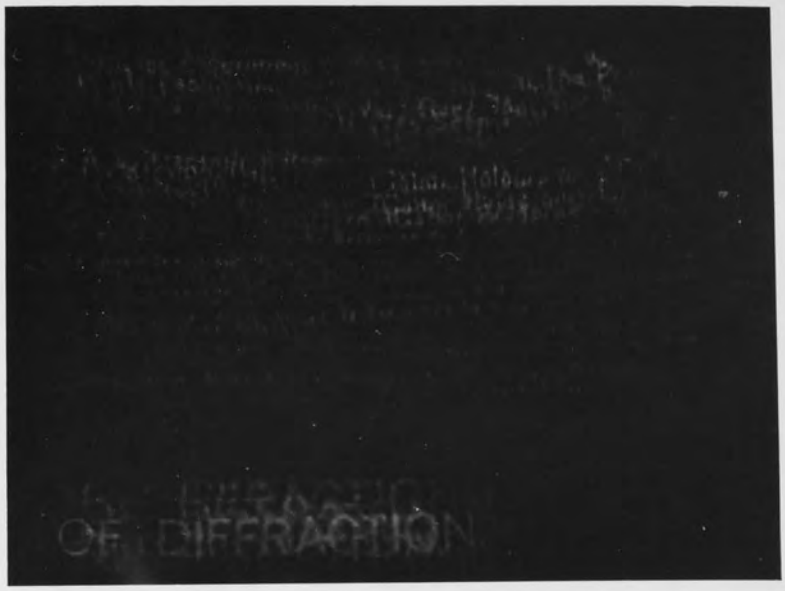

Figure 3.30. Decoded dilute picture (coherent experiment using 5 random-dots of nonequal weight)

Figure 3.31 Decoded continuous-tone picture (coherent experiment using 5 random-dots of nonequal weight)

3.33, 3.34 and 3.35) when the coded pictures were turned upside down in the coherent correlator. This position corresponds to the convolution position of the dots. The convolution pattern of the five dots has 25 dots. These are supposed to have equal intensities when the signal beam falls exactly on the centre of the hologram. But as the hologram is shifted laterally away from the lens focus, the dots start to twinkle. A position along the hologram, may exist in which some of the dots have intensities higher than the rest. One of these dots, or may be an assembly of them may act as delta function which decodes the pictures. The decoded dilute picture shown in Figure 3.35 illustrates this theory. The convolution pattern has 25 dots, therefore, one expects to see 25 letters for each letter to be coded. But since some of the letters are brighter than the rest,therefore, they show better in the decoded picture, especially if the toe of the H & D curve is used. This can be shown more clearly in the decoded letter O of the word OF, where it is easy to see that it is brighter than the rest of letters O.

The experiment reported in this section was repreated using a code consisting of 15 random dots (Figure 3.36). The autocorrelation pattern of the dots is shown in Figure 3.37. The central peak has a weight of 15 dots and is surrounded by 210 dots. The decoded dilute and continuous-tone pictures are

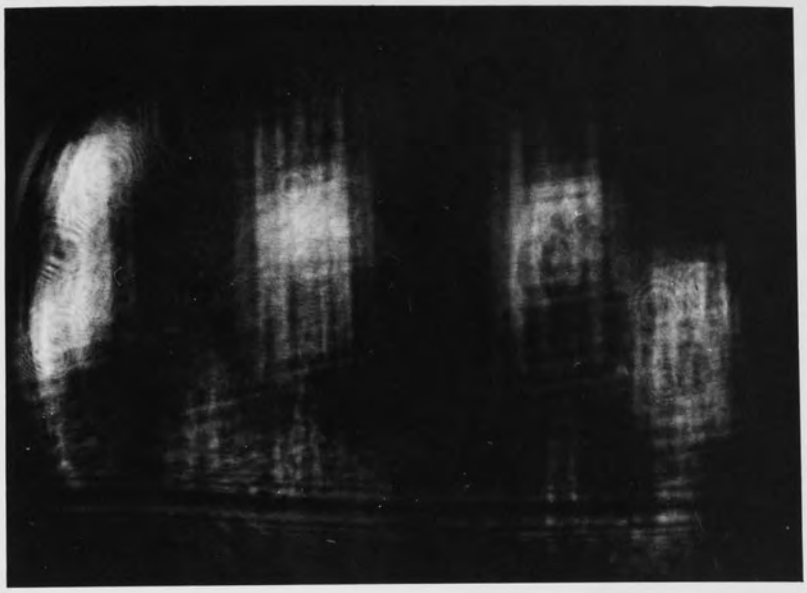

Figure 3.32 Decoding with the convolution position of the five equal dots (continuous-tone picture)

Figure 3.33 Decoding with the convolution position of the five equal dots (dilute picture)

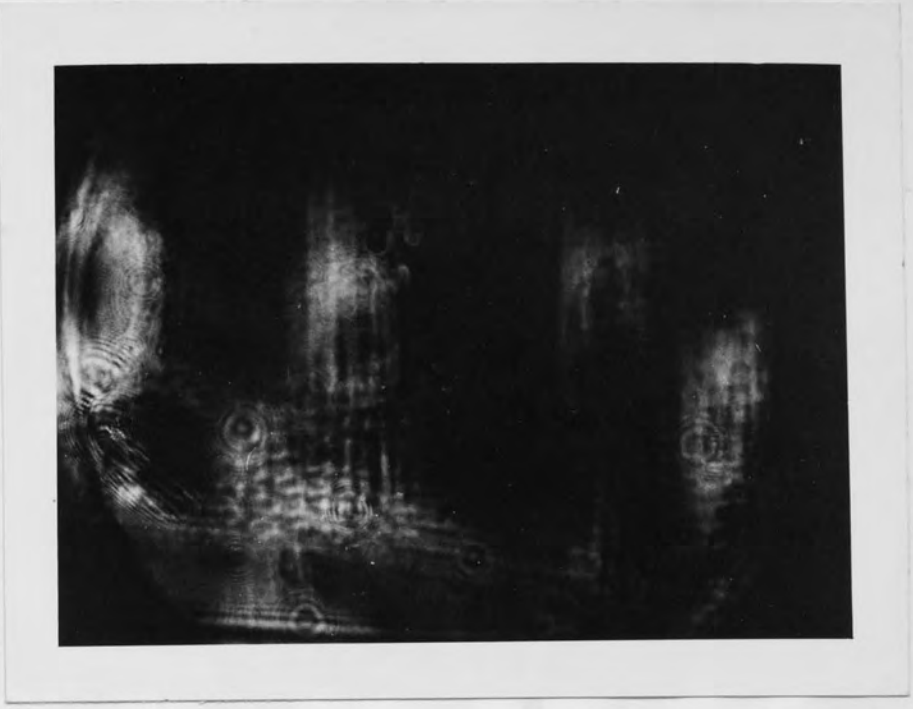

Figure 3.34 Decoding with the convolution position of the five nonequal dots (continuous-tone picture)

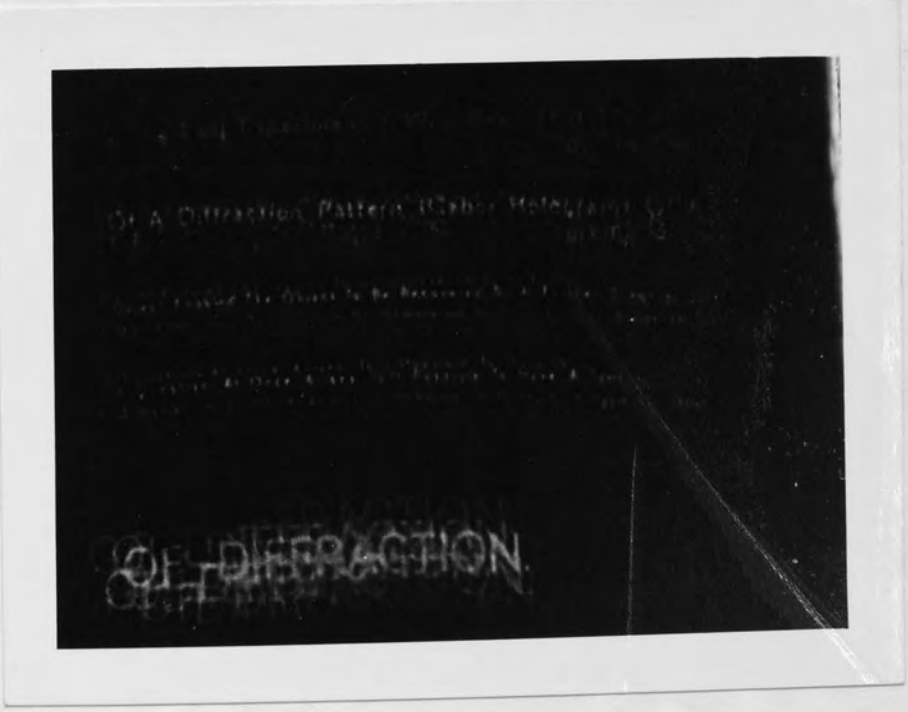

Figure 3.35 Decoding with the convolution position of the five nonequal dots (dilute picture)

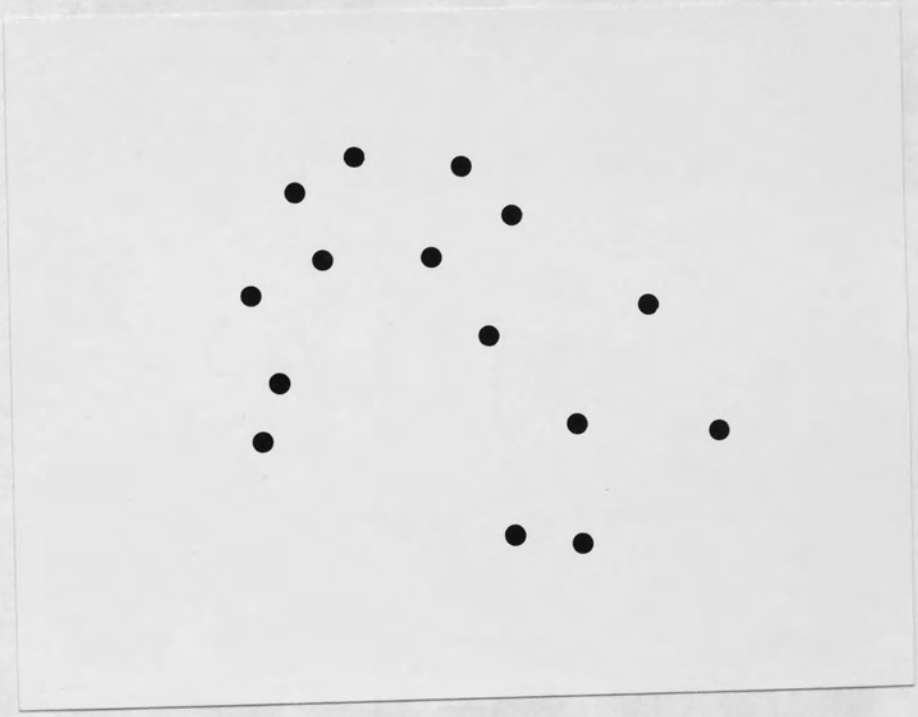

Figure 3.36 15 random-dots code

Figure 3.37 Autocorrelation pattern of the 15 random-dots

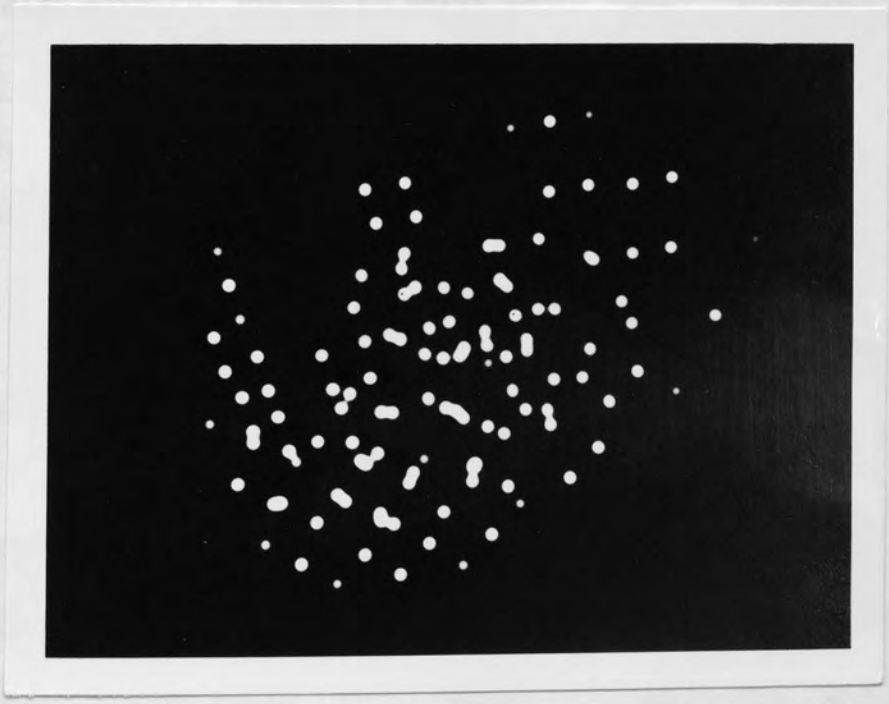

Figure 3.38 Convolution pattern of the 15 random-dots

shown in Figures 3.39 and 3.40.

The 15 dots decode the dilute picture better than the 5 dots. The peak of the 15 dots autocorrelation pattern has a weight of 15 dots while that of the 5 dots has a weight of 5 dots. In both cases each dot in the shoulder region has a weight of 1. Since most of the noise fall outside the main lines of the picture therefore the contrast of the decoded dilute picture is higher when 15 dots code is used. Hence the 15 dots decode better.

The decoded continuous-tone picture, on the other hand, shows less improvement when 15 dots are used. This is due to the fact that the signal to noise ratio in the case of the 15 dots is lower than that of the 5 dots. The SNR is shown, in section 3.4, to be equal to $1/(N-1)$. Therefore, as the number of dots increases the SNR decreases.

The dilute picture doesn't get affected by the increase of the amount of noise because most of the noise fall outside the main lines of the picture. Therefore, by careful decrease of the exposure time, the noise intensity is decreased and we end up with a decoded picture with high contrast.

The continuous-tone picture,however, does get affected

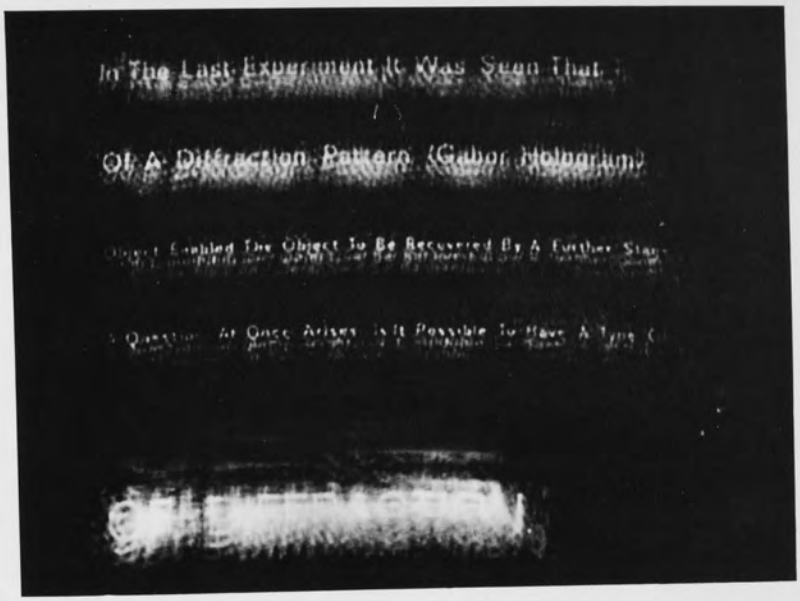

Figure 3.39 Decoded dilute picture (coherent experiment with 15 random-dots)

Figure 3.40 Decoded continuous-tone picture (coherent experiment with 15 random- dots)

by the increase of the amount of noise and decreasing the exposure time cannot reduce the effect of the noise. Therefore, as the number of dots in the code increases, the contrast of the decoded continuous-tone picture decreases.

3.6 The noncoherent decoding

Noncoherent light was used to decode the dilute and continuous-tone pictures shown in Figures 3.1 and 3.2. The method employed was based on the idea of reversing the rays involved in the process of coding.

The 15 random dots code shown in Figure 3.36 was used for producing the coded pictures. (Figures 3.41 and 3.42). The coding process was the same as the one described in Section 5.2 and the same apparatus was used.

The apparatus used for decoding the coded pictures is shown in Figure 3.43. It consists of a 1/1 magnification lens, which was constructed from two 20 cm. F/2.9 lenses, combined by placing together their object sides. A light box with a diffuse window was placed on one side of the lens and a ground-glass screen on the other side. The code transparency was put on the light-box window; its position and that of the ground-glass screen were arranged so that an image of the same size as the object was formed on the screen. A contact-printing frame was

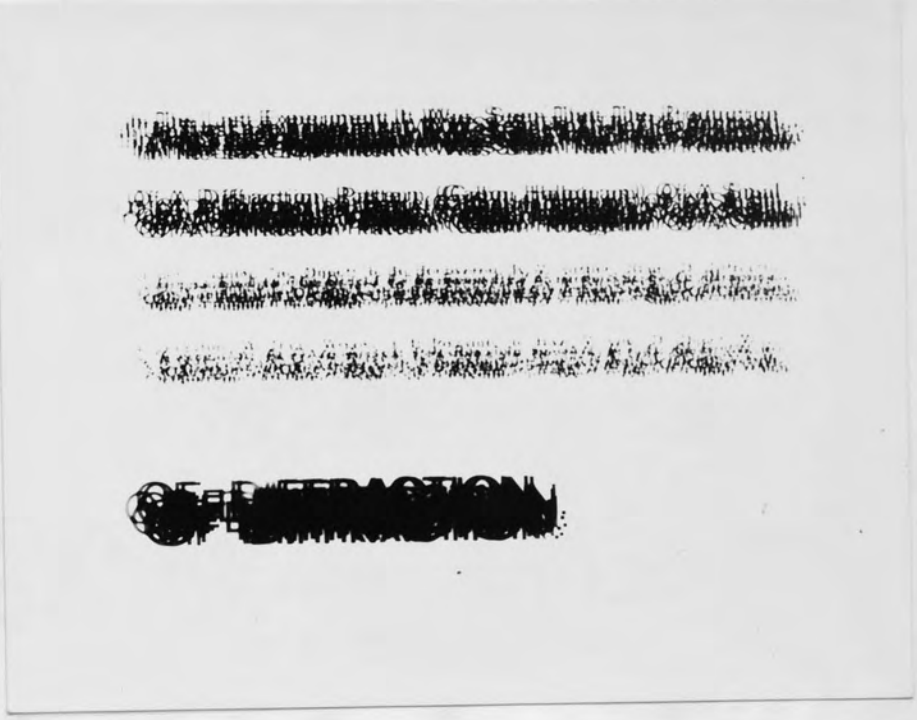

Figure 3.41 Coded dilute picture (15 random-dots)

Figure 3.42 Coded continuous-tone picture (15 random-dots)

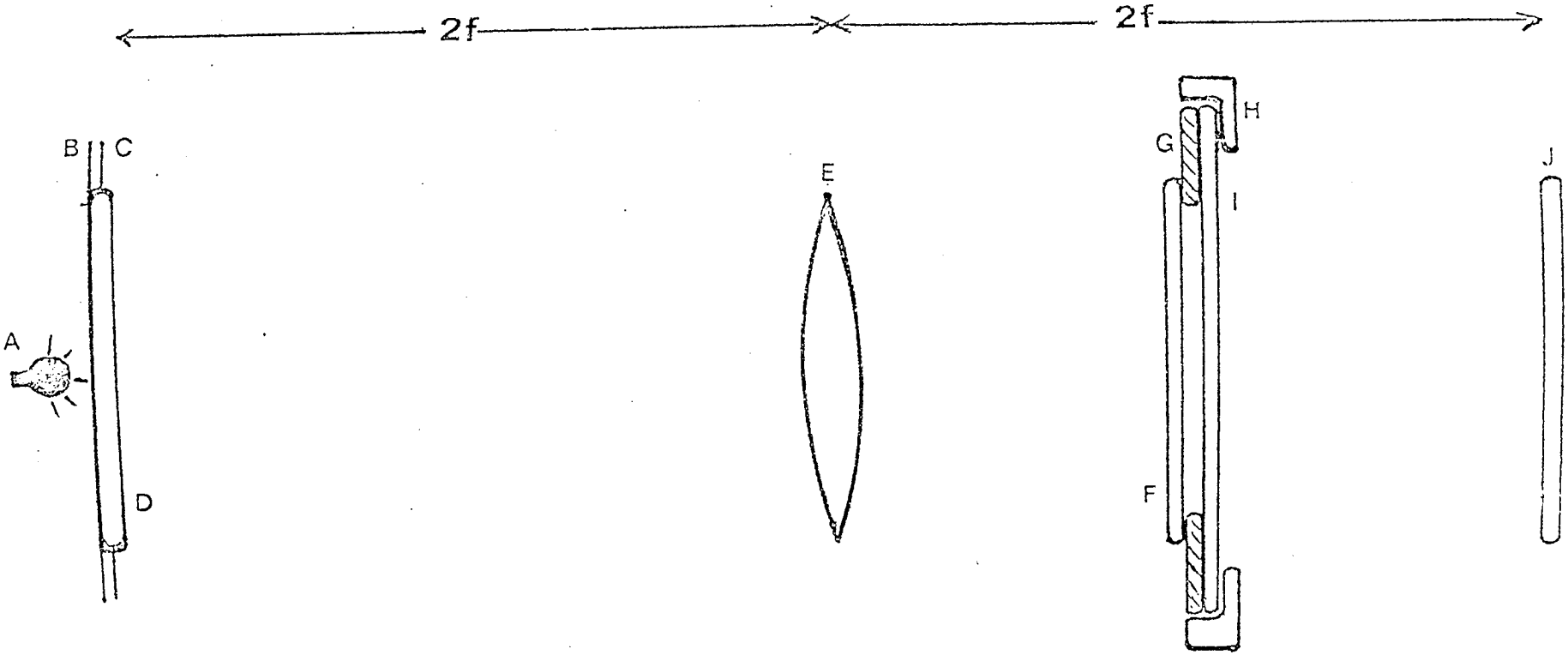

Figure 3.43 Apparatus for decoding the coded pictures.
A = Diffuse light source; B = ground-glass screen;
C = black cover to obstruct stray light;
D = random-dots plate; E = 1:1 magnification lens;
F = coded picture; G = spacer; H = contact-printing
frame; I = photographic plate; J = ground-glass
screen

inserted between the lens and the screen, 12 cm from the latter. The frame contained a photographic plate, the 3 mm spacer, used in the coding process, and the coded photograph. The coded photograph was the negative of the photograph produced by the process of coding. This was placed so that it was oriented the same way as it was in the coding apparatus.

In decoding the photograph, the photographic plate was exposed at the toe (Figure 3.10) of its H and D curve. This would reduce the amount of noise in the decoded photograph.

Ilford HP3 photographic plates were used to record the decoded image. The plates were developed with P Q Universal developer diluted by 1/9; development time was three minutes. The plates were then fixed, washed and dried as before.

The exposure time needed to decode the dilute picture; was 0.5 seconds. The continuous-tone picture needs shorter exposure time in order to be decoded. Therefore,a large sheet of neutral density filter was put over the code transparency in order to increase the exposure time for the continuous-tone object. The best exposure time needed to decode the continuous-tone picture was found to be two seconds. The decoded dilute and continuous-tone pictures are shown in Figures 3.44 and 3.45 respectively.

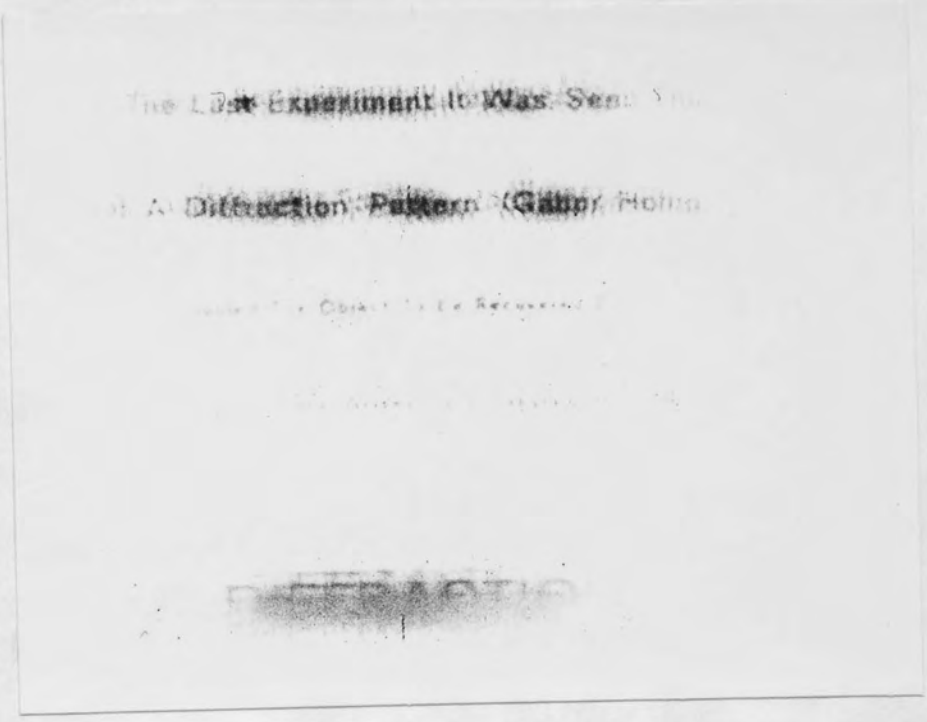

Figure 3.44 Noncoherently decoded dilute picture

Figure 3.45 Noncoherently decoded continuous-tone picture

a non redundant autocorrelation pattern, the peak has weight N and the integrated surround weigh N(N-1). Therefore, the signal to noise ratio is 1/(N-1). This assumes that the correlation is in intensity. If in amplitude, the signal to noise ratio is higher, viz $1/\sqrt{(N-1)}$. Therefore the coherent correlator is to be expected to give better results than the noncoherent.

3.8 Resolution Consideration

If we have got a large number of randomly distributed dots then the theoretical limiting resolution is determined by the minimum distance between them. A single dot or a pinhole of diameter D gives the same spatial resolution as an irregular system of dots with minimum distance between dots D.

The only frequencies F_{nm} in the object that get decoded are those which fall in the passband of the random-dots code. If these frequencies are denoted by H then the condition for resolution is

$$\sum_{n=o}^{360^o} \sum_{m=o}^{0.36\ mm} F_{nm} \leq H \leq \sum_{n=o}^{360^o} \sum_{m=2.37mm}^{\infty} F_{nm}$$

Where 0.36 mm and 2.37 mm are the minimum and maximum distances, respectively, between dots in the out of focus point spread function of the 15 dots.

The size of the out of focus point spread function is of the same order of magnitude as the size of OF DIFFRACTION letters

and the minimum distance between dots is of the same order of magnitude as the height of the fourth row of the dilute picture. Therefore, the first, second and third rows decode well, because they fall in the middle of the passband of the dots, the fourth and the sixth show little improvement and the fifth does not show any sign of decoding.

As the defocus distance, in the coding process increases the scale of the out of focus point spread function increases and therefore the resolution lower limit increases. Therefore, we do not expect any decoding when the defocus distance is increased so that the lower band width frequency of the code is higher than the upper band width frequency of the object.

References

1. Gabor D. Proc.Roy.Soc (London) 127, 454 (1949)
2. Rogers G.L. Nature, 166 237 (1950)
3. Mertz L. and Young N.O. Proc. of the International Conference on Optical Instrumentation (Chapman and Hall, London 1961) P.305
4. Barrett H.H. J.of Nuclear Medicine 13 382 (1972)
5. Rogers W.L. Han K.S. Jones L.W. and Beirwalters W.H. J. of Nuclear Medicine 13 612 (1972)
6. Rogers W.L. Jones L.W and Bierwalters W.H. Optical Engineering 12 13 (1973)
7. Barret H.H. Wilson D.T. De Meester G.D. and Schorman H. Optical Engineering 12 8 (1973)

8. Barret H. Garewal K. and Wilson D.T. Radiology 104 429 (1972)

9. Barrett H.H. Wilson D.T. and De Meester G.D. Optics Communications, 5 398 (1972)

10. Wilson D.T. De Meester Barrett H.H. and Barsak E. Optics Communications 8 384 (1973)

11. Dicke R.H. Astrophysics J., 153 101 (1968)

12. Alqazzaz L.and Rogers G.L. J.O.S.A. 65 695 (1975)

13. Weis, in Proc of the International Optical Computing Conference (I.E.E.E. Zurich 1974) P.41

14. Stroke G.W. "An Introduction to Coherent Optics and Holography, "Academic Press (1966) P82

15. Klotz E and Weiss H. Optics Communications 11 368 (1974)

16. McLachlan D, J.O.S.A. 52 454 (1962)

17. Vander Lugt A.B. I.E.E.E. Trans. Information Theory 10 139 (1964)

18. Rogers G.L. J.Sci.Instrum. 43 763 (1966)

CHAPTER 4

FOURIER IMAGES

4.1. Introduction

The idea of forming an image of an object in two stages has long been recognized. In 1873 Ernst Abbe (1) succeeded in formulating the principles involved in the formation of images in the microscope. According to Abbe's theory, the image in the microscope is formed in two steps. In the first step Fraunhofer diffraction pattern of the object is formed at the back focal plane of the lens. In the second step the Fraunhofer pattern diffracts into a Fresnel pattern, at a further distance from the lens, which is the image. These two steps, although in reality following each other immediately, nevertheless can be separated if so desired.

Image formation by holography (2,3) is a two stage process as well. A Fresnel diffraction pattern of the object is recorded in the first stage. The record is called a hologram and it contains amplitude as well as phase information about the object. The second stage involves reconstructing this hologram by illuminating it with an unomdulated coherent beam.

A question may arise. Does there exist an object which diffracts into an image of itself in a single stage of diffraction ? An observation made by Fox Talbot (4) in 1836 showed that

such an object exists. This object is, in its simplest form, a linear diffraction grating. If the grating is illuminated with coherent light, then at finite distances from the grating, exact images of the grating are formed. Lord Rayleigh (5) first deduced the distance between reconstructions of the grating for parallel monochromatic light. Cowley and Moodie (6) obtained a Fourier series expression for the amplitude of the diffraction images and therefore called them Fourier images.

Intermediate images, other than the object's reconstruction, were also observed (6,7,8). These were termed Fresnel images by Winthrop and Worthington (9). Fresnel images were thought to play a role in the vision of insects (10,11).

Fourier images may be regarded as a special case of in-line holography wnere the object and its hologram are identical. If a parallel beam of light is used to produce the Fourier images then the distance between the hologram and its reconstruction is the focal length of the hologram, as defined by zone plate analogy (12). According to the calculations of Rayleigh (5) the focal length of a linear diffraction grating is $\frac{2a^2}{\lambda}$ where a is the repeat distance of the grating. Rogers (11) however, found that a replica of the grating can be found at a distance of $\frac{a^2}{\lambda}$ from the grating, but this is shifted by $\frac{a}{2}$. He called this a half order image. Square and hexagonal lattices

have focal lengths of $\frac{2a^2}{\lambda}$ and $\frac{3a^2}{2\lambda}$ respectively.

A collimated beam of light produces a large number of Fourier images. Each image acts as its own hologram and produces the next image. These images are produced at distances of Nf from the diffraction grating. When N is an integer representing the order number and f is the focal length of the grating. The number of orders produced depends on the lateral extent of the grating and on the coherence length of the light source.

Suborders or intermediate images can be observed at distances $\frac{f}{n}$ from each reconstruction.These suborders differ from the main orders in phase and in general are more complex than the main orders. It is desirable that the original grating be largely opaque to develop clear suborders (13).

Rogers(11) compiled a list of multiplicities of the suborder image patterns of a grating and a hexagonal array of pinholes. In order to account for his experimental results he made calculations by computer for both the linear grating (14) and the hexagonal array (15). In these calculations he established the position, spacing and phases of the diffraction images.

Winthrop and Worthington (9) presented a theory of Fresnel images for plane periodic object. Their analysis resulted from applying the Fresnel-Kirchoff equation to a plane periodic

object in monochromatic light. This leads to consideration of multiplicity, shift of origin, phases, and intensities of the Fresnel patterns.

4.2. Confusion in recognition of images formed in coherent light

Coherent light is, quite often, used for illuminating the object in microscopy. This is particularly true in the case of electron microscopy, where the electrons proceed from a very fine source and the illumination is therefore very coherent. Such coherent illumination gives rise to definite diffraction patterns (17) which may have higher contrast and greater subjective sharpness than the true image of the object. If there is not a priori knowledge or hypothesis about a given structure, one can focus through a series of diffraction patterns and not know which to choose as the true image.

Coherently illuminated repeated objects give rise to Fourier Images. These are usually high contrast repeated structures. Therefore, if one does not know the object forming the Fourier Images then one may choose, as the true image, an Intermediate Fourier Image of a certain shape that may resemble a different object. It has been shown (16) that such confusion occurs between one of the intermediate Fourier Images of a graphite structure lattice and one of the main order Fourier Images of a hexagonal array of black dots.

Cowley and Moodie (6) claimed that diffraction processes could be used in electron microscopy to produce an enlarged image of a crystal lattice or other repeated structure, and that the image could be isolated from the rest of diffraction patterns. This claim conflicts with the idea expressed above and was modified later (8). But the fact that it was made, confirm the idea of confusion.

4.3. Theorems governing the formation of Fourier Images

(1) Huygens' principle

According to Huygens' principle, every point of a wavefront may be considered as the source of a small secondary wavelet which spreads in all directions from the point at the wave propagation velocity. A new wavefront is found by constructing a surface tangent to all the secondary wavelets. Therefore given the amplitude and relative phase of a wavefront on an initial surface, the amplitude and phase of the wavefront at any subsequent time can be calculated. By an extension of the method, an amplitude-phase pattern can also be calculated at any prior time. The pattern in this case is regarded as a virtual pattern, observable only by an imaging system receiving light after passage through the initial surface.

Fourier Images, in all cases,are Fresnel diffraction patterns of the original repeated object. Therefore, they are, by Hugyhens principle, equivalent to each other. If photographs are taken for these Fourier Images then the phase

information will be lost and the recorded images will look different.

Huygens principle can also be used to calculate the Fourier transform of complex objects. If a complex object is placed in the front focal plane of a lens and illuminated by collimated coherent light then the amplitude-phase or complex pattern formed in the back focal plane of the lens is called the Fourier transform of the complex object. The amplitude content of the Fourier transform is called the Fraunhofer diffraction pattern. We cannot, of course, see the amplitude but we see its squared modulus, or the intensity pattern.

Fourier images generated from the same object have Fourier Transforms that have the same amplitude but different phase. The phase of any of these transforms differs from the phase of another by a term of the form

$$\mathrm{Exp}\left\{ \frac{2\pi i}{\lambda} \quad p \quad \frac{\alpha^2}{2} \right\},$$

where α is the angle between the axis and a ray from the centre of the transform lens to a given point in the back focal plane and p represents the Newtonian distance from the front focal plane of the lens to the planes of the Fourier images. The transforms of the Fourier Images thus appear the same visually, i.e. they have the same Fraunhofer pattern, as defined above. The fact that these images all have the same Fraunhofer diffraction pattern

is a reason for the belief that they are not easily distinguished.

Figure 4.1 shows five photographs of Fourier Images with their corresponding Fraunhofer diffraction patterns. Four of these images were derived from a graphite structure lattice and the fifth was from a lattice of small hexagonal dots (the graphite structure lattice and the small hexagonal dots lattice are shown in Figure 4.2). The Fourier images derived from the graphite structure have the same Fraunhofer pattern. This is different from the Fraunhofer pattern of the Fourier image derived from the small hexagonal dots lattice.

The Fourier images derived from the same object have the same spatial frequencies and this is the reason why they have the same Fraunhofer pattern. The Fourier image derived from the different object, on the other hand, has different spatial frequencies and therefore it produces different Fraunhofer pattern.

Photographs of Fourier images derived from the same object look different (Figure 4.1). The reason is that the lateral phase of the Fresnel diffraction pattern (the Fourier image) changes along the beam. This phase change tends to redistribute the spatial frequencies in the Fourier image. Therefore, photographs taken at different positions along the beam show different Fresnel patterns because of the

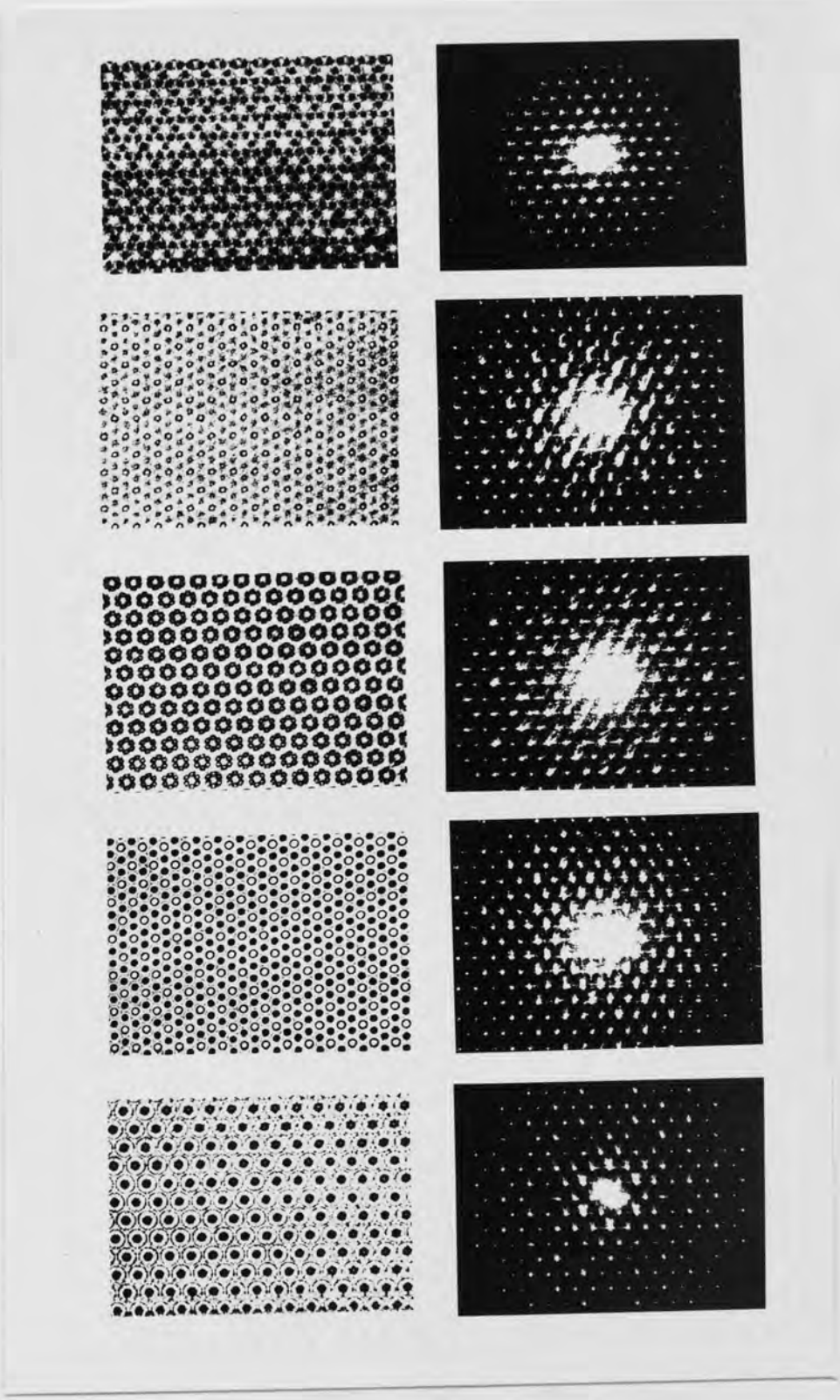

Figure 4.1 Fourier images with their corresponding Fraunhofer diffraction patterns

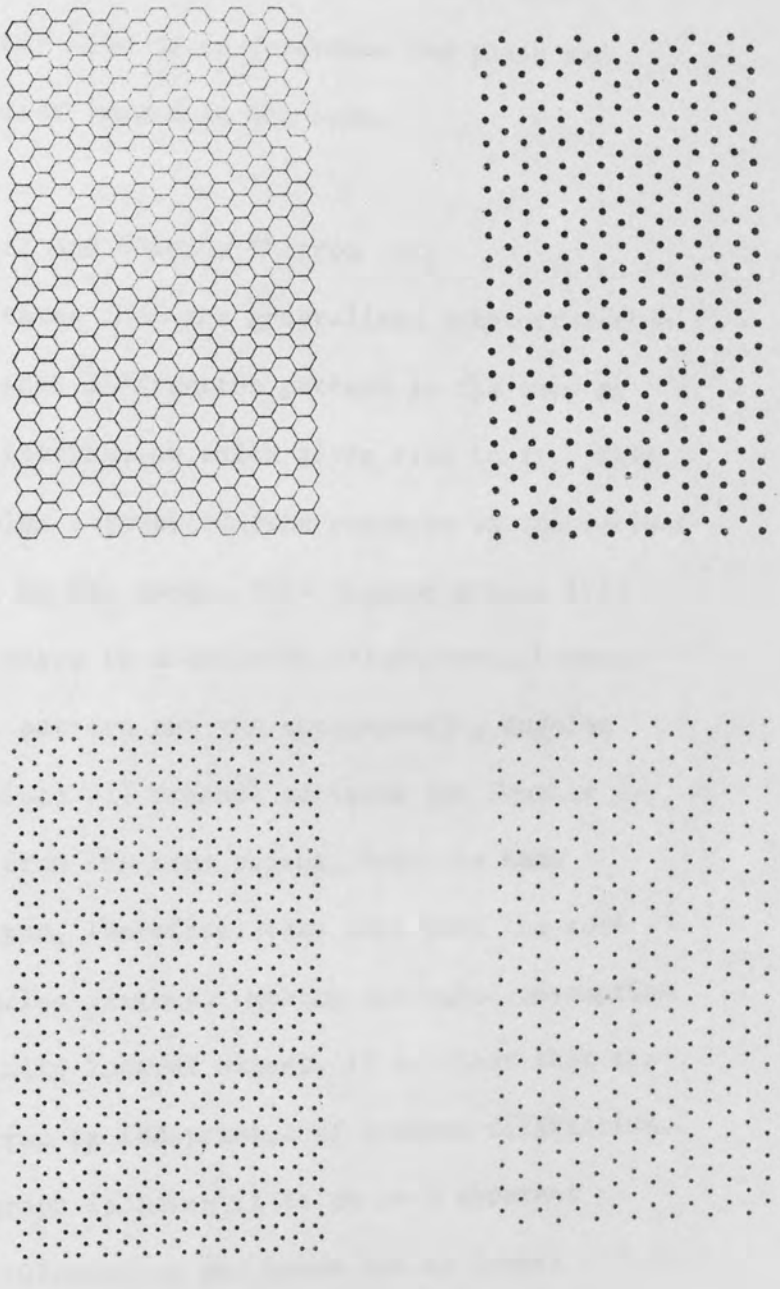

Figure 4.2 Lattices for demonstrating Fourier images

different arrangement of the spatial frequencies. Study of these arrangements may lead us to determine the phase and position of the Fourier images in the beam.

(2) Booker, Ratcliff and Shinn's Theorem (11)

This theorem states that the generalized autocorrelation function of the Fresnel diffraction pattern is the same as that of the field distribution which gives rise to it. This means that the complex autocorrelation patterns of the various Fourier images must be the same. This theorem arises from the fact (19) that there is a definite relationship between the autocorrelation pattern and the corresponding angular power spectrum. Since all Fresnel patterns (or Fourier images), generated from the same object, have the same angular power spectrum, therefore, they must have the same complex autocorrelation pattern. Making the usual assumption of patterns of infinite lateral extent, it is clear that the angular power spectrum is independent of Fresnel diffraction. As soon as a photograph is taken it is at once apparent that we lose phase information and hence can no longer calculate the complex autocorrelation pattern of the field from the photograph. Nevertheless it is reasonable to expect that the basic repeat distances of the original object will feature in the photograph, except in the interesting case where an amplitude contrast object has transformed into a pure phase contrast image. It has also been observed (15) that

other repeat distances appear prominently, but these are harmonies of the basic frequency.

The Booker, Ratcliff and Shinn theorem is one of the greatest power and generality. It defines a property of any coherent system of Fresnel diffraction patterns. It can be regarded as defining a minimal degree of information conveyed by the wavefront, information which is invariant and indestructible in normal uninhibited propagation. The complex autocorrelation function is thus the invariant representation of the minimal information in the beam.

It was thought useful to make correlation experiments between a number of Fourier image photographs. In view of the confusion mentioned in section 4.2 between simple hexagonal lattices and graphite structures, examples from each series are included. The results serve only to confirm the possibility of confusion.

4.4 . Coherent correlation experiment

The Fourier images transparencies, used in this experiment, were originally made by Mr.Barry Brooks, for use on a different experiment. Drawings of small hexagonal dots, large hexagonal dots, honeycomb lattice and graphite structure (Figure 4.2) were photographed so that their dimensions were reduced to about 2.5 x 4 mm. The photographic plate was mounted between two optical flats and was put in a parallel coherent beam of light.

Fourier images were produced. The Fourier images that had an interesting arrangement were photographed by a 35 mm camera moving along the beam. The Fourier images were then printed on Ilford N30 plates so that they had dimensions of 4 x 2.5 cm.

Five transparencies were used as objects in this experiment. Each was derived as a Fourier image, four of them were from a graphite structure, the fifth was from a lattice of small hexagonal clots. Each one of these transparencies was put between two optical flats.

4.4.1 Initial Procedure

A circular hole of about 2 mm, in diameter was punched on middle of large piece of black cellotape. The cellotape was arranged to cover the small dots transparency such that only one or two cells can appear. The transparency was then put at the front focal plane of the transform lens of the coherent correlater used in Chapter 3. Fourier transform hologram was recorded at the back focal plane of the lens.

After processing this hologram it was mounted on its original position, such that the holographic spot fell on the focus of the transform lens. This was checked with a watchmaker's lens. In order to check for the correlation efficiency of the hologram its reconstruction efficiency has to be checked. The signal beam was obstructed and the hologram reconstruction

was viewed by looking along the obstructed beam. The reference beam was then obstructed and the telescope was put behind the hologram so that its objective facing the holographic spot and its optical axis parallel to the direction of the obstructed reference beam. When the signal beam was allowed to fall on the hologram, correlation spots were observed on the object's cells. When the cellotape was removed from the transparency, correlation spots were seen to cover all the dots pattern, the reason for that is because the pattern is of similar cells.

One hologram was taken, by the same method described above, for each of the four graphite structure lattices and for the small hexagonal dots lattice. Each of these five holograms was allowed to correlate with each of the five lattice patterns and the correlation patterns produced were photographed using Fed F/2.8 camera Ilford FP4 film. The extent of correlation in these patterns is illustrated in the following table :

Transparency No	Hologram of transparency No 26 (small hexagonal dots)	Hologram of transparency No 29 (Graphite Structure)	Hologram of transparency No 30 (Graphite Structure)	Hologram of transparency No 32 (Graphite Structure)	Hologram of transparency No 33 (Graphite Structure)
26	Good	Good	Good	Good	Good
29	Bad	Good	Good	Good	Good
30	Good	Good	Good	Good	Good
32	Bad	Bad	Good	Good	Good
33	Bad	Bad	Bad	Bad	Bad

Table 4.1

4.4.2 Practical consideration

The transform lens in the coherent correlator produces a very fine diffraction pattern on the hologram plate. This is more evident when the object used to form the hologram is large. In this case the intensity of the signal beam over the plate will be about 3 or 4 orders of magnitude greater than the reference beam. This will produce low contrast holographic fringes and the reconstruction will therefore be very poor. This can be overcome in either or both of two ways.

1. Introducing neutral density filter into the signal beam :

Neutral density filters absorb light of all wavelengths equally throughout the visible spectrum and thus permits the reduction of light intensity by a definite ratio.

Kodak Wratten neutral density filters were used. These are gelatine filters of density running from 0.1 up to 2.0 according to the manufacturer's specifications. Other densities can be built up by combining two or more filters. The use of gelatine filters has the advantage that they are thin and therefore do not produce any change in the signal beam path length, even when they are combined. Care was taken in handling the filters since they are easily vulnerable to pollution.

The filter's aim is to equate the intensity of the signal beam with the reference beam and therefore produce high contrast holographic fringes. The value of the filter used depends on the size and the intensity transmittance of the object. The

filters were usually put in front of the transform lens.

2. Recording the hologram outside the transform lens focus:

The hologram was usually shifted out of the focal plane by an amount of 2 - 10 % of the basic focal length, during recording and brought back to the focal plane during reconstruction. This was done in order to utilize higher light intensity during reconstruction corresponding to relatively weaker one during recording. This would produce brighter and more evident reconstructions. The intensity of the signal beam in the recording would be reduced as well, resulting in improvement in the fringes contrast and therefore the reconstructed image.

4.4.3 .Improving the matched filter

Correlation tables between number of transparencies and their holograms should be symmetrical round their autocorrelation axes, and their autocorrelation positions should show good correlation (i.e. bright distinct dots). This is not the case with Table 4.1 which shows a bad symmetry as well as having a bad autocorrelation pattern.

The main source of error in the experiment was the matched filter.Synthesis of the matched filter needed critical combination of neutral density filter, defocusing and exposure time. In the experiment of Section 4.4.1, 3 cm defocus distance, ND.O.8 neutral density filter and two seconds exposure time

were used. For producing better results the following techniques were suggested :

1. Use of low contrast developer

In order to use all the information in the holographic spot, the hologram was recorded with very short defocus distance. This needed more neutral density filters to be put into the signal beam.

Ilford Holographic plates were usually used for recording the holograms. These were developed with Kodak D8 developer diluted by 1 :1. The D8 developer is a high contrast developer which tends to increase the density of the holographic spot, especially at the central part. If a hologram is recorded near the transform lens focus then the central part of the spot will act as a stop that reduces the resolution of the reconstructed image.

In order to overcome this problem, a low contrast developer like Ilford PQ Universal was used instead of the D8 developer. The development time was pushed up to 5 minutes instead of the 3 minutes used with the D8 developer.

Five holograms for the five transparencies used in Section 4.4.1 were recorded and developed with PQ Universal. The exposure time was 4 seconds, defocus distance was 3 mm, and a ND. 1.5 neutral density filter was in the beam.

The transparencies were allowed to correlate with the hologram and the correlation table was drawn (Table 4.2)

Transparency No.	Hologram of Transparency No 26 (small hexagonal dots)	Hologram of Transparency No 29 (Graphite Structure)	Hologram of Transparency No 30 (Graphite Structure)	Hologram of Transparency No 32 (Graphite Structure)	Hologram of Transparency No 33 (Graphite Structure)
26	Good	Good	Good	Good	Good
29	Good	Good	Good	Good	Good
30	Good	Good	Good	Good	Bad
32	Bad	Good	Good	Good	Bad
33	Good	Bad	Bad	Bad	Good

Table 4.2

2. Bleaching the filter

The matched filter may be bleached to form a phase hologram with a high diffraction efficiency. The bleaching process dissolves (or changes into transparent compounds) the metallic silver from the emulsion, leaving "holes" that introduce an effective phase variation in the wave transmitted.

Chromium Intensifier (with double strength HCl) was employed to bleach the five holograms used to produce Table 4.2. The holograms were put in the bleach for 3 minutes, washed in running water for 10 minutes then dried. They were then mounted on their original position in the optical bench and reconstructed

by the unmodulated reconstructing beam. The reconstructed image was brighter than before but it was degraded by flare light. The degradation was more severe when the hologram was reconstructed with the signal beam. The correlation image in this case was completely obstructed by noise and flare.

The flare light was primarily caused by a low frequency modulation due to the speckle pattern that was recorded on the plate. These modulations could be reduced by processing the plate with the reversal bleach process (20). In this process the index of refraction is greatest when the emulsion is thinnest. This causes a partial cancellation of the low spatial frequency modulation and therefore reduces the flare about the image.

Five holograms were recorded for the five transparencies that were used in the experiment. The recording was made with the holograms 3 mm. out of focus and a ND. 1.5 neutral density filter in the signal beam. The holograms were processed with the reversal bleach process. A detailed description of the process can be shown in Reference 20.

The transparencies were allowed to correlate with the holograms and the correlation table was drawn (Table 4.3)

Transparency No.	Hologram of Transparency No 26 (small hexagonal dots)	Hologram of Transparency No 29 (Graphite Structure)	Hologram of Transparency No 30 (Graphite Structure)	Hologram of Transparency No 32 (Graphite Structure)	Hologram of Transparency No 33 (Graphite Structure)
26	Good	Good	Good	Good	Good
29	Bad	Good	Good	Good	Bad
30	Good	Good	Good	Good	Good
32	Bad	Bad	Bad	Good	Good
33	Good	Good	Good	Good	Good

Table 4.3

3. Centring the holographic spot

In this method, the five holograms processed by the reversal bleaching were centred, more accurately, at the lens focus.

Each one of the holograms was first placed at the transform lens focus by the usual method described in 4.4.1. The undiffracted light emerging from the hologram was then received on a white sheet of paper. The shadow of the hologram was observed on the paper. The hologram was then moved along the bench till the shadow covers the whole aperture of the undiffracted light. This brought the hologram exactly on the focal plane of the lens. The pinhole filtering the laser beam was then dealigned so that weak beam of light emerged from it. A microscope was

placed in a horizontal position along the bench so that it focussed on the Fraunhofer diffraction pattern of the object. The holographic spot was then brought to the diffraction pattern so that its zero order fell on the middle of the spot. The microscope was then removed, the laser realigned and the correlation position viewed.

The correlation patterns of the five transparencies were observed. The extent of the correlation is shown in Table 4.4.

Transparency No.	Hologram of Transparency No 26 (small hexagonal dots)	Hologram of Transparency No 29 (Graphite Structure)	Hologram of Transparency No 30 (Graphite Structure)	Hologram of Transparency No 32 (Graphite Structure)	Hologram of Transparency No 33 (Graphite Structure)
26	Good	Good	Good	Good	Good
29	Good	Good	Good	Bad	Good
30	Good	Good	Good	Good	Good
32	Bad	Bad	Bad	Good	Good
33	Bad	Bad	Good	Good	Good

Table 4.4

Five holograms were prepared with ND.0.7 neutral density filter, 3 mm. defocus distance and 4 seconds exposure time. These were processed with PQ Universal in the usual way. They were then positioned at the transform lens focus and centred there by the method described above. The correlation patterns were observed and the correlation table was drawn (Table 4.5).

Transparency No	Hologram of Transparency No 26 (small hexagonal dots)	Hologram of Transparency No 29 (Graphite Structure)	Hologram of Transparency No 30 (Graphite Structure)	Hologram of Transparency No 32 (Graphite Structure)	Hologram of Transparency No 33 (Graphite Structure)
26	Good	Good	Good	Bad	Good
29	Bad	Good	Good	Bad	Good
30	Good	Good	Good	Good	Good
32	Bad	Bad	Bad	Good	Bad
33	Bad	Good	Good	Good	Good

Table 4.5

4. Correlating with a larger object sample

The hole in the mask used in recording the hologram was increased in size such that it covered one fourth of the lattice structure. Holograms were recorded for the five lattices and processed in the usual way. They were then allowed to correlate with the five lattices using the holographic spot centring technique. The extent of correlation is shown in Table 4.6

Transparency No	Hologram of Transparency No 26 (small hexagonal dots)	Hologram of Transparency No 29 (Graphite Structure)	Hologram of Transparency No 30 (Graphite Structure)	Hologram of Transparency No 32 (Graphite Structure)	Hologram of Transparency No 33 (Graphite Structure)
26	Good	Good	Good	Good	Good
29	Good	Good	Good	Good	Good
30	Good	Good	Good	Good	Good
32	Bad	Bad	Bad	Good	Bad
33	Good	Bad	Good	Good	Good

4.4.4. Conclusions

The main source of difficulty in formulating Tables 4.1 - 4.6 was the judgment on whether a particular correlation pattern represents a good or a bad correlation.This arises from the fact that there is no distinct limit between the two.

The different methods of improving the correlation in the coherent correlater did not produce perfect symmetry in the correlation table. Nevertheless it can be seen, in general, that transparency No. 32 has bad correlation with transparencies No. 26, 29 and 30 and transparency No. 33 has bad correlation with transparency No. 29. Therefore the optimum correlation table can be put as shown in Table 4.7.

Transparency No	Hologram of Transparency No 26 (small hexagonal dots)	Hologram of Transparency No 29 (Graphite Structure)	Hologram of Transparency No 30 (Graphite Structure)	Hologram of Transparency No 32 (Graphite Structure)	Hologram of Transparency No 33 (Graphite Structure)
26	Good	Good	Good	Bad	Good
29	Good	Good	Good	Bad	Bad
30	Good	Good	Good	Bad	Good
32	Bad	Bad	Bad	Good	Good
33	Good	Bad	Good	Good	Good

Table 4.7

Bleaching the holograms with the reversal bleach process and centring it over the transform lens focus with the microscope was the best method for producing better correlation. It produced a single deviation from the optimum correlation table cited above.

The coherent correlater does not correlate the spatial frequencies of the Fourier images only, but the phases between them as well. We shall call this Complex Spatial Frequency.

Fourier Images produce good correlation when their complex spatial frequencies are similar, or in other words the arrangement of their spatial frequencies is similar.

The small hexagonal dots and the graphite structure have common spatial frequencies. Therefore, there may exist a Fourier Image derived from one of them, which has similar complex spatial frequencies as a Fourier image derived from the other and therefore produce good correlation. On the other hand, there may exist some Fourier Images derived from the same object but have different complex spatial frequencies and therefore produce bad correlation.

Table 4.7 confirms this idea. It shows that transparency No 26, of small hexagonal dots, correlate with transparency No 30, of graphite structure. It shows as well that transparency No 29 does not correlate with transparency No 32 in spite of both being from the same graphite structure. Figures 4.3, 4.4 and 4.5 show

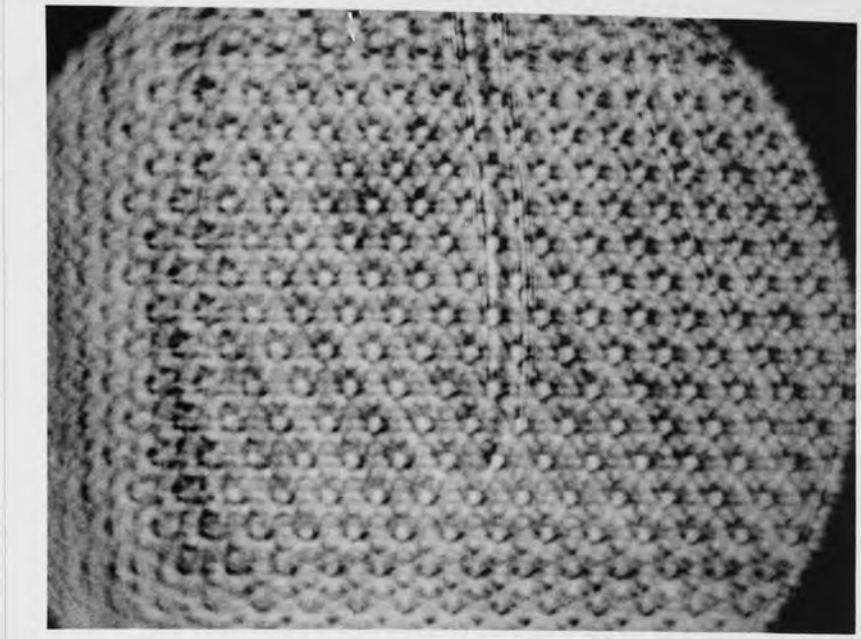

Figure 4.3 Autocorrelation pattern of transparency No. 29

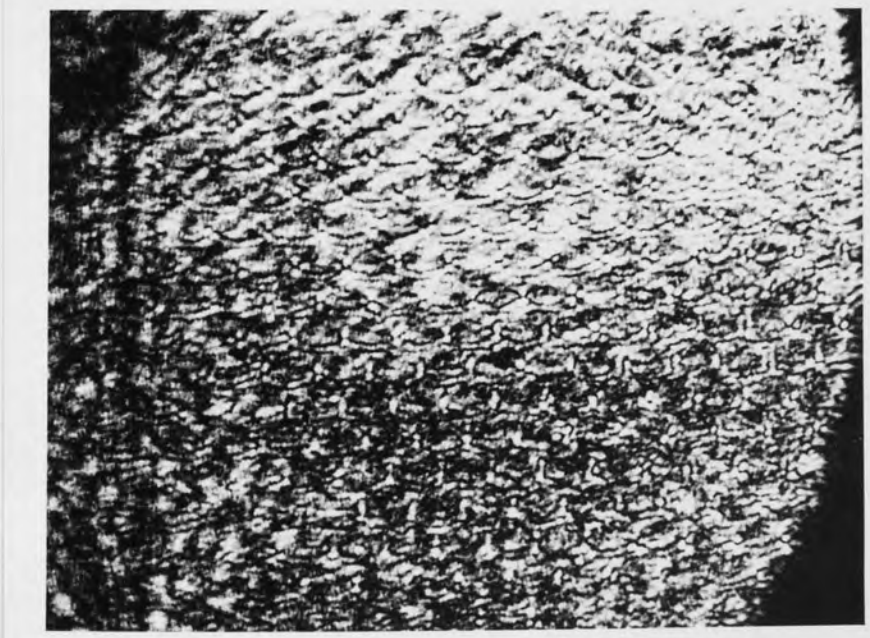

Figure 4.4 Bad correlation between transparency No. 30 of graphite structure and transparency No. 32 of graphite structure too

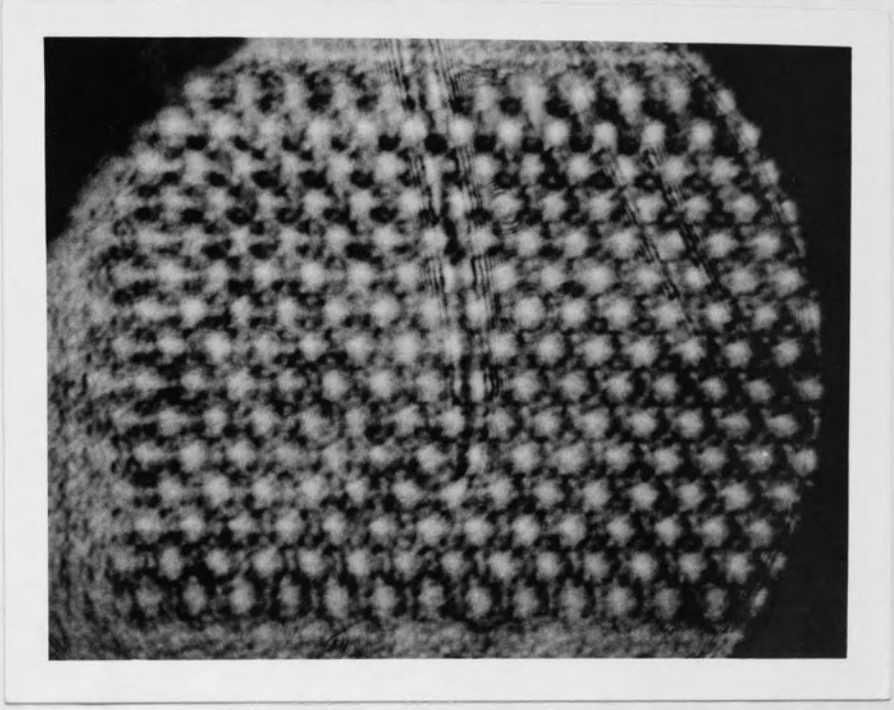

Figure 4.5 Good Correlation between transparency No. 33 of graphite structure and transparency No. 26 of hexagonal dots

three examples of the correlation of Fourier images, an auto-correlation pattern, a bad correlation between two Fourier images derived from the graphite structure lattice and a good correlation between two Fourier images derived from the graphite structure lattice and the small hexagonal dots lattice.

Fourier images derived from the same object are expected to produce good correlation when they are correlated with each other. On the other hand they are expected to produce bad correlation when they are correlated with Fourier images derived from a different object. The fact, illustrated in Table 4.7, that they do not follow this rule confirms the idea of confusion reported in 4.2.

4.5. Noncoherent correlation experiment

Five new Fourier images were printed on Ilford N30 plates from the 35 mm film mentioned in 4.4 that contains photographs of the Fourier images. Two of these images were derived from the honeycomb lattice, two from the graphite structure lattice and one from the large hexagonal dots lattice. The noncoherent correlater (Figure 3.15) mentioned in Chapters 2 and 3 was used to correlate the five resulting transparencies.

4.5.1. Producing the correlograms

The photographic densities of the five transparencies were different. The following method was used for calculating the exposure times needed for recording the different correlation patterns:

The five transparencies were masked with a black tape such that they all had the same aperture, viz. 35 x 23 mm. They were then placed over a masked light box, and a light meter was used to record their intensity transmittances. These were as follows

Transparency No.	Light meter reading	Normalized intensity transmittance	Normalized intensity transmittance approximated to nearest 0.50
13	9.75	1.00	1.00
29	9.50	0.97	1.00
31	9.50	0.97	1.00
33	4.80	0.49	0.50
38	5.20	0.53	0.50

Table 4.8

The intensity transmittance of a combination of transparencies can be found by mutliplying their corresponding intensity transmittances. The normalized intensity transmittance

approximated to nearest 0.25, of any combination of two of the five transparencies is shown in the following table :

Transparency No.	13	29	31	33	38
13	1.00	1.00	1.00	0.50	0.50
29	1.00	1.00	1.00	0.50	0.50
31	1.00	1.00	1.00	0.50	0.50
33	0.50	0.50	0.50	0.25	0.25
38	0.50	0.50	0.50	0.25	0.25

Table 4.9

The exposure time multiplying factor is 1/the normalized intensity transmittance. Therefore, Table 4.9 can be written in terms of the exposure time multiplying factor as

Transparency No	13	29	31	33	38
13	1	1	1	2	2
29	1	1	1	2	2
31	1	1	1	2	2
33	2	2	2	4	4
38	2	2	2	4	4

Table 4.10

In order to record the autocorrelation patterns, another set of Fourier images was printed on the same scale and using the same exposure time as the first set. The resultant transparencies were then masked with a similar mask as before.

Each transparency of the first set was allowed to correlate with the transparencies of the second set. The exposure times were 3 seconds, 6 seconds and 12 seconds, depending on the multiplying factor, shown in Table 4.10, of the two transparencies.

The Fourier Images were symmetrical round their x and y axes. Therefore, inverting one of the transparencies would not produce any change in the correlation pattern. However, the transparencies needed to be squared up very well with respect to each other so that no error would arise due to a transparency rotation.

The apparatus (Figure 3.15) used in correlating the Fourier image transparencies consisted of a diffuse light source, two metal frames for holding the two transparencies, f/2.9 lens. and a dark slide holder with a ground glass screen. The screen fell at the focal plane of the lens when no dark slide was in the holder. When a dark slide was inserted in the holder the photographic plate in the dark slide fell at the focal plane of the lens.

The correlation patterns observed on the ground glass screen

had low contrast; for this reason, high contrast photographic plates like Ilford N40 were used. These were developed with 1:1 Kodak D8 developer. The correlograms, however, looked as if they were nonuniformly exposed. This slow variation in the photographic density was thought to be due to two factors. The first was that the source was not perfectly diffuse, in other words it was not truly Lambertian. The second was that some of the rays were missing the lens and therefore giving rise to what is called vignetting.

4.5.2 Correcting the correlograms

Several methods were tried to produce uniform correlation patterns. These are

1. Printing the correlograms with their defocussed image.

A diffuse light source was placed at the back focal plane of an f/6.3 aircraft camera lens. The focussing of the source with respect to the lens was done with the help of a pre-set collimating telescope as described in 3.5.4. The lens gave rise to a variety of bundles of parallel rays (each from one source point) at angles round the lens axis. The nonuniformly exposed correlogram was placed, over the optical bench, behind the collimating lens. A ground glass screen was placed over another carrier behind the correlogram. This was moved along the bench so that the correlogram image was completely blurred. It was then replaced with Ilford N30 photographic plate.

In order to get complete cancellation of the slow variations in density the contrast in the photographic plate should be adjusted for a gamma equal to 1. For this reason a small photographic wedge was placed in front of the photographic plate so that it covered a small part of the plate. This was supported with a window glass plate as shown in Figure 4.6. The wedge was compared with its reproduction; if they looked the same, then the gamma is 1. Another way of checking the contrast was to combine the wedge with its reproduction; if they produced a uniform grey at the middle then the gamma is 1.

The photographic plates were developed for 5 minutes in Kodak Universal developer diluted by 1:15. The best exposure time was found to be 64 minutes. This produced a very dim mask. The correlogram was combined with this mask and the combination was printed on grade 4 paper with a printing projector. The exposure time needed to produce the print was inconveniently long. It was noted, as well, that the print was still having some variations in density. This was due to the fact that exposing and processing the mask was so critical that it was very difficult to get a mask with a gamma exactly equal to 1.Figure 4.7 shows a nonuniformly exposed photograph and its "corrected" image. Figure 4.8 shows the mask used for the correction.

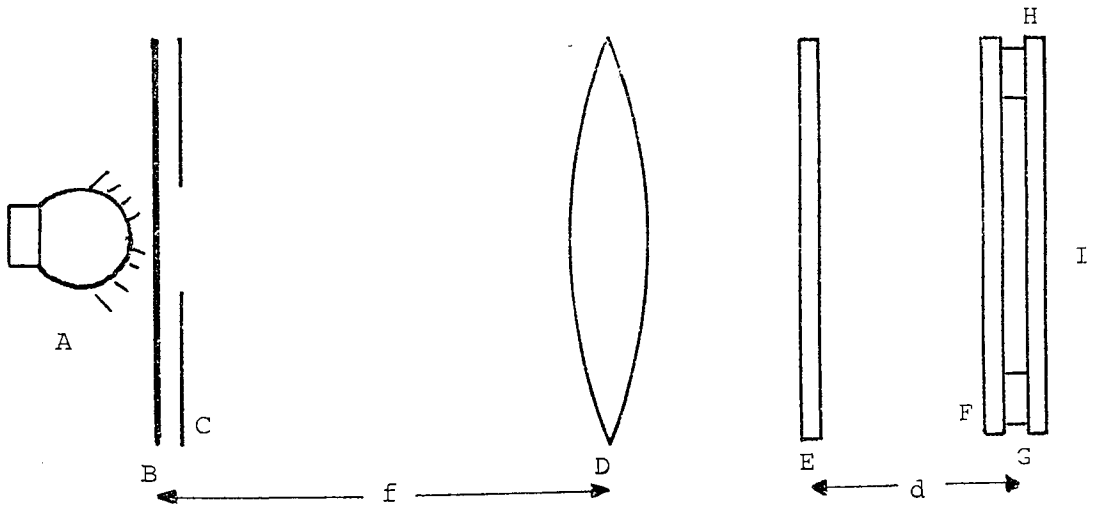

Figure 4.6 The arrangement used for producing density-variation correction mask. A = Diffuse light source; B = Ground-glass screen; C = mask for controlling the size of the source; D = collimating lens; E = correlogram plate; F = ordinary glass plate for holding the photographic wedge; G = photographic wedge; H = spacer of the same thickness as the wedge; I = photographic plate; d = defocus distance; f = the front focal plane of the lens

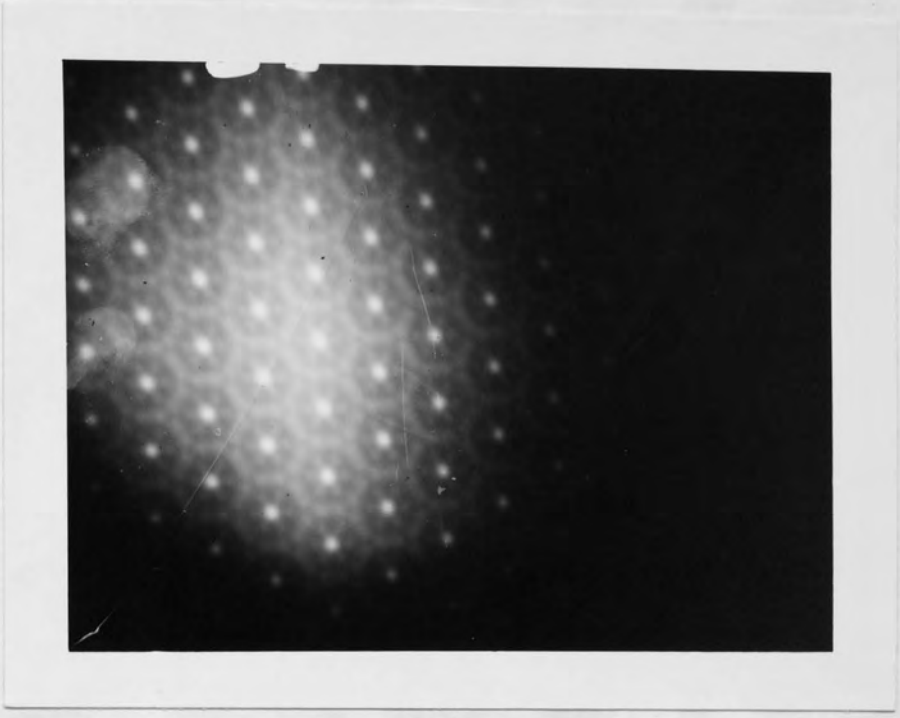

(a)

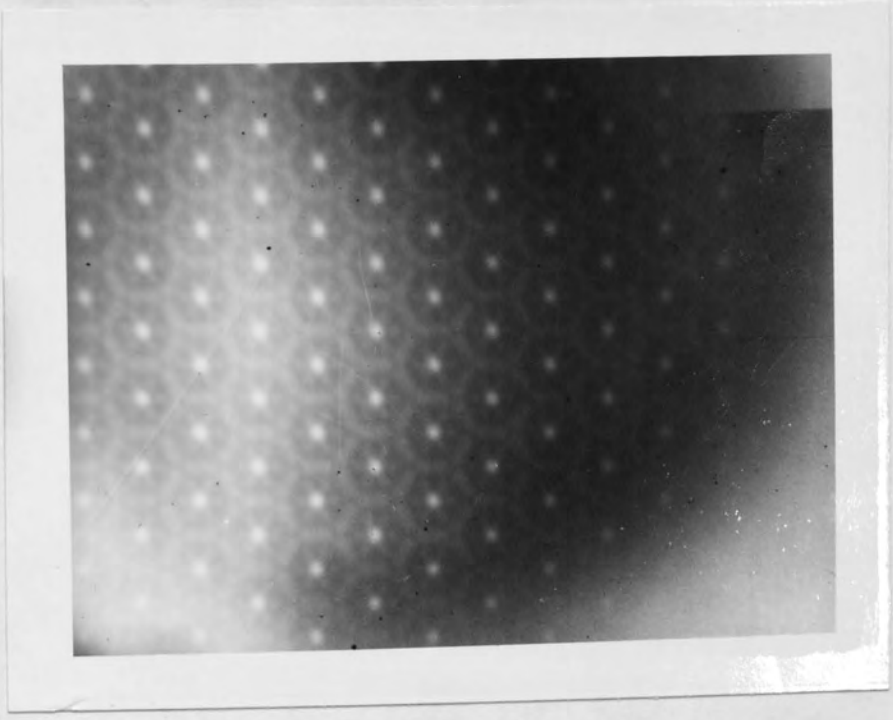

(b)

Figure 4.7 Correction of a nonuniformly exposed photograph by its blurred image mask, (a) The photograph, (b) its "Corrected" image

Figure 4.8 Mask used for producing Figure 4.7b.

2. Masking the light source or the photographic plate with the autocorrelation pattern of the transparencies apertures.

In this method, the noncoherent correlater was used to produce the autocorrelation pattern of the metal frames used for holding the Fourier image transparencies. In other words, it was used to produce the autocorrelation pattern of the transparencies apertures. The pattern represents the nonuniformity of the output of the correlation system. If this was used to mask the light source or the photographic plate of the system then the density variation at its output would be corrected or reduced.

The photographic plate used to produce the mask was Ilford N30. This was processed in the same way as in the first method. Several exposures were tried and the resultant plates were put consecutively over the light source, the transparencies were placed on their holders and the correlation pattern was observed over a ground glass screen at the correlater's output. The mask that gave a uniform density distribution was chosen. This was combined with Ilford N40 process plate and the combination was placed at the correlater's output. The process plate was exposed and proceesed in the usual way. The resultant correlation pattern had low contrast and low resolution. The mask had acted as a diffuser and therefore reduced the contrast and the resolution of the pattern.

A thin, transparent glass plate was mounted, with Sira mountant, over the mask. This would produce a uniform emulsion thickness and therefore reduce the light scattering. The mounted mask was tried. The correlation pattern obtained showed some improvement but it was still not quite satisfactory. Figure 4.9 shows a nonuniformly exposed photograph and its "corrected" image. Figure 4.10 shows the mask used for the correction.

3. Dodging

The two preceding methods had the disadvantage that they need critical exposure time and critical processing. The grain structures of the mask and the original plate add and therefore increase the noise in the corrected correlation pattern

In dodging, the printing projector was used to project the image of a nonuniformly exposed correlogram on a high contrast photographic paper. A circular hole was made in a black piece of cardboard. This was inserted between the projector's lens and the printing frame and was moved so as to control the exposure time of the different parts of the correlation pattern.

After some practice this method produced quite uniform correlation patterns. Figure 4.11 shows a nonuniformly exposed photograph and its corrected image.

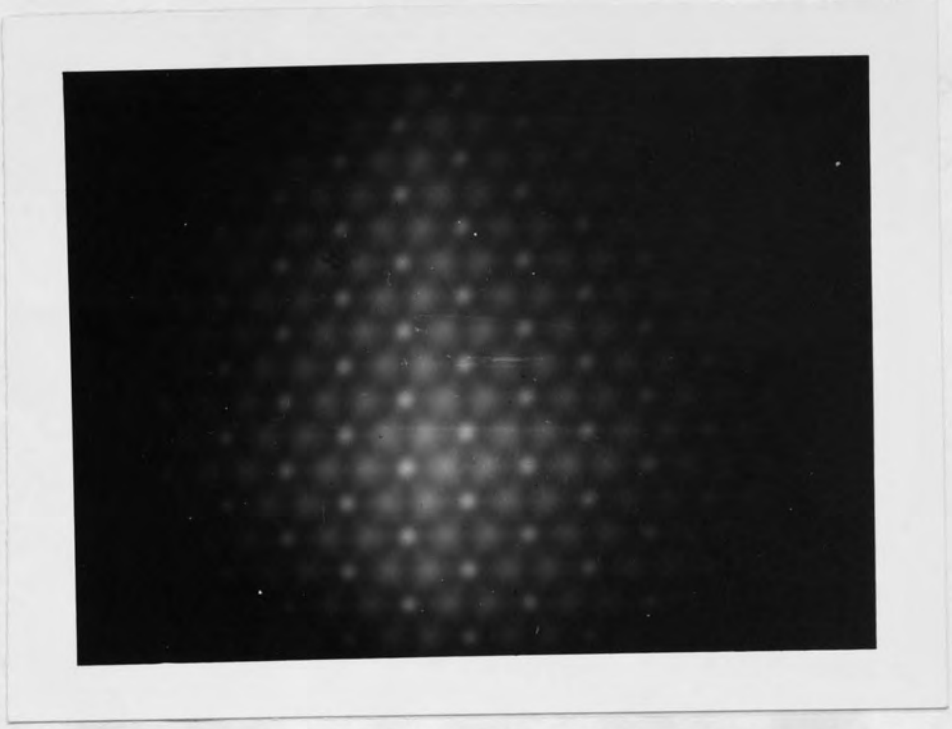

(a)

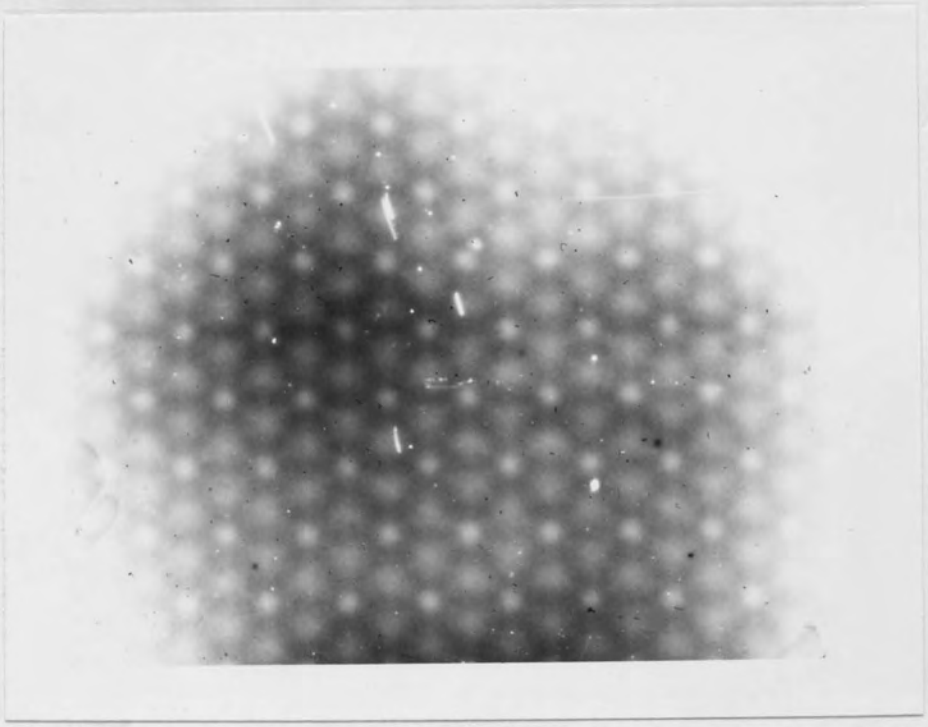

(b)

Figure 4.9 Correction of a nonuniformly exposed correlogram by masking the photographic plate (a) A noncorrected correlogram (b) Its corrected image

Figure 4.10 Mask used for producing Figure 4.9b.

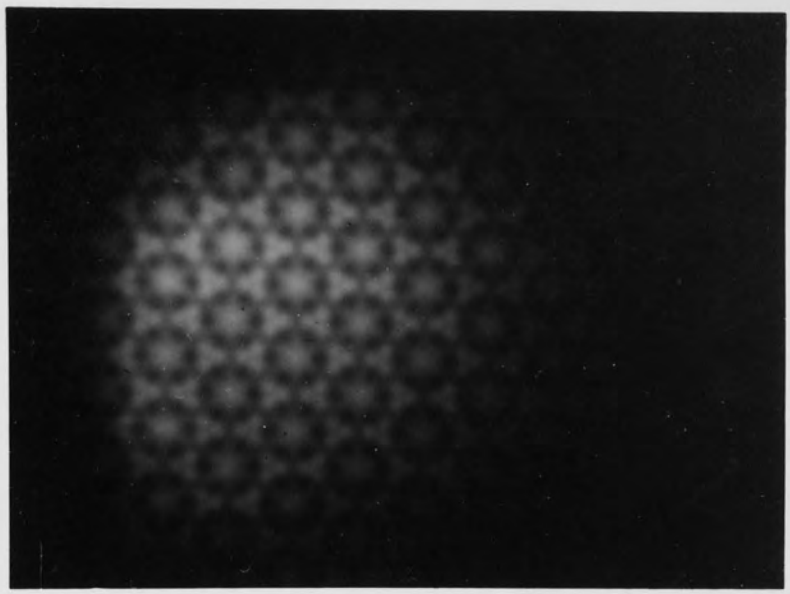

(a)

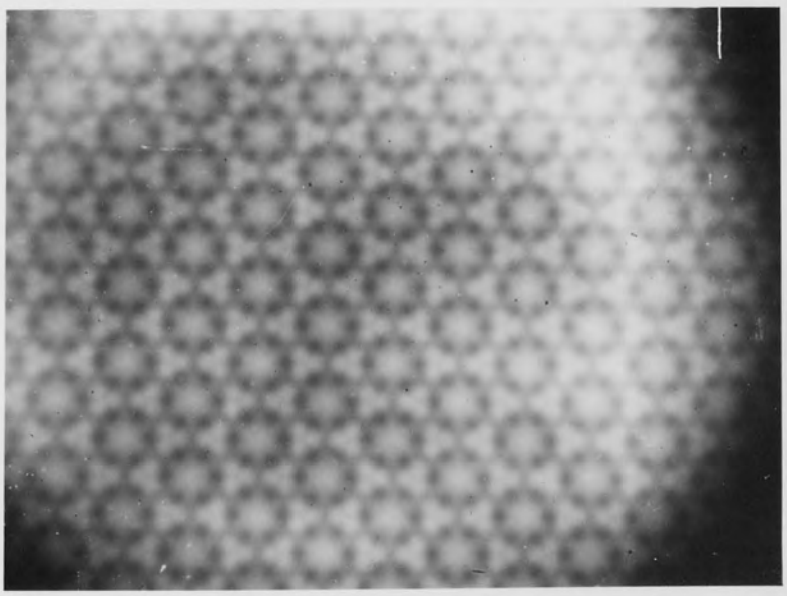

(b)

Figure 4.11 Correction of a nonuniformly exposed photograph by the dodging method (a) The photograph (b) its corrected image

4.5.3 Conclusions

Figure 4.12 shows a set of patterns representing the correlation between the five Fourier images used in this experiment. All the patterns were corrected by the dodging method.

The pattern set shows a very good symmetry round its autocorrelation axis. The autocorrelation patterns show good bright (white) peaks. Other patterns show either white or black peaks.

Bearing in mind that change in the exposure time and in the focussing of the printing projector changes the details of the correlation pattern photographs; it can be seen that some of the correlograms are similar. For example, 31 * 31 correlogram (both of honeycomb lattice) is similar to 31 * 33 of honeycomb structure and graphite structure.

A graphite structure Fourier image correlates with a honeycomb Fourier image and produces the same correlation pattern as a honeycomb Fourier image correlates with itself, tells us that the Fourier images of both lattices can easily be confused with each other.

It is noted as well that some of the correlation patterns are, roughly, negatives of others (e.g. 29 * 38 correlogram of

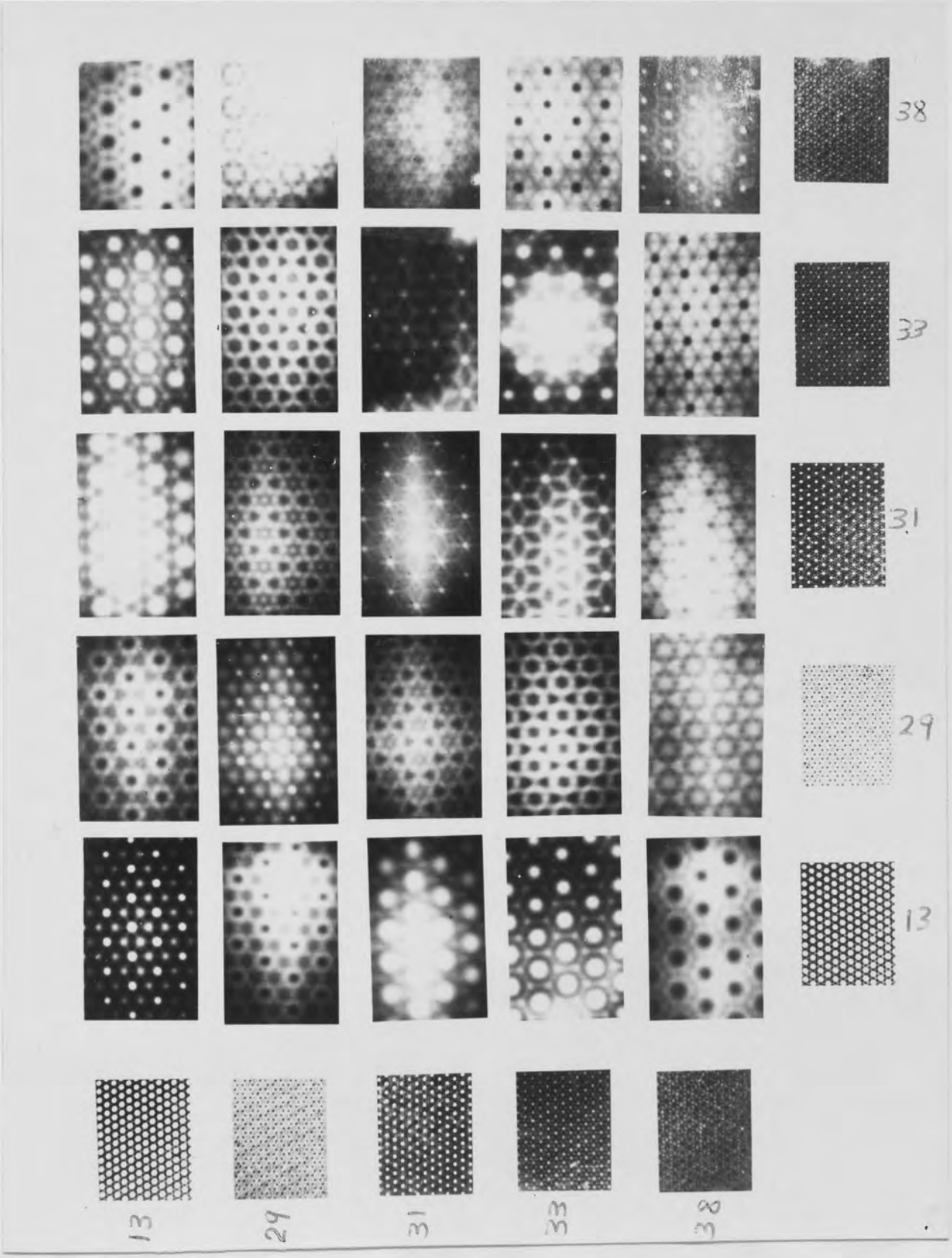

Figure 4.12 Correlation patterns of the five Fourier images used in the noncoherent correlation method

graphite structure and honeycomb lattice is the negative of 33 * 29 of graphite structure and graphite structure)

A correllogram negative of another means that one of the correlating transparencies in the negative correlogram differs from its corresponding one in the positive correlogram by 90^{o} (This can be proved by comparing the correlogram of two sine zone plates with the correlogram of a sine and a cosine zone-plates). The same idea of confusion mentioned above applies to these correlation patterns.

4.6 Reconstruction of Fourier images by the computer

Consider the problem of a coherent light wave travelling in the z direction and incident normally on a thin linear diffraction grating. The grating is situated at plane 0 (Figure 4.13). In order to calculate the Fresnel diffraction pattern at plane P, consider Huygens' principle.

For upward going wave we have a phase path to the wavefront of D cos θ and an extra phase path to plane P of x sin θ . For lower wave we have a phase path to the wavefront of D cos θ less a phase path of x sin θ .

Let us confine ourselves to a small angle. Therefore, $\sin \theta \simeq \theta$ and $\cos \simeq 1 - \frac{\theta^2}{2}$.

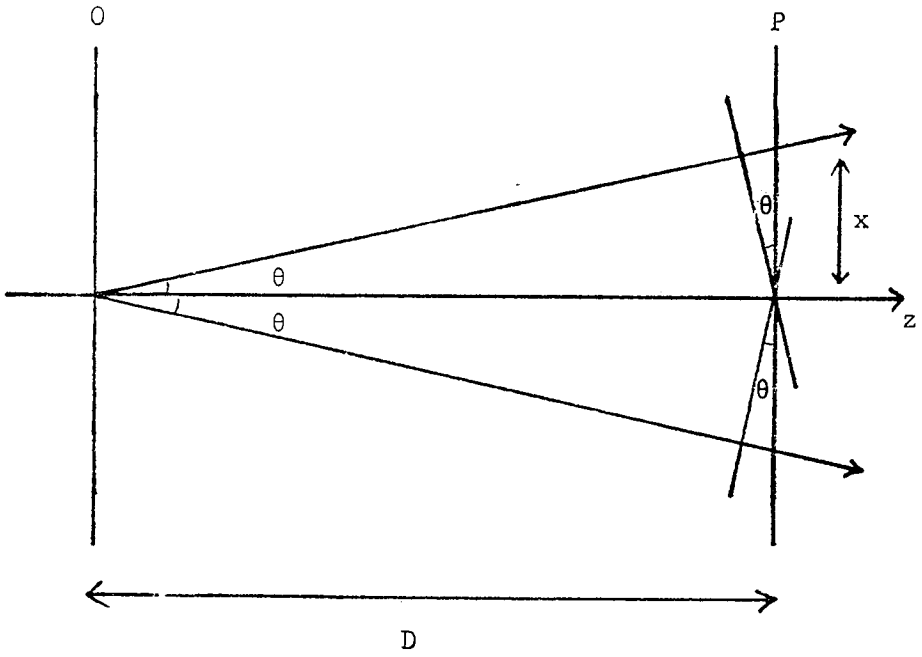

Figure 4.13 Formation of Fourier images by Fresnel diffraction

The disturbances arriving at P are

The amplitude A_o of phase path D

The amplitude A_1 of phase path D cos θ+ x sin θ

The amplitude A_{-1} of phase path D cos θ - x sin θ

If we take as zero the phase path D associated with A_o and subtract it from the rest then the above three formulas become

Zero phase path

D (cos θ - 1) + x sin θ

D (cos θ - 1) - x sin θ

Using now our approximation above we get

0

$D(-\frac{\theta^2}{2})+ x \theta$

$D\left(-\frac{\theta^2}{2}\right) - x \theta$

The diffraction pattern, at plane P, is therefore represented by the series

$$\sum_{n=-p}^{n=+p} A_n e^{-\frac{2\pi i}{\lambda}\left\{x\theta_n - \frac{\theta_n^2 D}{2}\right\}}$$

where A_n is the symmetrical Fourier Coefficient of the object and p is the number of orders taken in the calculation.

Let f be the focal length of the diffraction grating. In other words f is the distance between two reconstructions of the grating. The suborder number m can therefore be defined

as

$$m = \frac{f}{D}$$

The distance D is shown, in 4.1, to be equal to $\frac{d^2}{m\lambda}$

From the grating's diffraction formula $d \sin \theta_n = n\lambda$ we get

$$\theta_n = \frac{n\lambda}{d}$$

hence, the Fresnel diffraction pattern expression becomes

$$\sum_{n=-p}^{n=+p} A_n \, e^{-i\left\{ nx\left(\frac{2\pi}{d}\right) - \frac{\pi n^2}{m} \right\}}$$

Wang mini-computer was used for calculating the Fourier images. The computer uses the language BASIC. One period of the grating was used as the input. This is shown in Figure 4.14. The height of the input was taken to be π, its width 2π and the black to white ratio 1:1. It must be noted that

$$P > \frac{md}{\ell}$$

where d is the grating repeat distance and ℓ is the amount of d which is white. Since d was put equal to 2π, therefore the series above becomes

$$\sum_{n=-p}^{n=+p} A_n \, e^{-i\left\{ nx - \frac{\pi n^2}{m} \right\}}$$

$\frac{\pi n^2}{m}$ represents the phase of the Fourier image and is called α_n.

The suborder number m is shown (13) to be equal to the lines

multiplicity of the Fourier image. Therefore, in order to calculate the object's reconstruction, m has to be put equal to 1; otherwise α_n can be put equal to zero.

In order to use the above series in the computer it has to be modified as follows :

$$f(x) = A_o + \sum_{n=\pm 1}^{\pm p} A_n \; e^{-inx+i\alpha_n}$$

$$= A_o + \sum_{n=\pm 1}^{\pm p} A_n \; (\cos nx - i \sin nx)\; (\cos \alpha_n + i \sin \alpha_n)$$

$$= A_o + \sum_{n=\pm 1}^{\pm p} A_n \; (\cos nx \cos\alpha_n + \sin nx \sin \alpha_n)$$

$$+i \sum_{n=\pm 1}^{\pm p} A_n \; (\cos nx \sin \alpha_n - \sin nx \cos \alpha_n)$$

where f(x) represents the amplitude of the resultant pattern

$$\text{Let } A_o + \sum_{n=\pm 1}^{\pm p} A_n(\cos nx \cos \alpha_n + \sin nx \sin\alpha_n) = a$$

$$\sum_{n=\pm 1}^{\pm p} A_n \; (\cos nx \sin \alpha_n - \sin nx \cos \alpha_n) = b$$

Therefore the intensity of the resultant pattern is

$$f^2(x) = a^2 + b^2$$

The coefficients A_o and A_n are calculated as follows

$$A_o = \frac{1}{2\pi} \int_{-\pi}^{\pi} f(x)\, dx$$

$$= \frac{1}{\pi} \int_{o}^{\frac{\pi}{2}} \pi \quad dx$$

$$= \frac{\pi}{2}$$

$$A_n = \frac{1}{2\pi} \int_{-\pi}^{\pi} f(x) \cos nx \quad dx$$

$$= \frac{1}{\pi} \int_{o}^{\frac{\pi}{2}} \pi \cos nx \quad dx$$

$$= \frac{1}{n} \sin \frac{n\pi}{2}$$

Figure 4.15 shows the reconstruction of the object shown in Figure 4.14. α was put equal to 0 and therefore all the Fourier Components of the object add in phase and we get the reconstruction. The program for doing this is shown in Appendix 1.

The reconstruction is sampled onto 32 points, M is the sampling number and p is 40.

A trial was carried out for getting the reconstruction of suborder numbers 2 and 4. In this case α_n was put equal to $\frac{n^2 \pi}{2}$ and $\frac{n^2 \pi}{4}$ respectively (Appendices 2 and 3). No satisfactory results appeared in the computer output. The

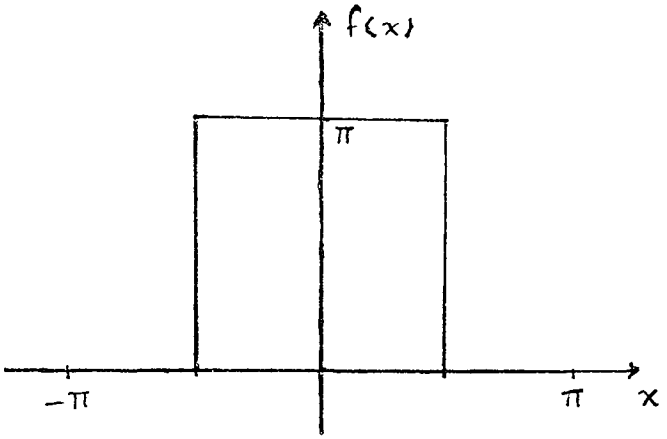

Figure 4.14 One period of a square wave diffraction grating used as an input for calculating the Fourier images by the computer

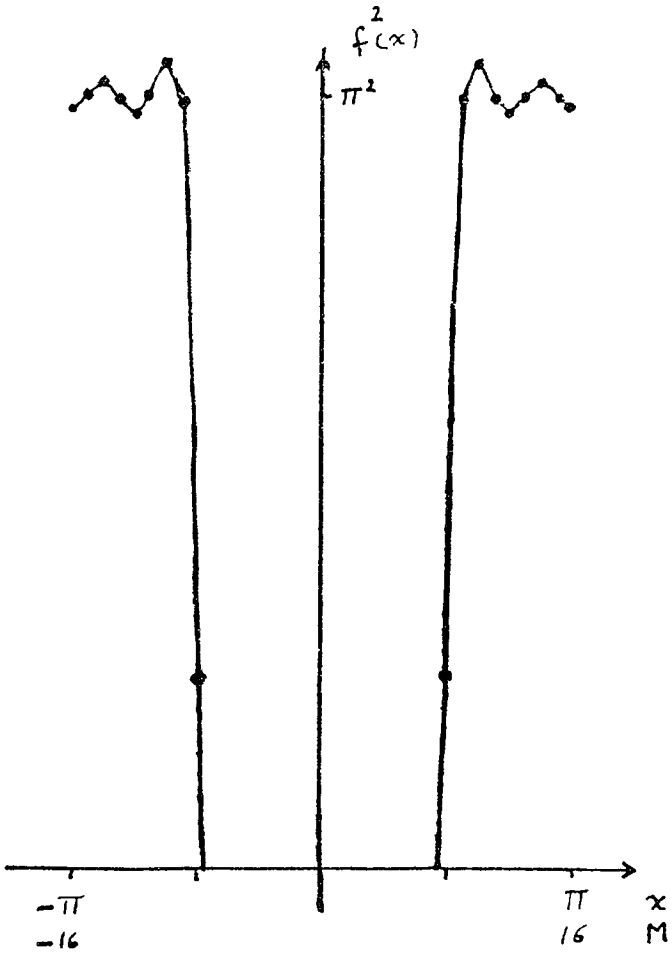

Figure 4.15 The Computer's reconstruction of one period of the square wave diffraction grating. The reconstruction is shifted by one half of the repeat distance (Section 4.1).

reason for that seems to be the conversion of the amplitude contrast object into phase contrast image. The values of the imaginary part of the series are indication of such conversion.

References

1. Abbe E. Arch.f.mikr. Anat. 9 413 (1873)
2. Gabor D. Nature 161 777 (1948)
3. Gabor D. Proc.Roy.Soc. A. 197 454 (1949)
4. Talbot F. Phil Mag. 9 401 (1836)
5. Lord Rayleigh. Phil.Mag. 11 196 (1881)
6. Cowley J.M. and Moodie A.F. Proc.Phys.Soc. Lond. 70 486, 497, 505, (1957)
7. Cowley J.M and Moodie A.F. Proc.Phys. Soc. Lond. 71 533 (1958)
8. Cowley J.M. and Moodie A.F. Proc. Phys.Soc. 76 378 (1960)
9. Winthrop J.T. and Worthington C.R. J.Opt.Soc.Am. 55 373 (1965)
10 Rogers G.L. New Scientist 12 570 (1961)
11 Rogers G.L. Proc.Roy.Soc.B 157 83 (1962)
12 Rogers G.L. Nature 166 399 (1950)
13 Rogers G.L. "Handbook of Gas Laser Experiments" Iliffe (1970)p.42.
14 Rogers G.L. Brit.J.Appl.Phys. 14 657 (1963)
15 Rogers G.L. Brit.J.Appl.Phys. 15 594 (1964)
16 Rogers G.L. J.of Mic. 89 121 (1969)
17 Conrady A.E. J.Roy.Micr.Soc. 610 (1904)
18 Booker H.G. Ratcliffe J.A. and Shinn D.H. Phil.Trans.Roy. Soc. A. 242 579 (1950)

19 Ditchburn R.W. "Light" 2nd Edition Blackie (1963) P207

20 Lamberts R.L. and Kurtz C.N. Appl.Opt. 10 1342 (1971)

CHAPTER 5.

NONCOHERENT SPATIAL FILTERING BY BLOCKING FILTERS

5.1. The Fourier Transformer

We have seen in Chapter 2 that any Fourier coefficient of an input pattern can be obtained by convolving the pattern with an appropriate sinusoidal grid.

If the pattern is represented by F(x,y) and the sinusoidal grid by cos(ux + vy) then the cosine Fourier coefficient will be

$$C(u,v) = \int_{-\infty}^{\infty}\int_{-\infty}^{\infty} F(x,y) \cos (ux + vy) \; dx \; dy$$

The convolution shift is assumed zero in this case. u and v define the spacing and orientation of the grid, and the direction of maxima in the detector plane.

The sine Fourier coefficient is obtained by convolving the pattern with a sine grid .

In order to get the Fourier transform, the pattern F(x,y) has to be convolved with a set of sinusoidal grids of different spacings and orientations. This can be obtained by different

ways (1,2). The simplest way is to make two zone-plates overlap (2,3). This generates linear fringes (moire pattern) whose spacing is inversely related to the separation of the zone-plate centres (4). By arranging that the zone-plates are not in the same plane, a range of frequencies can be observed simultaneously. Parallax effects as the observer moves around will thus generate moire fringes of variable frequency. The pattern F(x,y) is then placed anywhere between the zone plates or behind them and an integrating lens is used to focus each skew parallel bundle of rays onto the corresponding point in the back focal plane of the lens. Any one of these points represents a Fourier coefficient and the whole pattern represents the Fourier transform (Figure 5.1).

The transform given by this device, however, is the cosine Fourier transform. If the sine Fourier transform is required then <u>one</u> of the zone-plates has to be replaced by a phase-shifted zone-plate (sine zone-plate). This is similar to the normal zone-plate (cosine zone-plate) except that the zones are shifted by 90^{o}.

If R_m represents the radius of the mth boundary between zones and R_1 represents the radius of the innermost boundary of the cosine zone-plate then R_m for the cosine zone-plate is

$$R_m = R_1 \sqrt{m} \qquad m = 1,2,3,.....$$

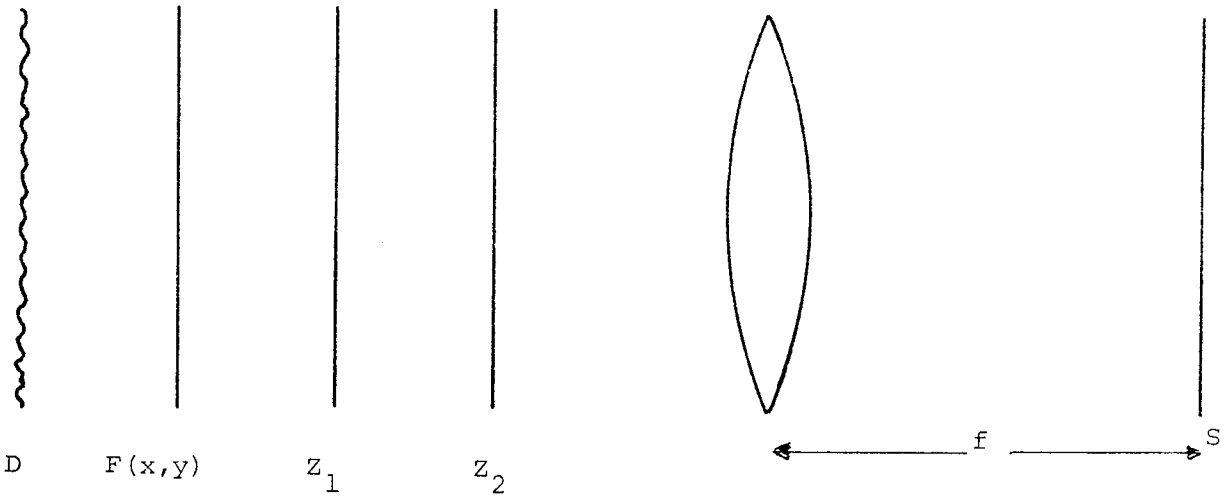

Figure 5.1 The Fourier transformer

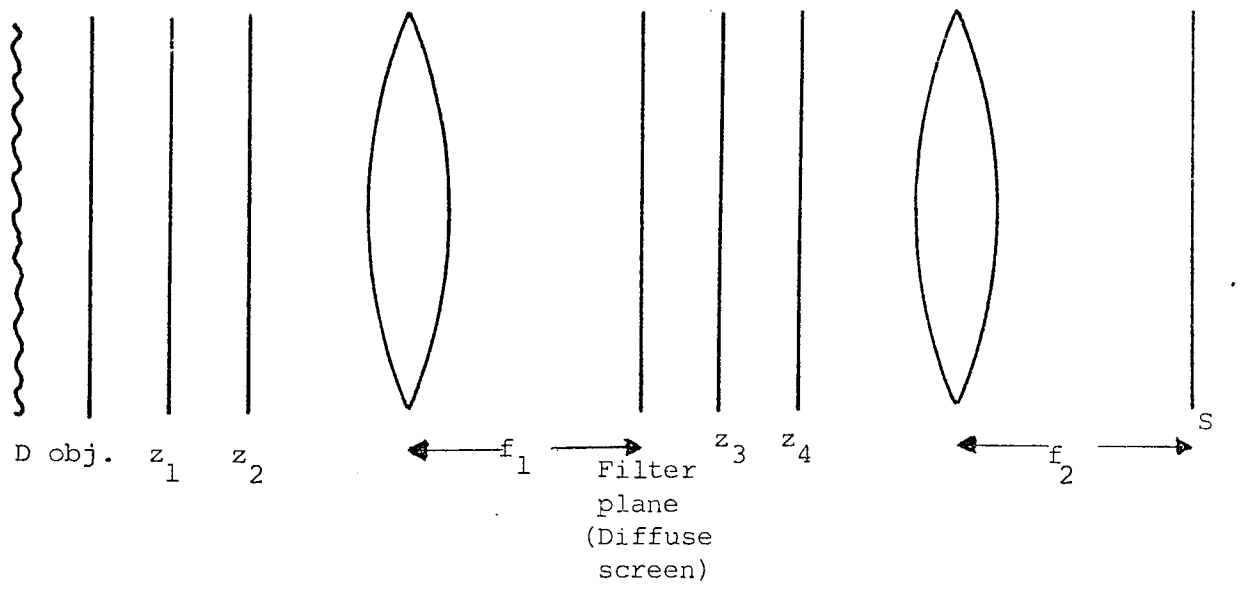

and for sine the zone-plate is

$$R_m = R_1 \sqrt{m-\tfrac{1}{2}} \qquad m = 1, 2, 3, \ldots\ldots\ldots$$

It is not necessary to use zone-plates in this device. Any plate that produces linear moire fringe system can be used. If two Girard Grids are used instead of two zone-plates a Fourier transform is still obtained. The output however, appears as though it is reflected in the line $x = y$ with respect to the zone-plates output.

This method of obtaining Fourier transforms is phase-sensitive. This can be seen by moving the object, for instance vertically, and observing the Fourier transform plane. The transform changes from light to dark and vice versa. This corresponds to the case of in-phase and anti-phase conditions between the waves generated by the zone-plates (moire fringes) and the Fourier components of the object.

The idea of obtaining the Fourier transform in this way is similar to the idea of obtaining the Fourier transform in the coherent way. In both cases, the function to be transformed is multiplied by a particular wavefront and integrated. In the noncoherent method the required wavefront is generated as a moire pattern between two suitably separated zone-plates. In the coherent method, the wavefront is the wedge fringe

system between the incident wavefront and the diffracted wavefront.

5.2. The spatial filtering system

Blocking filters are used in coherent optical data processing to perform many useful spatial filtering operations (e.g. Raster removal, additive noise removal, Half-tone removal...etc) They are usally placed in the back focal plane of the Fourier transform lens to block out the unwanted frequencies of the object. The rest of the spectra is then transformed back, with another lens, to form the filtered image (Figure 2.1).

If the output of the noncoherent Fourier transformer mentioned in the last section is used as an input for another similar transformer then the object's frequencies will be transformed twice. This will form an image similar to the original object at the second transformer output. Blocking filters may then be placed at the first transformer output to omit the unwanted frequencies (Figure 5.2)

This system has all the advantages of the noncoherent systems. The input can be represented in a variety of ways, e.g. an opaque copy, transparency, television screen, optical image, reflection....etc. Therefore, real time techniques can be easily applied to this system. It has the added advantages

of being phase sensitive, redundant and less expensive.

The Fourier transform pattern produced by the noncoherent transformer is different from that produced in a coherent light. Every spot in the noncoherent Fourier transform contains all the information about the object. Therefore, blocking out part of the spectrum with a blocking filter does not prevent all the frequencies of the object from passing through. For this reason a ground glass screen was placed at the output of the first Fourier transformer. The would distort all the information in the filter plane and change it into an intensity variations.

5.3 Experiment

The object used in the experiment was a cross-grating (Figure 5.3). This has a Fourier transform of the shape shown in Figure 5.4. The filter was a horizontal slit cut into a white sheet of paper. The sheet was oiled with a machine-oil so that no sharp edge would appear on the diffuse screen. This would prevent the sharp edge of the filter from being transformed by the second transformer and therefore prevent the unwanted ringing effect, mentioned in 2.2.1, from occurring. The horizontal slit was designed to produce a linear grating of vertical lines at the system's output.

The diffuse light source was a 100 watts lamp. This

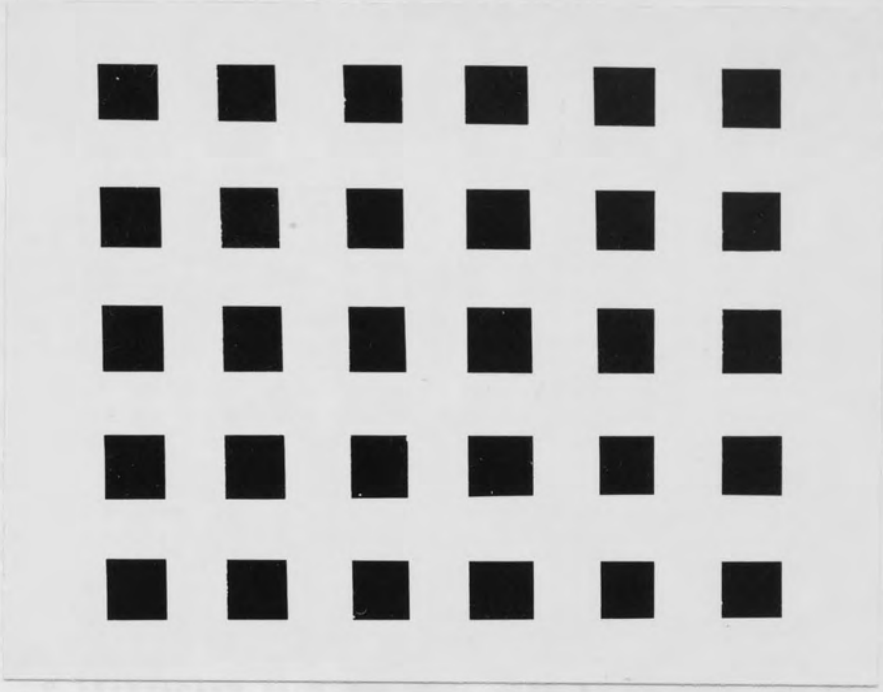

Figure 5.3 The Cross-grating

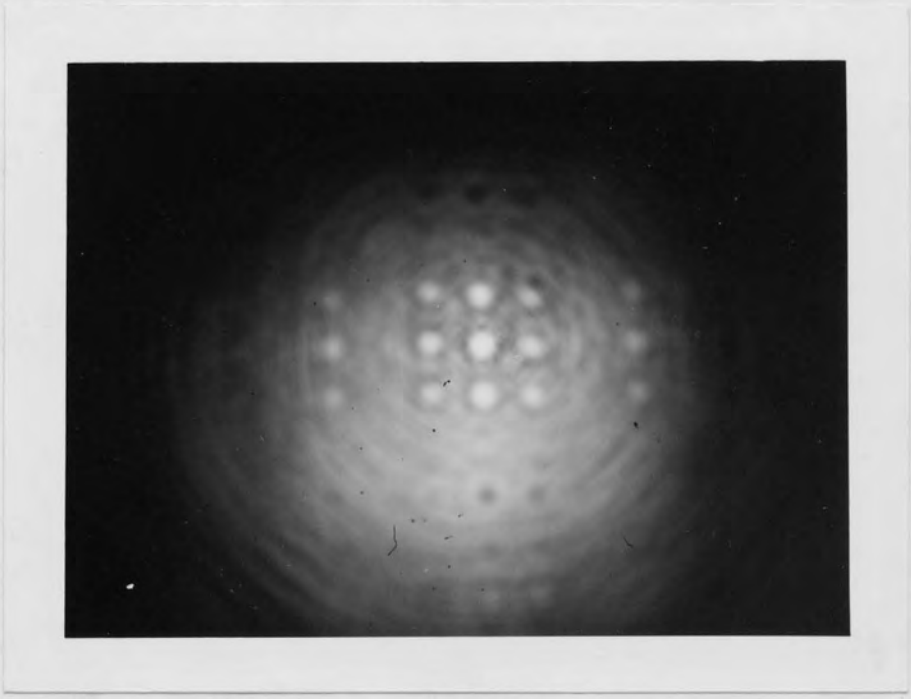

Figure 5.4 The Fourier transform of the cross-grating

was found to be not strong enough to produce a Fourier transform pattern with a high intensity and contrast. Kodak Carousel projector was, therefore, used as a light source. Several diffuse screens were placed behind the object to render the projected light diffuse. The Fourier transform pattern was still not bright enough, the contrast was not high enough and no image could be observed at the system's output.

A television link was next used to enhance the brightness and contrast. The output of the first transformer was displayed on a television screen. This was used as an input for the second transformer. The contrast was very good but the brightness of the spots was poor. Any attempt to increase the brightness of the television monitor would decrease the contrast of the Fourier transform pattern.

References

1. Born M. Furth R. and Pringle R.W. Nature 156 756 (1945)
2. Richardson J.M. U.S. patent No. 3669528 (1972)
3. Stephens N.W.F. and Rogers G.L. Phys.Ed. 9 331 (1974)
4. Oster G. Wasserman M. and Zwerhing C. J.Opt.Soc.Am. 54 169 (1964)

```
10 FOR M=0TO 16
20 Q=0:P=0
30 FOR N=1TO 40
40 T=1/N*SIN(N*#PI/2)*(COS(N*M*#PI/16)*COS(NT2*#PI)+SIN(N*M*#PI/
16)*SIN(NT2*#PI))
50 Q=Q+T
60 NEXT N
70 FOR N=-40TO -1
80 T=1/N*SIN(N*#PI/2)*(COS(N*M*#PI/16)*COS(NT2*#PI)+SIN(N*M*#PI/
16)*SIN(NT2*#PI))
90 Q=Q+T
100 NEXT N
110 R=0
120 FOR N=1TO 40
130 U=1/N*SIN(N*#PI/2)*(COS(N*M*#PI/16)*SIN(NT2*#PI)-SIN(N*M*#PI
/16)*COS(NT2*#PI))
140 R=R+U
150 NEXT N
160 FOR N=-40TO -1
170 U=1/N*SIN(N*#PI/2)*(COS(N*M*#PI/16)*SIN(NT2*#PI)-SIN(N*M*#PI
/16)*COS(NT2*#PI))
180 R=R+U
190 NEXT N
200 T=Q+2*R+P
210 PRINT M;N;Q;R;I
220 NEXT M
```

```
0  -1   2.49844934E-02 -1.01961425E-10   6.24221415E-04
1  -1  -1.26344222E-04  3.50000000E-12   1.59628662E-08
2  -1  -2.70371989E-02  1.90400000E-10   7.31010125E-04
3  -1   4.99879386E-04  1.63800000E-10   2.49878401E-07
4  -1   3.52898124E-02 -8.28000000E-11   1.24537065E-03
5  -1  -1.66488810E-03 -2.12300000E-10   2.77185241E-06
6  -1  -6.49399959E-02 -1.73800000E-10   4.20343917E-03
7  -1   1.49599051E-02 -1.10200000E-10   2.20813808E-04
8  -1   1 5707963296786   0   2.4674011002
9  -1   3.12673948437   1.09700000E-10   9.7764583055
10 -1   3.20642658972   1.73900000E-10   10.2811747
11 -1   3 1432575417   2.12400000E-10   9.88006797e4
12 -1   3.10620294119l   8.32000000E-11   9.64911/3412
13 -1   3.14109975205 -1.63700000E-10   9.8664b88224
14 -1   3.16862995508 -1.90300000E-10   10.040215142
15 -1   3.14171899781A -3.50000000E-12   9.870396e2612
16 -1   3.11660829131   1.01961425E-10   9.7132466601
```

APPENDIX 1

Program for reconstructing a main order Fourier image of a square wave diffraction grating

```
10 FOR M=1TO 16
20 Q=#PI/2
30 FOR N=1TO 40
40 T=1/N*SIN(N*#PI/2)*(COS(N*M*#PI/16)*COS(N+2*#PI/2)+SIN(N*M*#P
I/16)*SIN(N+2*#PI/2))
50 Q=Q+T
60 NEXT N
70 FOR N=-40TO -1
80 T=1/N*SIN(N*#PI/2)*(COS(N*M*#PI/16)*COS(N+2*#PI/2)+SIN(N*M*#P
I/16)*SIN(N+2*#PI/2))
90 Q=Q+T
100 NEXT N
110 R=0
120 U=1/N*SIN(N*#PI/2)*(COS(N*M*#PI/16)*SIN(N+2*#PI/2)-SIN(N*M*#
PI/16)*COS(N+2*#PI/2))
130 R=R+U
140 NEXT N
150 FOR N=-40TO -1
160 U=1/N*SIN(N*#PI/2)*(COS(N*M*#PI/16)*SIN(N+2*#PI/2)-SIN(N*M*#
PI/16)*COS(N+2*#PI/2))
170 R=R+U
180 NEXT N
190 I=Q+2+R+2
200 PRINT M;N;Q;R;I
210 NEXT M
```

```
 0  -1   1.570796326697   1.545811903334   4.8569355405
 1  -1   1.570796326758   1.570922671015   4.9351991385
 2  -1   1.570796326862   1.597933525712   5.0204730764
 3  -1   1.570796326826   1.570296448408   4.9332320363
 4  -1   1.570796326698   1.535506514394   4.8251813557
 5  -1   1.570796326745   1.572461214907   4.9400353725
 6  -1   1.570796326892   1.635630262183   5.1426874552
 7  -1   1.570796326891   1.555936521647   4.88833956
 8  -1   1.570796326795   9.47292894E-12   2.4674011003
 9  -1   1.570796326701  -1.555936521646   4.8883395594
10  -1   1.570796326701  -1.635630262183   5.1426874546
11  -1   1.570796326843  -1.572461214904   4.9400353728
12  -1   1.570796326896  -1.535506514396   4.8251813564
13  -1   1.570796326765  -1.570296448406   4.9332320361
14  -1   1.570796326729  -1.597833525712   5.0204730?6
15  -1   1.570796326832  -1.570922671019   4.9351991387
16  -1   1.570796326891  -1.545811903334   4.8569355411
```

APPENDIX 2

Program for reconstructing a Fourier image of suborder No 2

```
10 FOR M=0TO 15
20 A=#PI/2
30 FOR N=1TO 40
40 T=1/N*SIN(N*#PI/2)*(COS(N*M*#PI/16)*COS(NT2*#PI/4)+SIN(N*M*#P
I/16)*SIN(NT2*#PI/4))
50 A=A+T
60 NEXT N
70 FOR N=-40TO -1
80 T=1/N*SIN(N*#PI/2)*(COS(N*M*#PI/16)*COS(NT2*#PI/4)+SIN(N*M*#P
I/16)*SIN(NT2*#PI/4))
90 A=A+T
100 NEXT N
110 B=0
120 FOR N=1TO 40
130 U=1/N*SIN(N*#PI/2)*(COS(N*M*#PI/16)*SIN(NT2*#PI/4)-SIN(N*M*#
PI/16)*COS(NT2*#PI/4))
140 B=B+U
150 NEXT N
160 FOR N=-40TO -1
170 U=1/N*SIN(N*#PI/2)*(COS(N*M*#PI/16)*SIN(NT2*#PI/4)-SIN(N*M*#
PI/16)*COS(NT2*#PI/4))
180 B=B+U
190 NEXT N
200 I=A^2+B^2
210 PRINT M;N;A;B;I
220 NEXT M
 0 -1   2.6639504046095   1.093054079268   8.2908662062
 1 -1   2.6816406400197   1.110810073386   8.4249119047
 2 -1   2.7006352480016   1.129838921252   8.5699667308
 3 -1   2.6811639939925   1.110367267156   8.4215536854
 4 -1   2.6565633954484   1.085767068878   8.2362192032
 5 -1   2.6896943150019   1.111897988204   8.433165924
 6 -1   2.7273615767701   1.1565652499   8.7761443474
 7 -1   2.6710095992337   1.100213265561   8.3447614721
 8 -1   1.5707963268803   5.70000000E-12   2.4674011003
 9 -1   .4705830612582 -1.10021326556   1.43191764724
 10 -1   .4142310768888 -1.1565652499   1.50923056236
 11 -1   .4588988338575 -1.111897988201   1.4469048e2135
 12 -1   .4950299257906 -1.08576706888   1.41414350892
 13 -1   .4604290596669 -1.110367267155   1.44491038699
 14 -1   .4409574065575 -1.129838921253   1.47097942153
 15 -1   .4599868253992 -1.110810073889   1.44548637241
 16 -1   .4777429749 -1.093054079268   1.42300487524
```

APPENDIX 3

Program for reconstructing a Fourier image of suborder No.4

JOURNAL OF THE OPTICAL SOCIETY OF AMERICA VOLUME 65, NUMBER 6 JUNE 1975

Coding and decoding of dilute and continuous-tone objects in incoherent light

Luay Alqazzaz and Gordon L. Rogers

Department of Physics, University of Aston in Birmingham, Gosta Green, Birmingham B4 7ET, Great Britain
(Received 15 October 1974)

ACKNOWLEDGMENTS

I am very much indebted to my Supervisor, Professor G.L. Rogers, for his continued guidance and encouragement throughout the research.

I would also like to thank Mr.B.Brookes for preparing the Fourier images transparencies; Mr.A.G.McKenzie for building the prism-lens holder of the coherent correlater; Mr.J.Davies for helping with the computer and Mrs.D.Hill for typing the manuscript.